DISSERTATION

LOW-COST ANALYTICAL TOOLS FOR COMPOSITIONAL ANALYSIS OF PARTICULATE MATTER

Submitted by

Jaruwan Mettakoonpitak

Department of Chemistry

In partial fulfillment of the requirements

For the Degree of Doctor of Philosophy

Colorado State University

Fort Collins, Colorado

Summer 2018

Doctoral Committee:

Advisor: Charles Henry

Delphine Farmer
George Barisas
John Volckens

ABSTRACT

LOW-COST ANALYTICAL TOOLS FOR COMPOSITIONAL ANALYSIS OF PARTICULATE MATTER

Particulate matter (PM) represents a major health problem to people worldwide, contributing to 4 million deaths annually as reported by the Global Burden of Disease (GBD) study (http://www.healthdata.org). PM toxicity is linked to its chemical composition. The toxic chemical components of PM include trace metals, reactive oxygen species, and organic compounds that cause DNA oxidative damage and/or carcinogenesis in the respiratory and cardiovascular systems. The advanced laboratory instrumentation, normally used for the compositional analysis in PM, hinders people in remote area accessing PM monitoring on time due to large, complicated, and expensive features. Microfluidic paper-based analytical devices (mPADs) allow people in developing countries and remote area get an access to analytical testing in wide-ranging application from pharmaceutical analysis to environmental monitoring. However, analytical performance of mPADs needs to be improved. Electrochemistry, integrated into an mPAD, is able to improve limits of detection (LOD) and selectivity. This dissertation presents two efforts towards developing low-cost, portable, and disposable electrochemical analytical devices for chemical characterization of PM.

First, simple electrochemical devices for analyzing trace metals including Zn, Cd, Pb, Co, and Ni in PM are presented. The device was fabricated using stencil-printing on a low-cost polyethylene transparency (PET) sheet to create carbon stencil-printed electrode (CSPE). For simultaneous Zn, Cd, and Pb detection, electrospray deposition of silver nanoparticles (AgNPs)

was chosen for electrode modification to enhance electrode performance. An enhanced dispersion of AgNPs on the electrode surface was observed resulting in increase of surface area and better electrochemical performance. In addition, Bi and Nafion were used as co-modifiers to enhance peak current. Finally, acetate buffer (pH 5.0) was found to be suitable to obtain the best limit of detection (LOD) and longest linear operating range. The AgNP/Bi/Nafion-modified CSPE provided LODs of 5.0, 0.5, and 0.1 μg L^{-1} for Zn, Cd, and Pb detection, respectively. The proposed method was used to measure Zn, Cd, and Pb in PM samples including incense, fly ash, cigarette, and solder. The results from the proposed method for Zn, Cd, and Pb detections were not significantly different from the results measured using ICP-MS (at 95% confidence). Besides the method developed for Zn, Cd, and Pb detection, CSPEs were also used for Co and Ni analysis because these metals can produce reactive oxygen species via Fenton-like reactions. The CSPE for Co and Ni determination was modified with Bi to improve signal. Furthermore, dimethylglyoxime (DMG) was used as a Co(II) and Ni(II) chelator with highly selective chemical precipitation for adsorptive stripping voltammetry. The approach gave LOD of 1.0 and 5.0 μg L^{-1} for Co and Ni, respectively. Finally, Bi-modified CSPEs were used to determine Co and Ni in aerosol samples. The amount of Co and Ni in the samples determined using the proposed method was not significantly different from the results obtained using ICP-MS at 95% confidence.

In addition to metals, other components in PM such as organic compounds are prevalent in PM but their analysis is normally restricted to complicated separation methods. To address this need, the last part of this dissertation focuses on developing a low-cost, high resolution electrophoretic laminated Parafilm-paper devices for further analysis of complicated compositions in PM samples. The essential electrophoretic parameters including Joule heating, electroosmotic flow, and electrophoretic mobility were studied. Colorimetry and fluorescence were used as the

detection methods. Method viability was first established using chlorophenol red and indigo carmine dyes. The parameters affecting the separation included paper type, channel width, and applied potential. Addition of an injection valve into the device improved resolution and reduced peak broadening. Moreover, the separation of fluorescein isothiocyanate (FITC) and glutamic acid labeled with FITC was used to demonstrate fluorescence detection. In conclusion, the low-cost methods for PM analysis were proposed with using CSPE to detect Zn, Cd, Pb, Ni and Co and using electrophoresis separation on mPAD prepared for effective complicated compounds analysis in the future.

ACKNOWLEDGEMENTS

I would first like to express my sincere thanks to my advisor, Dr. Charles Henry, for his advice, supports, and patience. He has provided me valuable opportunities to do the research matching to my temperaments and the comprehensive knowledge in chemistry. His motivation and flexibility encourage me overcome numerous obstacles I have been facing through my research. His positive thinking attitude inspires me to replace negative thoughts with some positive ones. I will be forever grateful to him.

I would like to give more meaningful thanks to my family for supporting me for all accounts, raising me up when facing with the problems, having patience over the time I have spent in the U.S., and always giving me unconditional love. All of my accomplishments owe to them.

Next, I would like to thank all of the faculty and research scientists including Dr. John Volckens, Dr. Melissa Reynolds, Dr. Scott Noblitt, Dr. Dan Miller-Lionberg, Dr. Thomas Reilly, for their collaboration and help. Moreover, I would like to thank former and current members of Henry lab for their feedback, helps, collaborations and of course friendship.

I am appreciative to the Development and Promotion of Science and Technology Talent Project scholarship, Thailand and Office of Educational Affairs Royal Thai Embassy, Washington DC to provide great opportunities, financial support, and advice.

Finally, I would like to thank my hopes and dreams.

TABLE OF CONTENTS

CHAPTER 1. INTRODUCTION TO LOW-COST ANALYTICAL TOOLS FOR COMPOSITIONAL ANALYSIS OF PARTICULATE MATTER

Introduction to particulate matter

Airborne particulate matter (PM) is a heterogeneous mixture of solid and liquid particles (with diameter between a few nanometers and several micrometers) suspended in the atmosphere[1] and is constantly being released from both natural and anthropogenic sources.[2] Primary PM is directly emitted from sources such as combustion, mining, agricultural harvesting, soil, and marine aerosols while secondary PM is formed in the atmosphere as a result of chemical reactions. Extensive research has demonstrated that PM exposure affects human health with impacts ranging from allergies to chronic diseases.[3,4] PM properties including particle concentration, size, and composition impact human health and the environment.[5]

- **Particle concentration and size**

Exposure to and intake of PM is influential on human health.[6] Different measures are commonly used to describe PM concentrations, including mass, surface area, and/or PM number by considering the distribution of ambient particles as the function of size as shown in Figure 1.1.[7] PM concentration based on mass shows the majority of particles have a diameter greater than ~0.1 μm while PM concentration based on particle number shows the majority of particles with diameter less than ~0.1 μm. Thus, the particles larger than 0.1 μm are frequently quantified using mass concentration (per unit volume of air) and the particles smaller than 0.1 μm (ultrafine) are generally characterized using number concentration. Ultrafine particles ($PM_{0.1}$: defined as the particles smaller than 0.1 μm) have considerably different properties from those of larger particles such as $PM_{2.5}$ and/or PM_{10}. Therefore, particles larger and smaller than 0.1 μm are discussed separately in this chapter.

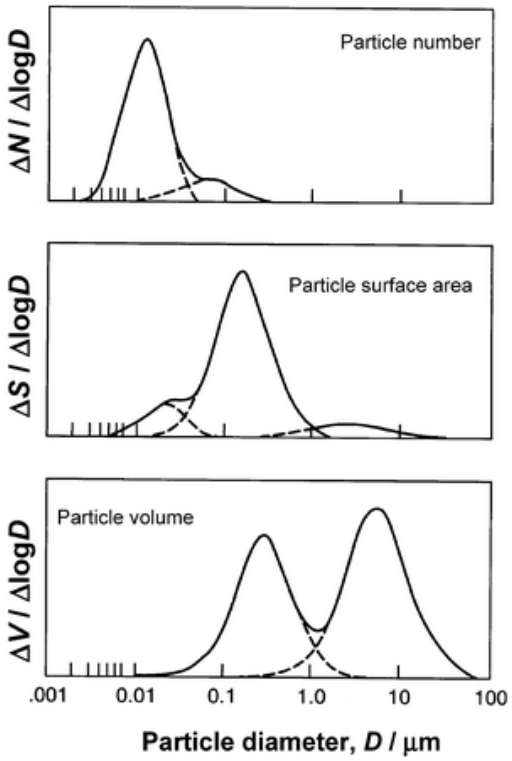

Figure 1.1: Ambient particle distribution as a function of particle diameter (D) based on particle number (N), surface area (S), and volume (V). The latter is equivalent to a mass distribution when variation in particle density is small.[7] Reprinted with permission from reference 7 with permission of The Royal Society of Chemistry.

Particles larger than 0.1 μm are also classified into fine and coarse size groups. Fine particles have a diameter less than 2.5 μm ($PM_{2.5}$) and coarse particles refer to particles with diameter between 2.5 μm to 10 μm ($PM_{2.5\text{-}10}$). Fine particles are formed by several pathways including chemical reactions, nucleation, condensation, coagulation, and cloud and fog processing.[5] Fine particles are released from combustion (coal, oil, gasoline, diesel, and wood), gas-to-particle conversion of NO_x, SO_2, and volatile organic compounds (VOCs), smelters, and mills.[5] In the case of coarse particles, they are generated by mechanical break-up of even larger solid particles and resuspension of dusts.[8] Coarse particles come from resuspension of soil from farming, mining, and unpaved roads, biological sources, construction and demolition, and ocean spray.[1] Although the lifetime of PM_{fine} in the atmosphere (days to week) is longer than that of

PM_{coarse} (minutes to days), toxicity of $PM_{2.5}$ and PM_{10} is hard to differentiate in epidemiological studies.[7] However, C.A. Pope *et al.* indicated that PM_{10} and PM_{15} associated with less mortality than that from $PM_{2.5}$ for long-term exposure.[9] In the case of short-term exposure, Brunekreef and Forsbergre suggested that $PM_{2.5-10}$ exhibited stronger short-term effect to the cardiovascular system than that from $PM_{2.5}$. The World health organization (WHO) has proposed air quality guidelines for $PM_{2.5}$ and PM_{10} for short-term (24-hours mean) and long-term (annual mean) exposure as shown in Table 1.1.[10]

Table 1.1: Current World Health Organization advisory air quality guidelines for $PM_{2.5}$ and PM_{10}.[10]

PM	**24-hour mean[a] (μg m^{-3})**	**Annual mean (μg m^{-3})**
$PM_{2.5}$	25	10
PM_{10}	50	20

[a] as 99th percentile (no more than 3 days exceedance/year)

Ultrafine particles (UFPs) are generated through the nucleation mode. Natural primary sources of UFPs include marine aerosols, emissions from volcanic eruptions, and forest fires,[7] while the anthropogenic sources of UFPs include off-road engines, gasoline automobiles, industrial emissions,[11,12] power plants,[13] ship exhaust,[14] construction,[11] cooking,[15] and biomass-burning. UFPs cause cardiovascular and respiratory diseases. They penetrate the lung wall to the pulmonary interstitium leading to cardiac symptom.[16] UFPs can enter to bloodstream affecting destabilization of atheromous plaques, which can increase the likelihood of an adverse cardiac event.[17] Large surface area of UFP can induce cellular DNA damage and oxidative stress.[18,19]

Previous reports indicated that smaller PM is closely associated with adverse health problems more than larger one.[20] Long-term exposure of ultrafine PM and fine PM relates to chronic disease in the cardiovascular and respiratory systems and increase of premature death.[20-

[23] Furthermore, fine PM also impacts visibility, the ecosystem, and the climate.[24] PM toxicity depends not only on physical characteristics of the particles (number, size, and mass), but also on chemical composition of PM. Thus, chemical composition of fine PM ($PM_{2.5}$) is discussed in the following section.

- **PM Composition**

Major components of PM include sulfate, nitrate, ammonium, sodium ions, chloride ions, elemental carbon, organic carbon, mineral material, and water.[7] The generation and main sources of each component are summarized in Table 1.2.[7] Phosphate and metals appear as minor components.[25] The exact composition of PM depends on particle size range, source and processing, and prevailing meteorology. An example of the fraction of each PM composition is shown in Figure 1.2.[26] Organic carbon is the dominant constituent as shown in Figure 1.2. As $PM_{2.5}$ brings serious problems to human and environment, this dissertation focuses on the compositions of $PM_{2.5}$.[24]

SO_x, NO_x, NH_3, and VOCs are the gaseous precursors of sulfate, nitrate, ammonium, and organic matter, respectively.[27] SO_x is emitted from anthropogenic sources, such as fuel combustion, industries, aircraft and highway vehicles and ships, and natural sources such as volcanic eruptions based on National Emissions Inventory (NEI) Data (2011). SO_x contributes to sulfate formation as shown in the following chemical reactions;

$$SO_2 + OH\bullet + M \rightarrow HOSO_2 + M$$

$$HOSO_2 + O_2 \rightarrow HO_2 + SO_3$$

$$SO_3 + H_2O + M \rightarrow H_2SO_4 + M$$

Where M is the third body such as N_2.[28] SO_2 is reacted with hydroxy radicals to produce sulfate.

Table 1.2: Main components of airborne PM and their major sources.[7]

Component	Sources	Notes
Sulfate	Present mainly as a secondary ammonium sulfate component ($(NH_4)_2SO_4$) from atmospheric oxidation of SO_2 followed by reaction with NH_3 gas derived mainly from agricultural sources, although there may be a small primary component derived from emissions of sea-salt particles or mineral matter such as gypsum.	-
Nitrate	A secondary component normally present as ammonium nitrate (NH_4NO_3), which results from the neutralization by NH_3 of HNO_3 vapor derived from oxidation of NO_x emissions, or as sodium nitrate ($NaNO_3$) due to displacement of hydrogen chloride from NaCl by HNO_3 vapor.	-
Ammonium	Generally present in the form of $(NH_4)_2SO_4$ or NH_4NO_3 from NH_3 emissions	-
Sodium ions and chloride ions	From primary emissions of sea-salt particles	-
Elemental carbon	It is formed during the high-temperature combustion of fossil and contemporary biomass fuels.	Including black and graphite carbon
Organic carbon	Primary organic carbon is from automotive or industrial sources and secondary organic carbon is from the oxidation of VOCs.	Including carbon in the form of organic compounds
Mineral material	They are present in primary coarse dusts that arise from, for example, wind-driven entrainment of soil and mineral material, quarrying, construction and demolition.	Including Al, Si, Fe, and Ca
Water	From the atmosphere	Water-soluble components, especially $(NH_4)_2SO_4$, NH_4NO_3 and NaCl, take up water at high relative humidity, turning from crystalline solids into liquid droplets.

In the case of nitrate, NO_x, is reacted with hydroxy radicals to produce nitric acid as the following chemical reaction;[29]

$$NO_2 + OH\bullet + M \rightarrow HNO_3 + M$$

Where M is the third body such as N_2.[30] Nitric acid can produce nitrate salt via the chemical reactions with ammonia, amine, dust, and sea salts in the aerosol phase. The chemical reaction between nitric acid and ammonia is shown in the following reaction;[5]

$$HNO_3(g) + NH_3(g) \leftrightarrow NH_4NO_3\ (s)$$

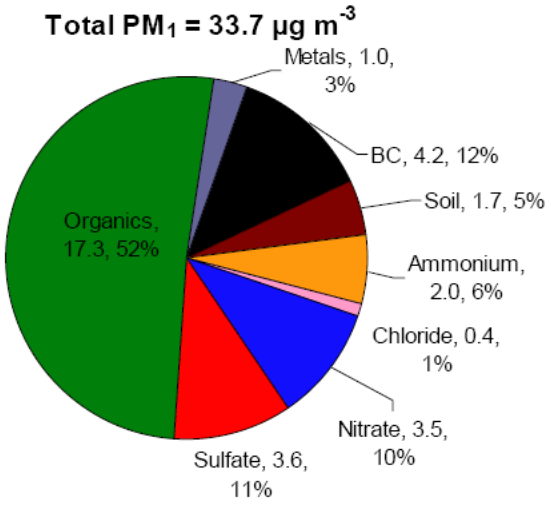

Figure 1.2: Average mass concentration of each PM component in Mexico City.[26] Reprinted with permission from reference 26 with permission of American Chemical Society.

NH_4NO_3 is the major chemical form of nitrate in urban fine PM.[5] Moreover, secondary source of ammonium is also attributional to ammonium sulfate salts. Previous reports showed that the common inorganic components including sulfate, nitrate, and acidity in the normal level of $PM_{2.5}$ exposure were not associated with the epidemiology and toxicology studies.[31] Sulfate at high levels of PM exposure can affect biological responses. In addition, sulfate levels may be used as the representative of secondary organic aerosols from the SO_2 oxidation products.[32]

As a result of lower impact to human health of the inorganic $PM_{2.5}$ components, the details of other toxic $PM_{2.5}$ components including elemental and organic carbon, toxic metals, and reactive oxygen species (ROS) are described as follow. Previous work indicated that elemental and organic carbons linked to cardiovascular mortality in California for long-term exposure.[33] Elemental carbon exposure is associated with an increase in the rate of asthma and lung diseases.[34] VOCs are

the gaseous precursors of organic carbon in PM. Vegetation is the dominant source of hydrocarbon emission.[35] VOCs are also produced from anthropogenic activities including vehicular emissions, petroleum products, petroleum combustion, coal and biomass burning.[36] Isoprene and terpene are the major species of VOCs emitted from plants.[35] Oxidation of isoprene produces CO, which represents about 16% of the global CO production.[37] Moreover, isoprene is reacted with other species including NO_x, peroxy radicals, and hydroperoxyl to produce methacrolein, methyl vinyl ketone, and 3-ethyfuran which are toxic when inhaled.[35] Oxidation of alkanes and aromatics with OH· generate a number of oxygenated organic compounds including aldehyde, ketone, alcohol, carboxylic acid, phenols, hydroperoxide, percarboxylic acid, and peroxyacyl.[38,39] Moreover, organic carbon is also directly emitted from vehicle emission and industrial sites. Polycyclic aromatic hydrocarbons (PAHs) and nitro-PAHs cause mutagenicity and carcinogenicity leading to many health concerns.[40] PAH-based quinone derivatives can contribute to oxidative stress and be more toxic than their parent PAH.[41] The photochemical reactions of organic carbons, such as quinones and aromatic carbonyls generate ROS, which contributes to health problems.

Aside from major PM components as mentioned above, there are common transition metals found in PM include Co, Cu, Fe, Mn, Ni, V, and Ti, while trace amounts of Pb, Cd, and Zn have been found.[4] Metals in PM such as Ni and V increase risks of acute cardiac function changes and short-term mortality.[42] Pb and Zn in PM are indicated to affect human health.[42] Previous work showed high concentrations of Pb, Br, Sb, and Cu were detected in urban areas while high concentrations of As and Cd were observed in industrial areas.[43] Bioavailability of trace metals in PM has been shown to cause cardiopulmonary injury.[44] Pt compounds in PM were found to be mutagenic in bacterial systems.[45] Fe found in PM increased production of ROS in vivo.[46] Moreover, some metals such as Fe and Cu are capable of producing ROS as described below.

Radical-generating capacity of PM produces ROS via photochemical reactions of organic chemical compounds (e.g., PAHs and quinones) and the Fenton reaction of transition metals (e.g., Fe and Cu).[47-49] ROS cause oxidative stress, which is defined as a serious imbalance between ROS and antioxidant defense in the body.[50] Oxidative stress from ROS in PM most widely proposed and promising hypothesis for adverse health effects in humans such as DNA mutation, DNA-adduct formation, induced oxidative protein damage.[4,17,19,51]

Current methods for monitoring toxic composition of PM

- **Elemental and organic carbons**

Elemental carbon is commonly determined using an optical reflectometer. Besides the quantitative analysis of elemental carbon used for monitoring air quality, elemental carbon measurement can be used for source apportionment of PM.[52,53] In the case of organic carbon, gas chromatography mass spectrometry (GC-MS) and liquid chromatography mass spectrometry (LC-MS) are traditionally used to analyze these compounds due to their capabilities for identification and sensitive detection.[36,54] Moreover, the developed method such as HPLC with fluorescence detection was also proposed to detect a signature group of 16 PAHs.[55] Additionally, the sensitivity for quinone detection in PM was improved by Cho *et al.*[56] Quinones were converted to their diacetyl derivatives before detecting those derivatives using gas chromatography electron impact mass spectrometry (GC-EIMS).[56]

- **Reactive Oxygen Species (ROS)**

Monitoring ROS in PM is conventionally carried out using mass spectrometry, chromatography, electron spin resonance spectroscopy, and electrophoresis.[57] Moreover, chemical assays to evaluate ROS generation in PM, including a dithiothreitol (DTT) assay,[58-62] thiobarbituric acid (TBA) assay,[63] and fluorescence assays,[64,65] have been proposed. For the

colorimetric DTT assay, ROS is indirectly measured by determining the decrease of DTT as a result from the reaction of ROS and DTT, as shown in Figure 1.3. In the case of the TBA assay, the oxidized deoxyribose, which is the product from the reaction of ROS and deoxyribose, is reacted with TBA to produce the colored product of TBA. The amount of ROS is proportional to the color intensity of the TBA's product.[63] For the fluorescence assay, 2′,7′-Dichlorodihydrofluorescein (DCHF), a fluorescent dye, is reacted with ROS to then produce 2′,7′-dichlorofluorescein, DCF, which can be measured via fluorescent spectroscopy.[64,65]

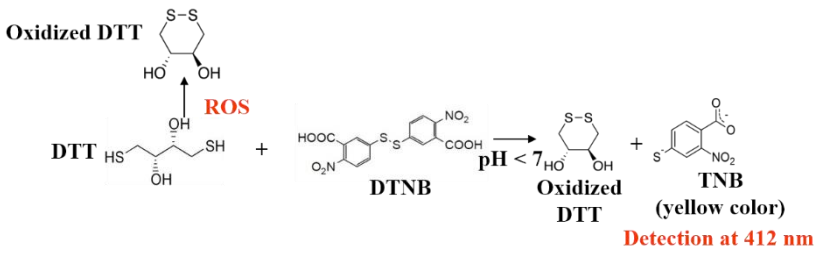

Figure 1.3: DTT assay (DTNB: 5,5'-dithiobis-(2-nitrobenzoic acid) and TNB: 2-nitro-5-thiobenzoate).

- **Trace metals**

Existing methods for measuring metal-containing PM include atomic absorption spectroscopy (AAS), inductively coupled plasma mass spectrometry (ICP-MS), electron microscopy coupled with energy-dispersive X-ray spectroscopy, or fluorescent probes, neutron activation analysis, fluorescence spectrometry, glow discharge atomic emission spectrometry, microwave plasma atomic emission spectrometry, and laser-induced breakdown spectroscopy.[43,66-69] In the urban area of Thessaloniki, Greece in 2002, As, Br, Co, Cr, Fe, K, La, Na, Sb, Sc, and Zn in PM_{10} were investigated using neutron activation analysis and using flame AAS and electrothermal AAS for Cd, Cu, Mn, Ni, Pb, and V analyses.[43] Scanning electron microscopy (SEM) and transmission electron microscopy (TEM) with energy dispersive X-ray spectrometry

(EDX or EDS) were also utilized to reveal single particle morphology and identify the elemental composition of PM.[67] This study classified the particles into ten elemental-rich groups and investigated the morphology of each group. For example, the Fe-rich group consisted of large (~10μm) and homogeneous particles that also contained Cl, Cu, Sn, and Mn. In 2013, ICP-MS was used for Ni and Cr determination for welders because these elements can accumulate in the lungs. The levels of Ni and Cr in welders were determined taking into consideration factors, such as smoking, use of respiratory protection, and/or types of welding process, by measuring elemental levels in welding fumes, urine, and erythrocytes. Limits of quantification (LOQs) for Ni and Cr in urine using ICP-MS were 1.5 μg L^{-1} and 1.0 μg L^{-1}, respectively.[68] Moreover, ICP-MS measurements were conducted to determine Pb, Cr, Zn, Cu, Ni, Fe, Mn, V, and K in airborne PM and to study the sources associated with these elements.[70] In 2014, K. H. Kim *et al.* used AAS to monitor the Cu levels in PM in Korea from 1991 to 2012. The trend showed Cu levels decreased with time. An LOD of Cu in airborne PM using this technique was 0.1 ng m^{-3}.[71] Besides development of analytical methods for trace metals detections in PM focusing on improving LOD, less expensive methods with simple operation such as electrochemistry and flow injection analysis were also investigated.[72,73] Square-wave stripping voltammetry offering direct measurements of heavy metals in indoor-airborne PM was suggested by O. A. Farghaly *et al.*.[72] They reported that the proposed electrochemical method could analyze eight metals including Cd(II), Pb(II), Cu(II), Zn(II), Co(II), Ni(II), Cr(VI), and Mo(VI) with low standard deviation (about 2%). LODs were 0.03, 0.4, 0.04, 0.1, 0.15, 0.05, 0.2, and 3.2 μg/kg for Cd(II), Pb(II), Cu(II), Zn(II), Co(II), Ni(II), Cr(VI), and Mo(VI), respectively. In the case of flow injection analysis, H. Mukai *et al.* suggested a cation-exchange resin column on-line in the flow injection system to determine Pt in PM.[73] The

proposed method could eliminate major matrix elements and hafnium, which suppressed signal intensity of Pt and a spectral interference by hafnium oxide.

These complicated and high-cost techniques for PM composition analysis cannot meet the demands of people living in developing countries and remote areas due to requirements of large sample volume, which results in long sample collection periods, long analysis times, and high cost for implementation. Low-cost, portable, simple microfluidic paper-based analytical devices (mPADs) for analyzing PM components were proposed.[74-78]

This dissertation focuses on trace metal detection in PM using low-cost analytical devices. mPADs using colorimetric and distance-based detection motifs were developed to make metal analysis in PM easier to perform in the field.[74-76] Despite these advancements, further work is needed to improve performance of metal measurements in PM. Thus, this dissertation, and specifically chapters 2 and 3, introduces low-cost, portable, disposable electrochemical analytical platforms for sensitive detection of trace metals in PM.[79,80] Aside from proposing the analytical devices for trace metals analysis, this work (chapter 4) also developed an electrophoretic mPAD that could ultimately be used for separation and analysis of complicated composition in PM. Details and previous mPADs, electrochemical microfluidic paper-based analytical devices (ePADs), and electrophoretic mPADs are provided as follows.

Microfluidic paper-based analytical devices (mPADs)

mPADs have been developed to provide fast, inexpensive point-of-need analyses.[81-85] mPADs are made of patterned paper acting as a microfluidic platform. The channel barrier of mPADs is created using hydrophobic materials such as photoresist, wax, and/or organic solvents, as shown in Figure 1.4.[82,83] Moreover, incorporating functionality to mPADs for timing and multistep processing using magnetic valves,[86] origami folding platforms,[87] and multiple paper

layers[88-90] have been demonstrated. For colorimetric detection, a variety of methods have been used, including mobile cameras, desktop scanners, and hand-held readers. Inexpensive materials, simple fabrication methods, and simple detection equipment make mPADs low-cost, portable, disposable, and easy to use. mPADs allow people in developing countries and remote area access primary analytical testing.[82,83,91]

The use of mPADs has been demonstrated in wide-ranging applications from clinical diagnosis to environmental testing.[81,82,84,85,91] For compositional analysis of PM, the portability and rapid detection of mPADs are applicable to trace metal measurements because some trace metals change over time via chemical processes.[92] Previous work introduced mPADs to analyze trace metals in PM.[75,93] mPADs were developed to measure Fe, Cu, Ni, and Cr in aerosol samples using colorimetric detection (Figure 1.5a)[93] and distance-based detection (Figure 1.5b).[75] However, the colorimetric and distance-based analyses are not sensitive enough to detect trace metals (in μg m^{-3} (i.e., ppb) level) in PM. Consequently, electrochemistry was integrated into mPADs to improve detection sensitivity.

Electrochemical paper-based analytical devices (ePADs)

ePADs were firstly introduced by W. Dungchai *et al.*.[94] ePADs consist of the electrodes fabricated on a paper substrate using various techniques such as inkjet printing, pencil drawing, and screen printing.[85] ePADs have become increasing utilized for detecting trace metals such as Au,[95] Cd, and Pb.[77,96-100] This dissertation focuses on the development of ePADs for Zn, Cd, Pb, Co, and Ni measurements in PM. ePADs for Cd and Pb detections in PM were proposed by P. Rattanarat *et al.* using square-wave anodic stripping voltammetry (ASV).[77] ASV is one interesting technique for trace elemental analysis capable of measuring very low concentrations. The preconcentration step in this technique provides LODs down to 10^{-10} M. Square-wave voltammetry

is commonly used as the measurement step in this technique because it can reduce background current. According to previous works using ePADs,[77,99,100] LODs for Zn, Cd, Pb, Co, and Ni needed to be improved to be low enough for measuring trace metal concentrations (in sub-ppb level) in PM. Thus, electrode modification methods to lower LODs were explored.

Previous work using ASV to determine Zn, Cd, and Pb in tap water and human hair used bismuth-film modified electrodes to enhance the signal and provided LODs of 0.2 µg L^{-1} for Cd

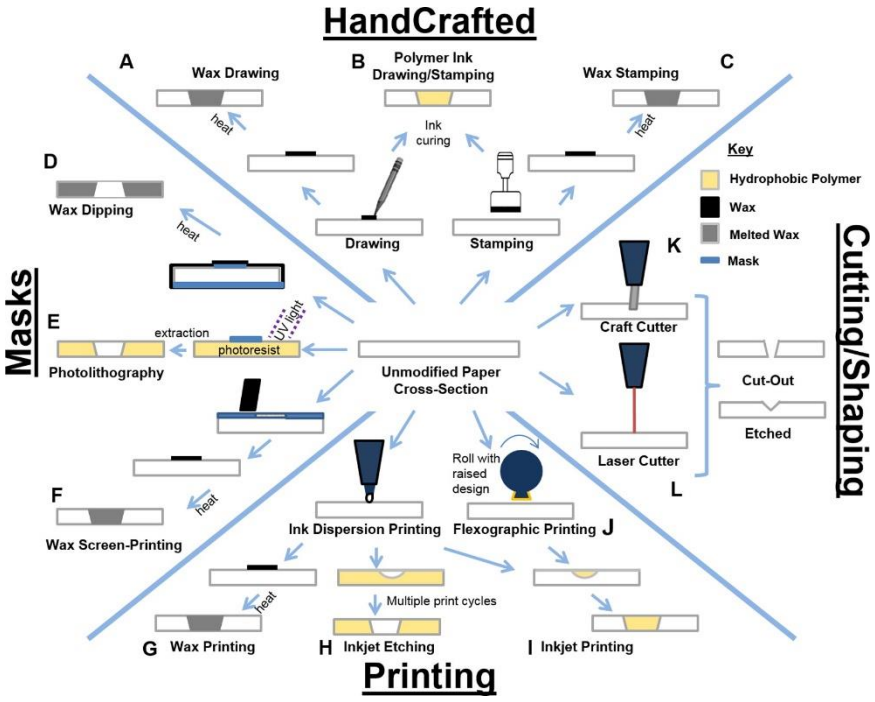

Figure 1.4: Fabrication methods for creating µPADs.[82] Reprinted with permission from reference 82. Copyright (2018) American Chemical Society.

and Pb, and 0.7 µg L^{-1} for Zn.[101] In another study, Zn, Cd, Pb, Cu, Mo, Cr, Ni, and Co in soil and indoor-airborne PM were measured used square-wave stripping voltammetry.[72] ASV was applied resulting in LODs of 0.03, 0.4, 0.04, and 0.1 µg kg^{-1} for Cd(II), Pb(II), Cu(II), and Zn(II), respectively. Using adsorptive cathodic stripping voltammetry with dimethylglyoxime as a complexing agent provided LODs of 0.15, 0.05, 0.2, and 3.2 µg kg^{-1} for Co(II), Ni(II), Cr(VI), and Mo(VI), respectively.[72] Cathodic stripping voltammetry was also applied for the determination of

metals such as Cu, Pb, Cd, Ni, Co and Zn in seawater. This method measured signal resulting from complex formation between these metals and ligands such as dimethylglyoxime, oxine, salicylaldoxime, and cyclohexane-1,2-dionedioxime. LODs of these metals were 0.3 nM Cu, 0.2 nM Pb, 0.1 nM Cd, 0.4 nM Ni, 0.6 nM Zn, and 0.02 nM Co.[102]

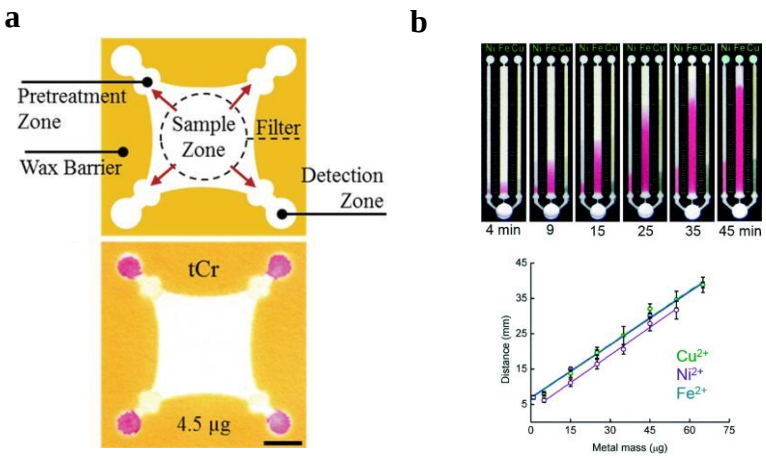

Figure 1.5: (a) Cr measurement using mPADs based on colorimetric detection.[93] Reprinted with permission from reference 93 with permission of Elsevier. (b) Cu^{2+}, Ni^{2+} and Fe^{2+} measurements using mPADs based on distance-based detection.[75] Reprinted with permission from reference 75 with permission of Royal Society of Chemistry.

The sensitivity of electrochemical detection can be improved by enhancing the surface area and increasing conductivity of the electrode. Metal-based nanoparticles such as silver nanoparticles (AgNPs) have small size, high conductivity, and high positive standard reduction potential that meet the criteria for increasing sensitivity.[103,104] Therefore, AgNPs were used for electrode surface modification via electrospray to lower LODs of Zn, Cd, and Pb as described in Chapter 2.[79] Additionally, low-cost electrochemical analytical devices to detect Co and Ni in PM using adsorptive cathodic stripping voltammetry are proposed in Chapter 3.[80]

Electrophoresis on Laminated parafilm paper devices

mPADs were applicable to detect PM components,[74-76,78,93] however, sample digestion and/or preparation to extract each component is still required. Sample digestion and preparation were performed using corrosive chemical reagents such as concentrated acids, organic solvents,

and instruments that are expensive, large, and complicated. Addition of a separation function into mPADs is an interesting concept to allow the sample extraction to be operated on low-cost mPADs. In lateral flow assays on paper, however, the fluid flow rate decreases with distance, leading to progressively slower migration of mobile phase, resulting in poor separation efficiency.[105] Electrophoresis, which is a well-known technique for analyzing complicated samples, is able to improve separation efficiency due to the presence of constant flow rate contributed from the electrokinetic forces.[106-112] Enhanced separation efficiency in electrophoresis is also resulted from lack of band broadening, which is described by the Van Deemter equation.[113] The multiple-path (Eddy diffusion) term and the mass-transfer term in the Van Deemter equation are eliminated because the electrophoretic separation is carried out in a single phase of uniformly flowing carrier liquid.[113] Paper electrophoresis has been used since 1961, but it has been replaced by more efficient separation methods such as capillary electrophoresis (CE) and high-performance liquid chromatography (HPLC).[114] To date, electrophoresis has been integrated into mPADs based on the hypothesis that a small mPAD channel could improve separation efficiency of paper electrophoresis, due to minimized heat dissipation and thermal gradients relative to a larger channel.[115] Electrophoretic mPADs could offer low-cost and simple methods for complicated sample analysis. Previous electrophoretic mPADs still obtained poor separation efficiency as shown in Figure 1.6.[105,116] Most electrophoretic mPADs were fabricated using wax-printing.[105,116-119] In these studies, the wax barrier was suggested as the part contributing to peak broadening due to low zeta potential.[120]

In this dissertation (Chapter 4), electrophoretic laminated Parafilm paper (l-paper) device is proposed to achieve a free-standing channel assisting to reduce peak broadening. The essential electrophoretic parameters such as Joule heating, electroosmotic flow, and electrophoretic

mobility were studied. The viability of l-paper devices was demonstrated by applied for colorimetric and fluorescent applications. In the future, the electrophoretic l-paper will be developed for separation and analysis of PM composition.

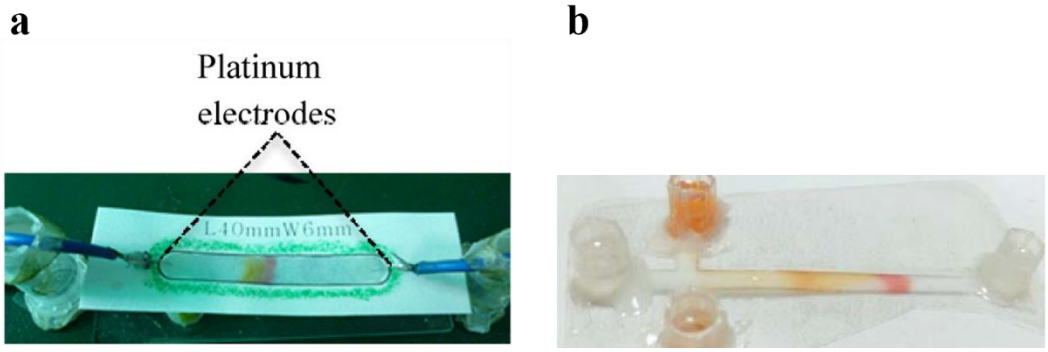

Figure 1.6: (a) carmine and sunset yellow FCF dyes separation using a electrophoretic wax-printed mPAD.[105] Reprinted with permission from reference 105. Copyright (2018) American Chemical Society. (b) An electrophoretic mPAD for carmine and sunset yellow FCF separation on a cut-paper channel using.[116] Reprinted with permission from reference 116 with permission of John Wiley and Sons.

In summary, this dissertation presents low-cost, portable, simple electrochemical analytical devices for trace metals analyses in PM and the electrophoretic l-paper towards the separation and analysis of other PM components, such as volatile organic compounds and pathogenic bacteria. These works would be a significant step forward in monitoring PM components and understanding chemical reactions in PM.

REFERENCES

1. J. H. Seinfeld and S. N. Pandis, *Atmospheric chemistry and physics: from air pollution to climate change*, John Wiley & Sons, 2016.
2. K.-H. Kim, E. Kabir and S. Kabir, *Environment international*, 2015, **74**, 136-143.
3. A. Valavanidis, K. Fiotakis and T. Vlachogianni, *J Environ Sci Health C Environ Carcinog Ecotoxicol Rev*, 2008, **26**, 339-362.
4. T. M. de Kok, J. G. Hogervorst, J. J. Briede, M. H. van Herwijnen, L. M. Maas, E. J. Moonen, H. A. Driece and J. C. Kleinjans, *Environ Mol Mutagen*, 2005, **46**, 71-80.
5. R. Zhang, G. Wang, S. Guo, M. L. Zamora, Q. Ying, Y. Lin, W. Wang, M. Hu and Y. Wang, *Chemical Reviews*, 2015, **115**, 3803-3855.
6. H. R. Anderson, *Atmospheric Environment*, 2009, **43**, 142-152.
7. M. R. Heal, P. Kumar and R. M. Harrison, *Chemical Society Reviews*, 2012, **41**, 6606-6630.
8. W. E. Wilson and H. H. Suh, *Journal of the Air & Waste Management Association*, 1997, **47**, 1238-1249.
9. C. A. Pope III, R. T. Burnett, M. J. Thun, E. E. Calle, D. Krewski, K. Ito and G. D. Thurston, *Jama*, 2002, **287**, 1132-1141.
10. WHO., *Air Quality Guidelines: Global Update 2005. Particulate Matter, Ozone, Nitrogen Dioxide and Sulfur Dioxide*, World Health Organization, 2006.
11. P. Kumar, M. Mulheron and C. Som, *Journal of Nanoparticle Research*, 2012, **14**, 771.
12. L. N. Posner and S. N. Pandis, *Atmospheric Environment*, 2015, **111**, 103-112.

13. Y. Li, A. Suriyawong, M. Daukoru, Y. Zhuang and P. Biswas, *Journal of the Air & Waste Management Association*, 2009, **59**, 553.

14. H. Saxe and T. Larsen, *Atmospheric environment*, 2004, **38**, 4057-4067.

15. G. Buonanno, L. Morawska, L. Stabile and A. Viola, *Atmospheric Environment*, 2010, **44**, 3963-3969.

16. A. Seaton, D. Godden, W. MacNee and K. Donaldson, *The lancet*, 1995, **345**, 176-178.

17. J. A. Araujo and A. E. Nel, *Part Fibre Toxicol*, 2009, **6**, 24.

18. W. G. Kreyling, M. Semmler and W. Möller, *Journal of Aerosol Medicine*, 2004, **17**, 140-152.

19. J. A. Araujo, B. Barajas, M. Kleinman, X. Wang, B. J. Bennett, K. W. Gong, M. Navab, J. Harkema, C. Sioutas and A. J. Lusis, *Circulation research*, 2008, **102**, 589-596.

20. R. Schlesinger, N. Kunzli, G. Hidy, T. Gotschi and M. Jerrett, *Inhalation toxicology*, 2006, **18**, 95-125.

21. G. Oberdörster, Z. Sharp, V. Atudorei, A. Elder, R. Gelein, W. Kreyling and C. Cox, *Inhalation toxicology*, 2004, **16**, 437-445.

22. A. W. Correia, C. A. Pope III, D. W. Dockery, Y. Wang, M. Ezzati and F. Dominici, *Epidemiology (Cambridge, Mass.)*, 2013, **24**, 23.

23. W. J. Gauderman, E. Avol, F. Gilliland, H. Vora, D. Thomas, K. Berhane, R. McConnell, N. Kuenzli, F. Lurmann and E. Rappaport, *New England Journal of Medicine*, 2004, **351**, 1057-1067.

24. IPCC, *Climate Change 2013: The Physical Science Basis. Contribution of Working Group I to the Fifth Assessment Report of the Intergovernmental Panel on Climate Change*,

Cambridge University Press, Cambridge, United Kingdom and New York, NY, USA, 2013.

25. J. M. Pacyna and E. G. Pacyna, *Environmental Reviews*, 2001, **9**, 269-298.

26. A. Aiken, D. Salcedo, M. J. Cubison, J. Huffman, P. DeCarlo, I. M. Ulbrich, K. S. Docherty, D. Sueper, J. Kimmel and D. R. Worsnop, *Atmospheric Chemistry and Physics*, 2009, **9**, 6633-6653.

27. S. Guo, M. Hu, M. L. Zamora, J. Peng, D. Shang, J. Zheng, Z. Du, Z. Wu, M. Shao and L. Zeng, *Proceedings of the National Academy of Sciences*, 2014, **111**, 17373-17378.

28. B. Long, J. L. Bao and D. G. Truhlar, *Physical Chemistry Chemical Physics*, 2017, **19**, 8091-8100.

29. H. Rodhe, P. Crutzen and A. Vanderpol, *Tellus*, 1981, **33**, 132-141.

30. D. M. Golden and G. P. Smith, *The Journal of Physical Chemistry A*, 2000, **104**, 3991-3997.

31. R. B. Schlesinger, *Inhalation Toxicology*, 2007, **19**, 811-832.

32. T. J. Grahame and R. B. Schlesinger, *Inhalation toxicology*, 2005, **17**, 15-27.

33. B. Ostro, W.-Y. Feng, R. Broadwin, B. Malig, R. Green and M. Lipsett, *Occupational and environmental medicine*, 2008, **65**, 750-756.

34. K. L. Jansen, T. V. Larson, J. Q. Koenig, T. F. Mar, C. Fields, J. Stewart and M. Lippmann, *Environmental Health Perspectives*, 2005, **113**, 1741-1746.

35. A. Kansal, *Journal of Hazardous Materials*, 2009, **166**, 17-26.

36. M. S. Alam, J. M. Delgado-Saborit, C. Stark and R. M. Harrison, *Atmospheric Environment*, 2013, **77**, 24-35.

37. P. J. Crutzen, *Faraday Discussions*, 1995, **100**, 1-21.

38. W. S. McGivern, I. Suh, A. D. Clinkenbeard, R. Zhang and S. W. North, *The Journal of Physical Chemistry A*, 2000, **104**, 6609-6616.

39. J. Fan and R. Zhang, *Environmental Chemistry*, 2004, **1**, 140-149.

40. J. F. Collins, J. P. Brown, G. V. Alexeeff and A. G. Salmon, *Regulatory Toxicology and Pharmacology*, 1998, **28**, 45-54.

41. S. Sidhu, B. Gullett, R. Striebich, J. Klosterman, J. Contreras and M. DeVito, *Atmospheric Environment*, 2005, **39**, 801-811.

42. L. C. Chen and M. Lippmann, *Inhalation toxicology*, 2009, **21**, 1-31.

43. D. Voutsa, C. Samara, T. Kouimtzis and K. Ochsenkühn, *Atmospheric Environment*, 2002, **36**, 4453-4462.

44. D. L. Costa and K. L. Dreher, *Environmental health perspectives*, 1997, **105**, 1053.

45. C. L. S. Wiseman and F. Zereini, *Science of The Total Environment*, 2009, **407**, 2493-2500.

46. M. B. Kadiiska, R. P. Mason, K. L. Dreher, D. L. Costa and A. J. Ghio, *Chemical Research in Toxicology*, 1997, **10**, 1104-1108.

47. P. Bautista, A. Mohedano, J. Casas, J. Zazo and J. Rodriguez, *Journal of Chemical Technology and Biotechnology*, 2008, **83**, 1323-1338.

48. M. Saran and W. Bors, *Klinische Wochenschrift*, 1991, **69**, 957-964.

49. J. Prousek, *Pure and applied chemistry*, 2007, **79**, 2325-2338.

50. T. Finkel and N. J. Holbrook, *Nature*, 2000, **408**, 239.

51. H. Bömmel, M. Haake, P. Luft, J. Horejs-Hoeck, H. Hein, J. Bartels, C. Schauer, U. Pöschl, M. Kracht and A. Duschl, *International immunopharmacology*, 2003, **3**, 1371-1379.

52. J. Sandradewi, A. S. Prévôt, S. Szidat, N. Perron, M. R. Alfarra, V. A. Lanz, E. Weingartner and U. Baltensperger, *Environmental science & technology*, 2008, **42**, 3316-3323.

53. B. Yan, D. Kennedy, R. L. Miller, J. P. Cowin, K.-h. Jung, M. Perzanowski, M. Balletta, F. P. Perera, P. L. Kinney and S. N. Chillrud, *Atmospheric environment*, 2011, **45**, 7478-7486.

54. T. Xia, P. Korge, J. N. Weiss, N. Li, M. I. Venkatesen, C. Sioutas and A. Nel, *Environmental health perspectives*, 2004, **112**, 1347.

55. C. F. Bassøe, N. Li, K. Ragheb, G. Lawler, J. Sturgis and J. P. Robinson, *Cytometry Part B: Clinical Cytometry*, 2003, **51**, 21-29.

56. A. K. Cho, E. Di Stefano, Y. You, C. E. Rodriguez, D. A. Schmitz, Y. Kumagai, A. H. Miguel, A. Eiguren-Fernandez, T. Kobayashi and E. Avol, *Aerosol Science and Technology*, 2004, **38**, 68-81.

57. U. Pöschl, *Angewandte Chemie International Edition*, 2005, **44**, 7520-7540.

58. Y. Wang, C. Arellanes, D. B. Curtis and S. E. Paulson, *Environmental science & technology*, 2010, **44**, 4070-4075.

59. V. Mugica, E. Ortiz, L. Molina, A. De Vizcaya-Ruiz, A. Nebot, R. Quintana, J. Aguilar and E. Alcántara, *Atmospheric Environment*, 2009, **43**, 5068-5074.

60. R. D. McWhinney, S. S. Gao, S. Zhou and J. P. Abbatt, *Environmental science & technology*, 2011, **45**, 2131-2136.

61. M. Y. Chung, R. A. Lazaro, D. Lim, J. Jackson, J. Lyon, D. Rendulic and A. S. Hasson, *Environmental science & technology*, 2006, **40**, 4880-4886.

62. S. Hu, A. Polidori, M. Arhami, M. Shafer, J. Schauer, A. Cho and C. Sioutas, *Atmospheric Chemistry and Physics*, 2008, **8**, 6439-6451.

63. M. W. Frampton, A. J. Ghio, J. M. Samet, J. L. Carson, J. D. Carter and R. B. Devlin, *American Journal of Physiology-Lung Cellular and Molecular Physiology*, 1999, **277**,

L960-L967.

64. F. Tietze, *Analytical biochemistry*, 1969, **27**, 502-522.

65. B. Halliwell and M. Whiteman, *British journal of pharmacology*, 2004, **142**, 231-255.

66. K. Naito, T. Tachikawa, M. Fujitsuka and T. Majima, *The Journal of Physical Chemistry C*, 2008, **112**, 1048-1059.

67. P. Sielicki, H. Janik, A. Guzman, A. Reynolds and J. Namieśnik, *Central European Journal of Chemistry*, 2010, **9**, 308-313.

68. T. Weiss, B. Pesch, A. Lotz, E. Gutwinski, R. Van Gelder, E. Punkenburg, B. Kendzia, K. Gawrych, M. Lehnert, E. Heinze, A. Hartwig, H. U. Kafferlein, J. U. Hahn, T. Bruning and W. Group, *Int J Hyg Environ Health*, 2013, **216**, 175-183.

69. Y.-J. Wang, Z.-Q. Tu, L. Zhou, Y.-J. Chi and Q. Luo, *Guang pu xue yu guang pu fen xi= Guang pu*, 2015, **35**, 1030-1032.

70. L. Niu, H. Ye, C. Xu, Y. Yao and W. Liu, *Chemosphere*, 2015, **119**, 112-121.

71. K.-H. Kim, *Atmospheric environment*, 2014, **94**, 1-10.

72. O. A. Farghaly and M. A. Ghandour, *Environmental Research*, 2005, **97**, 229-235.

73. H. Mukai, Y. Ambe and M. Morita, *Journal of Analytical Atomic Spectrometry*, 1990, **5**, 75-80.

74. D. M. Cate, P. Nanthasurasak, P. Riwkulkajorn, C. L'Orange, C. S. Henry and J. Volckens, *The Annals of Occupational Hygiene*, 2014, **58**, 413-423.

75. D. M. Cate, S. D. Noblitt, J. Volckens and C. S. Henry, *Lab on a Chip*, 2015, **15**, 2808-2818.

76. M. M. Mentele, J. Cunningham, K. Koehler, J. Volckens and C. S. Henry, *Analytical chemistry*, 2012, **84**, 4474-4480.

77. P. Rattanarat, W. Dungchai, D. Cate, J. Volckens, O. Chailapakul and C. S. Henry, *Analytical chemistry*, 2014, **86**, 3555-3562.

78. Y. Sameenoi, P. Panymeesamer, N. Supalakorn, K. Koehler, O. Chailapakul, C. S. Henry and J. Volckens, *Environmental Science & Technology*, 2013, **47**, 932-940.

79. J. Mettakoonpitak, J. Mehaffy, J. Volckens and C. S. Henry, *Electroanalysis*, 2017, **29**, 880-889.

80. J. Mettakoonpitak, D. Miller-Lionberg, T. Reilly, J. Volckens and C. S. Henry, *Journal of Electroanalytical Chemistry*, 2017, **805**, 75-82.

81. J. Adkins, K. Boehle and C. Henry, *ELECTROPHORESIS*, 2015, **36**, 1811-1824.

82. D. M. Cate, J. A. Adkins, J. Mettakoonpitak and C. S. Henry, *Analytical chemistry*, 2014, **87**, 19-41.

83. A. W. Martinez, S. T. Phillips, G. M. Whitesides and E. Carrilho, *Journal*, 2009.

84. N. A. Meredith, C. Quinn, D. M. Cate, T. H. Reilly, J. Volckens and C. S. Henry, *Analyst*, 2016, **141**, 1874-1887.

85. J. Mettakoonpitak, K. Boehle, S. Nantaphol, P. Teengam, J. A. Adkins, M. Srisa-Art and C. S. Henry, *Electroanalysis*, 2016, **28**, 1420-1436.

86. X. Li, P. Zwanenburg and X. Liu, *Lab on a Chip*, 2013, **13**, 2609-2614.

87. H. Liu and R. M. Crooks, *Journal of the American Chemical Society*, 2011, **133**, 17564-17566.

88. W.-B. Young, *Colloids and Surfaces A: Physicochemical and Engineering Aspects*, 2004, **234**, 123-128.

89. H. S. Wiklund and T. Uesaka, *Physical Review E*, 2013, **87**, 023006.

90. J. Cai and B. Yu, *Transport in porous media*, 2011, **89**, 251-263.

91. Y. Yang, E. Noviana, M. P. Nguyen, B. J. Geiss, D. S. Dandy and C. S. Henry, *Analytical Chemistry*, 2017, **89**, 71-91.

92. E. Chevallier, R. D. Jolibois, N. Meunier, P. Carlier and A. Monod, *Atmospheric Environment*, 2004, **38**, 921-933.

93. P. Rattanarat, W. Dungchai, D. M. Cate, W. Siangproh, J. Volckens, O. Chailapakul and C. S. Henry, *Analytica chimica acta*, 2013, **800**, 50-55.

94. W. Dungchai, O. Chailapakul and C. S. Henry, *Analytical Chemistry*, 2009, **81**, 5821-5826.

95. A. Apilux, W. Dungchai, W. Siangproh, N. Praphairaksit, C. S. Henry and O. Chailapakul, *Analytical Chemistry*, 2010, **82**, 1727-1732.

96. S. N. Tan, L. Ge and W. Wang, *Analytical Chemistry*, 2010, **82**, 8844-8847.

97. J. Shi, F. Tang, H. Xing, H. Zheng, B. Lianhua and W. Wei, *Journal of the Brazilian Chemical Society*, 2012, **23**, 1124-1130.

98. J. Cui, G. Lisak, S. Strzalkowska and J. Bobacka, *Analyst*, 2014, **139**, 2133-2136.

99. N. Ruecha, N. Rodthongkum, D. M. Cate, J. Volckens, O. Chailapakul and C. S. Henry, *Analytica chimica acta*, 2015, **874**, 40-48.

100. S. Chaiyo, E. Mehmeti, K. Žagar, W. Siangproh, O. Chailapakul and K. Kalcher, *Analytica chimica acta*, 2016, **918**, 26-34.

101. G. Kefala, A. Economou, A. Voulgaropoulos and M. Sofoniou, *Talanta*, 2003, **61**, 603-610.

102. C. Colombo and C. M. van den Berg, *Analytica chimica acta*, 1997, **337**, 29-40.

103. J. Yang, J. Y. Lee, L. Chen and H.-P. Too, *The Journal of Physical Chemistry B*, 2005, **109**, 5468-5472.

104. Z. Peng, Z. Jiang, X. Huang and Y. Li, *RSC Advances*, 2016, **6**, 13742-13748.

105. C. Xu, W. Lin and L. Cai, *Journal of Chemical Education*, 2016, **93**, 903-905.

106. D. A. Skoog, F. J. Holler and S. R. Crouch, *Principles of Instrumental Analysis*, Thomson Brooks/Cole, 2007.

107. N. H. Martin and G. T. Franglen, *Journal of Clinical Pathology*, 1954, **7**, 87-105.

108. L. F. J. Parker, *Analyst*, 1955, **80**, 638-651.

109. G. Hanrahan, R. Montes and F. A. Gomez, *Analytical and Bioanalytical Chemistry*, 2008, **390**, 169-179.

110. A. Tiselius, *Discussions of the Faraday Society*, 1953, **13**, 29-33.

111. W. L. Dunn and R. H. Pearce, *Canadian Medical Association Journal*, 1961, **84**, 272-280.

112. A. A. Benson, *Journal of the American Chemical Society*, 1958, **80**, 5010-5010.

113. B. Gaš, M. Štědrý and E. Kenndler, *ELECTROPHORESIS*, 1997, **18**, 2123-2133.

114. C. Wunderly, *Principles and applications of paper electrophoresis*, 1961.

115. P. G. Righetti and A. Guttman, *Capillary electrophoresis*, Wiley Online Library, 1996.

116. C. Xu, M. Zhong, L. Cai, Q. Zheng and X. Zhang, *ELECTROPHORESIS*, 2016, **37**, 476-481.

117. L. Ge, S. Wang, S. Ge, J. Yu, M. Yan, N. Li and J. Huang, *Chemical Communications*, 2014, **50**, 5699-5702.

118. C. L. S. Chagas, F. R. de Souza, T. M. G. Cardoso, R. C. Moreira, J. A. F. da Silva, D. P. de Jesus and W. K. T. Coltro, *Analytical Methods*, 2016, **8**, 6682-6686.

119. L. Luo, X. Li and R. M. Crooks, *Analytical Chemistry*, 2014, **86**, 12390-12397.

120. T. Rosenfeld and M. Bercovici, *Lab on a Chip*, 2018.

CHAPTER 2. AgNP/Bi/NAFION-MODIFIED DISPOSABLE ELECTRODES FOR SENSITIVE Zn(II), Cd(II), AND Pb(II) DETECTION IN AEROSOL SAMPLES

Chapter Overview

A new method for modifying electrodes with Ag nanoparticles (AgNPs) using electrospray deposition for sensitive, selective detection of Zn(II), Cd(II), and Pb(II) in aerosol samples when combined with Bismuth and Nafion coating and square-wave anodic stripping voltammetry (SWASV) is reported. Carbon stencil-printed electrodes (CSPEs) fabricated on a polyethylene transparency (PET) sheet were produced for an inexpensive, simple to fabricate, disposable sensor that can be used with the microliter sample volumes for analysis. Sensor performance was improved by modifying the electrode surface with electrospray-deposited AgNPs. The use of electrospray deposition resulted in more uniform particle dispersion across the electrode surface when compared to drop-casting. Using AgNP-modified electrodes combined with Bi and Nafion, experimental detection limits (LODs) of 5.0, 0.5, and 0.1 μg L^{-1} for Zn(II), Cd(II), and Pb(II), respectively, were achieved. The linear working ranges were 5.0-400.0 μg L^{-1}, 0.5-400.0 μg L^{-1}, and 0.1-500.0 μg L^{-1} for Zn(II), Cd(II), and Pb(II), respectively. Interference studies showed Cu(II) was the only metal that interfered with this assay but inference could be eliminated with the addition of ferricyanide directly to the sample solution. This electrochemical sensor was applied for the simultaneous determination of Zn(II), Cd(II), and Pb(II) within source particulate matter (PM) samples collected on filters using an aerosol test chamber. This work was published in *Electroanalysis*.[1]

Introduction

Human exposure to aerosolized particulate matter (PM) has been recognized worldwide as a major contributor to morbidity and mortality.[2-4] PM is chemically complex, containing a wide

range of inorganic and organic molecules that can cause adverse health effects. Understanding exposure can be difficult due to the spatial heterogeneity of PM and the large variety of PM sources.[5,6] Further exacerbating problems associated with PM exposure, particularly for human health, is that the quantity of PM is increasing as a result of globalization and urban expansion, especially within the developing world.[7-9] The toxic components of PM2.5 (PM less than 2.5 μm in aerodynamic diameter) include polycyclic aromatic hydrocarbons (PAHs), nitro PAHs, metals, and reactive gases. In this work, we focused on measuring Zn, Cd, and Pb in PM samples as part of a long-standing effort to quantify toxic metals in aerosols for human exposure studies using filter samples collected from personal aerosol samplers.

Zn, Cd, and Pb levels in PM are typically quantified using laboratory analytical instrumentation such as inductively coupled plasma-mass spectrometry (ICP-MS) or atomic absorption spectrometry.[10] These methods use large and expensive machines that are complicated to use and maintain, limiting their use to sophisticated laboratories that charge a high price for analysis. Faster, less expensive, and easier to use tools for analyzing samples would enable wide-spread testing in both developed and developing countries.[11] X-Ray Fluorescence (XRF) has been used as a less expensive, portable alternative to ICP-MS methods.[12] XRF, however, still requires purchase of a relatively expensive measurement unit. Among low-cost analytical methods, colorimetric detection using either visual or imaging-based techniques is simple and low-cost.[13] However, colorimetry has limited sensitivity, selectivity, and high limits of detection (LOD) for trace metals such as Zn, Cd, and Pb.[14] Electrochemical detection integrated with inexpensive portable instrumentation has the ability to overcome limitations of colorimetric methods.[14-18] Electrochemical detection can substantially improve sensitivity, selectivity, and LOD and can be optimized with methods such as electrode modification and analyte preconcentrate.[19,20] Many low-

cost electrode fabrication methods exist, including screen-printing,[21] inkjet-printing,[22] and pencil drawing[23] but many of these electrodes have relatively high electron transfer resistance resulting in sub-optimal detection limits.

In this work, stencil-printed carbon electrodes were fabricated on a simple PET film and used for voltammetric detection of Zn, Cd, and Pb. Square-wave anodic stripping voltammetry (SWASV) was used for its ability to provide low LODs *via* on-electrode preconcentration.[24] Many methods have been used to modify electrodes to improve Zn(II), Cd(II), and Pb(II) detection, including antimony[25] or bismuth[26,27] co-deposition or modification with nafion-graphene nanocomposites.[28] A new surface modification strategy using electrospray deposited silver nanoparticles (AgNPs) with Bi and Nafion modification to improve metal detection is reported here.

AgNPs are attractive because of their small size, simple low-cost synthesis[29], and good electron transfer kinetics.[30] AgNP-modified electrodes have primarily been generated using electrodeposition or drop-casting methods;[31,32] electrospray deposition offers an alternative method for electrode modification. Electrospray produces submicron-sized droplets with a large surface area and narrow size distribution.[33] Here, electrospray deposition improved the dispersion of AgNPs on a carbon stencil-printed electrode (CSPE) relative to drop-cast coatings, resulting in better electrode performance. The electron transfer kinetics were measured using a standard redox probe, ($Ru(NH_3)_6Cl_3$), for both bare and AgNP-modified electrodes and showed a decreased peak potential separation (ΔE) for modified electrodes. Using the modified electrodes, the optimum supporting electrolyte conditions for Zn(II), Cd(II), and Pb(II) detection were determined and a pH 5.0 acetate buffer was found to give the best combination of low detection limits and large linear working range. Selectivity was also determined from tolerance ratios for potential interfering

metals. Of the common metals found in PM, only Cu significantly interfered with the analysis but the interference could be addressed using $Fe(CN)_6^{3-}$. Under optimized detection conditions, AgNP-modified CSPEs were successfully used to measure the amount of Zn(II), Cd(II), and Pb(II) in PM samples collected from a variety of PM samples

Experimental

Materials and methods

Zinc(II) nitrate, cadmium(II) nitrate, lead(II) nitrate, copper(I) chloride, chromium(III) chloride, cobalt(II) chloride hexahydrate, vanadium(III) chloride, hexaaminеruthenium(III) trichloride, bismuth(III) oxide, sodium borohydride, sodium acetate trihydrate, sodium dodecyl sulfate (SDS) and trimethylsilylated Nafion® were purchased from Sigma–Aldrich (St. Louis, MO). Iron(II) sulfate, iron(III) nitrate, potassium dichromate, manganese(II) chloride tetrahydrate, silver(I) nitrate, and sodium carbonate were purchased from Fisher Scientific (Waltham, MA). Copper(II) nitrate and nitric acid were purchased from Mallinckrodt (St. Louis, MO). Glacial acetic acid was purchased from EMD Millipore (Billerica, MA). Trisodium citrate dehydrate was purchased from Alfa Aesar (Ward Hill, MA). Milli-Q water from Millipore ($R \geq 18.2$ MΩ cm) was used for all experiments. All chemicals were used as received without further purification. Carbon Ink (Acheson, Bangkok, Thailand), graphite powder (diameter <20 μm, Sigma–Aldrich, St. Louis, MO), and transparency film PP2200 (3M, St. Paul, MN) were used for electrode fabrication. A 30 W Epilog Zing Laser Cutter and Engraver (Golden, CO) was used to create electrode patterns on a transparency sheet using Corel Draw X4 program for stencil printing. A CHI832 potentiostat (CH Instruments) was used for all electrochemical measurements. The high voltage power supply used for electrospraying was purchased from Gamma High Voltage Research (Ormond Beach, FL). The syringe pump (NE-300) was purchased from New Era Pump

Systems, Inc. (Farmingdale, NY). Electrodes were imaged using a JSM-6500F scanning electron microscope (JEOL USA Inc., Peabody, MA).

AgNP synthesis

AgNPs were prepared as described previously by Yang et al.[29] A 5 mL aliquot of 12.6 mM sodium citrate was added to 50 mL of 0.3 mM silver nitrate, followed by the addition of 2 mL of 37 mM sodium borohydride under continuous stirring. When AgNPs formed, the solution changed to a bright yellow color. The size of the synthesized AgNP obtained from a dynamic light scattering technique was 13.1±0.5 nm.

Fabrication of CSPE

Custom electrode inks were fabricated by adding 5% (w/w) graphite to the commercial carbon ink followed by hand mixing until homogeneous. Electrodes were stencil printed on a PET

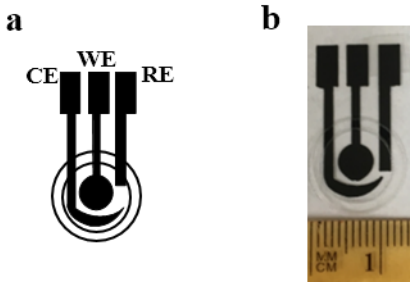

Figure 2.1: Electrode design showing stencil-printed carbon electrodes with a clear packing tape ring for solution containment (a), and CSPE photograph(b)

sheet through a laser-cut stencil. After printing, the electrodes were dried at 65^0C for 1 hr. A laser-cut, ring-shaped piece of adhesive tape was used for confining the solution droplet to the electrodes (Figure 2.1a). Figure 2.1b shows a photograph of a final representative CSPE.

Electrospray electrode modification

A homemade electrospray system consisting of a high-voltage power supply, syringe pump, plastic 3 mL syringe with a stainless-steel needle (26 G), and ground-collector (12 cm apart from the needle tip) was used for AgNP deposition. A flow rate of 12.0 mL h^{-1} was used for all

experiments. The high-voltage power supply was connected to the needle tip and ground-collector. CSPEs were covered using aluminum foil with openings to expose the underlying working electrode and attached to the ground-collector. A 12 kV potential was applied for five min to generate AgNP-modified working electrodes. The electrospraying process was repeated four times for each electrode to ensure consistent coating with a drying time of five minutes between each electrospraying process. Six CSPEs were able to be modified by electrospraying AgNP in the same time under these optimum conditions by covering CSPEs with the same sheet of aluminum foil.

Electrochemical measurement

Cyclic voltammetry (CV) of 0.1 M KNO_3 was carried out for observing the existence of AgNP on the electrode surface; the potential was swept from -0.7 to 0.7 V with scan rate of 50 mV s^{-1}. For electrode characterization, CV of 1.0 mM $Ru(NH_3)_6Cl_3$ was performed for electrode characterization; the potential was swept from 0.1 to -0.5 V for unmodified CSPE and 0 to -0.5 V for AgNP-modified CSPE versus a carbon pseudo-reference electrode with scan rates of 10-100 mV s^{-1}. Electrochemical impedance spectroscopy (EIS) of 1.0 mM $Ru(NH_3)_6Cl_3$ was done for measuring uncompensated resistance with initial potential at 0.194 V, high and low frequency of 100000 Hz and 0.1 Hz, respectively, amplitude of 0.01 V, and quiet time of 2 s. The electrolyte potential window of 0.1 M KNO_3 was also determined using CV, and the potential was swept from -2 to 2 V. Electrode modification for SWASV detection of Zn(II), Cd(II), and Pb(II) was accomplished by drop casting 1 µL of 0.5% Nafion dissolved in 50% v/v isopropanol/water onto the working electrode, and allowing it to dry. For measurements, 50.0 µL of standard Zn(II), Cd(II), and Pb(II) solutions, 3.2 µL of 10 mg L^{-1} Bi(III) dissolved in 0.1 M acetate buffer pH 5.0, and 0.1 µL of 500.0 µg L^{-1} ferricyanide were pipetted onto the electrode. An optimum deposition potential (-1.6 V) and time of -1.6 V and 360 s, respectively, were used for all measurements. Stripping

voltammetry was performed after a 10 s equilibration time from -1.8 to 0 V, and with an optimized step potential of 15 mV, amplitude of 75 mV, and frequency of 10 Hz.

Interference study

The mass ratios between other metals such as Cu(I), Cu(II), Fe(II), Fe(III), Cr(III), Cr(VI), Mn(II), Ni(II), Co(II), and V(III) and the target metals, Zn(II), Cd(II), and Pb(II), were studied to determine detection tolerance ratios. The tolerance ratio is defined as the mass ratio that creates a change in peak current of ±5%.[34]

Sample collection and sample preparation

Aerosol samples, including incense, fly ash, cigarette, and solder, were collected on 37-mm and 47-mm diameter Pallflex filters (Pall Corporation, Port Washington, NY). Aerosols were generated in a controlled test chamber. Incense and cigarette smoke was generated by burning locally purchased supplies of each. Fly Ash 2 (RT Corp., Laramie, WY) was mixed with filtered water and aerosolized using a Collison nebulizer (Mesa Labs, Butler, NJ). Soldering aerosols were generated by performing a soldering operation inside the chamber. Ultrasonic personal aerosol samplers (UPAS) and URG 16.7 LPM 2.5 um cutpoint cyclones (Chapel Hill, NC) were used for collecting the aerosol samples.[35] Gravimetric analysis was used to determine sample weights and aerosol concentrations. The PM weight is shown in Table 2.1. A 3-mm diameter punch was removed from the 37-mm diameter filter for SPCE analysis. Before quantifying Zn(II), Cd(II), and Pb(II), the punches were digested using a modification to a previously published procedure.[36] The digestion was performed by adding 8 µL of 5% w/v SDS in Milli-Q water to aid in filter wetting and 2 µL of concentrated nitric acid onto the 3-mm diameter punch. The punch was then placed in a microwave on high power for 15 s and repeated for a total of three times (45 s total). A 15 µL aliquot of 5% SDS was added to the punch between each heating step. Each punch was

then neutralized with 2 M Na_2CO_3 after the last digestion step. Verification that the punch was neutralized was performed with pH paper. Zn(II), Cd(II), and Pb(II) were measured by placing the 3-mm digested sample filter onto the electrode and adding 50.0 µL of 0.1 M acetate buffer pH 5.0, 3.2 µL of 10 mg L^{-1} Bi(III), and 0.1 µL of 500.0 µg L^{-1} ferricyanide. SWASV was performed for Zn(II), Cd(II), and Pb(II) determination using the optimal settings described above from three punches of each sample filter to create replicate measurements.

Table 2.1: Aerosol generation and collection details. All samples were collected as $PM_{2.5}$.

Sample	Collected PM Mass (mg)
Incense	1.401
Nebulized Fly Ash	0.203
Cigarette Smoke	1.546
Solder Fume	2.243

Results and Discussion

Electrode characterization

Previous methods for making low cost electrodes have utilized more expensive electrode materials and/or more complicated modifiers to achieve low detection limits.[28,37-39] In an effort to improve electrode performance using low-cost starting materials and simple modification methods, electrospray AgNP deposition was explored. Electrode modification was first studied using scanning electron microscopy (SEM) to measure the nanoparticle distribution on the electrode surface (Figure 2.2). Figure 2.2a shows the unmodified CSPE and its characteristic graphite sheet nature. For surface modification, 13.1±0.5 nm AgNP were either electrosprayed (Figure 2.2.b) or drop cast (Figure 2.2.c) onto a bare CSPE. Figure 2.2b shows well-dispersed AgNPs following electrospray deposition. The number of AgNPs on the working electrode were counted as approximately 9 particles per μm^2 using a custom MATLAB program.[40] In contrast, drop-cast

deposited AgNPs resulted in significant particle aggregation. Improvements in AgNP deposition uniformity on the electrode surface is likely due to the transfer of colloidal nanoparticles to gas phase, where droplets often contain one particle prior to deposition and are well dispersed.[33,41]

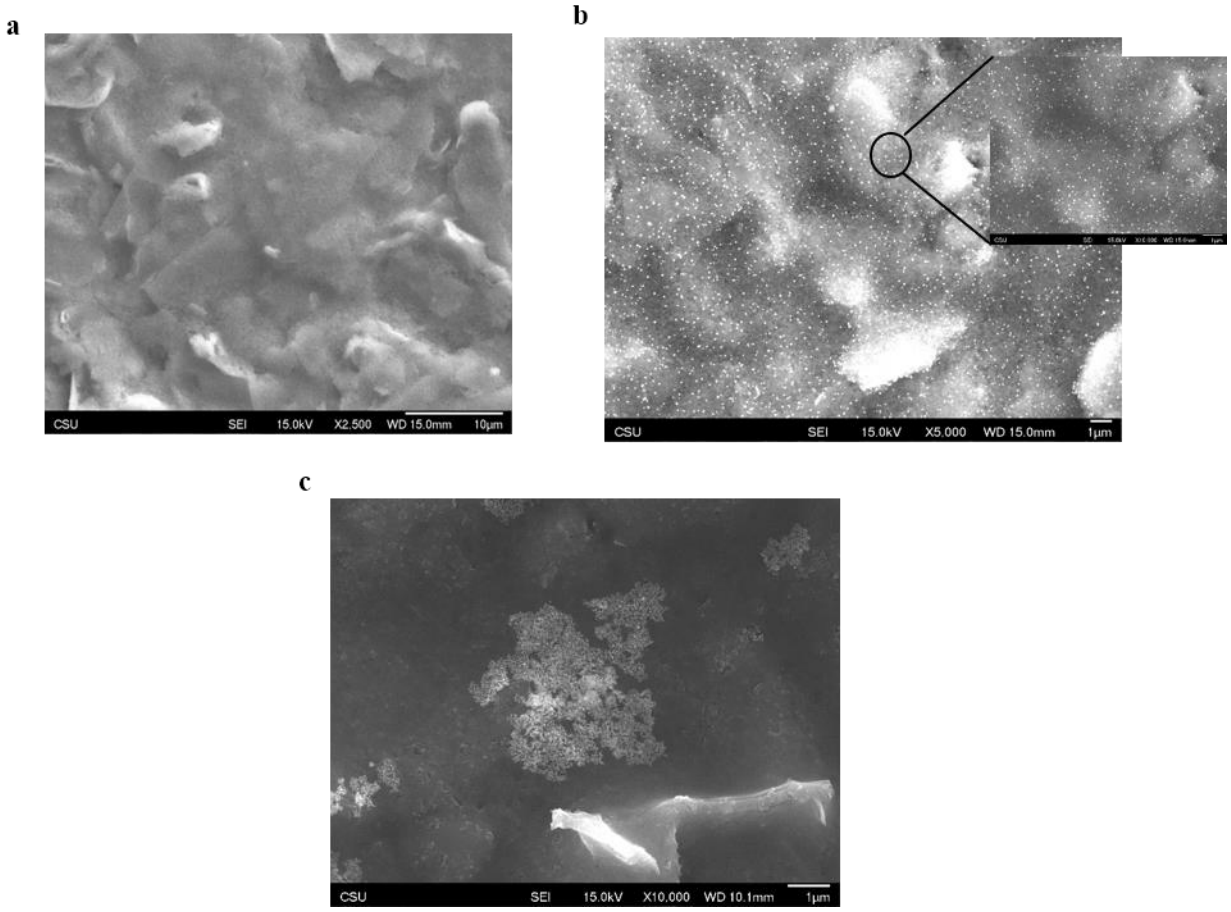

Figure 2.2: SEM images of an unmodified CSPE (a), an electrospray deposited AgNP modified CSPE (b) with and inset showing 10,000 times magnification of the AgNP modified CSPE (inset b), and a drop-cast and dried AgNP CSPE (c).

Electrochemical characterization

The existence of AgNP was also confirmed by a cyclic voltammogram of AgNP-modified CSPE compared with that of unmodified CSPE as shown in Figure 2.3. The oxidation and reduction potentials of AgNP deposited on CSPE surface appeared at 0.19 V and -0.31 V, respectively. The electrochemical performance was characterized using $Ru(NH_3)_6Cl_3$. $Ru(NH_3)_6^{2+/3+}$ is an outer-sphere redox system that is sensitive to electronic structure of carbon and

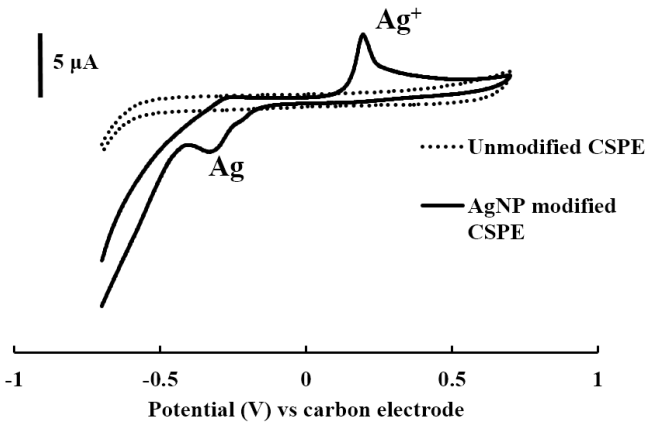

Figure 2.3: Cyclic voltammograms of unmodified and AgNP modified CSPE using 0.1 M KNO_3 the supporting electrolyte.

widely used to study the electron transfer kinetics.[42] Electron transfer rates are correlated with ΔE in the cyclic voltammograms of $Ru(NH_3)_6^{2+/3+}$, where a lower ΔE typically indicates a lower resistance.[43] Cyclic voltammograms as a function of scan rate for the reversible $Ru^{2+/3+}$ electrochemistry at bare and AgNP modified electrodes are shown in Figure 2.4a and b. As expected, given fast kinetics and modest scan rates, the current increases as a function of scan rate in a predictable and similar manner for both electrodes. Figure 2.4c shows the ΔE as a function of scan rate for AgNP-modified and unmodified CSPEs. As previously reported, the peak separation of $Ru(NH_3)_6^{2+/3+}$ in cyclic voltammograms causes from the resistance of the system which is the combination of uncompensated resistance and charged transfer resistance.[44] Thus, the uncompensated resistance of both unmodified and AgNP-modified CSPE was measured from Nyquist plots using EIS as shown in Figure 2.5 and summarized in Table 2.2. The results showed uncompensated resistance of AgNP-modified CSPE (280 ± 12 Ω) was lower than that of unmodified CSPE (335 ± 11 Ω) causing lower ΔE of AgNP-modified CSPE. The calculated difference of iR drop (peak current times to uncompensated resistance) causing from uncompensated resistance between both electrode was 0.004 V which is lower than the difference

of ΔE of both electrodes at 50 mV s^{-1} (0.006 V). It seems reasonable to assume then that the silver particles have a negligible effect on the electron transfer kinetics to $Ru(NH_3)_6^{2+/3+}$ under these conditions. Interestingly, the peak current dropped by ~ 30% (9 μA/29 μA), which would imply that the electrospray process is diminishing the specific electrochemically active surface area for this redox probe.

Table 2.2: Uncompensated resistance of unmodified and AgNP modified CSPEs measured by EIS (n=3).

Electrode	Uncompensated resistance (Ω)
Unmodified CSPE	335 ± 11
AgNP modified CSPE	280 ± 12

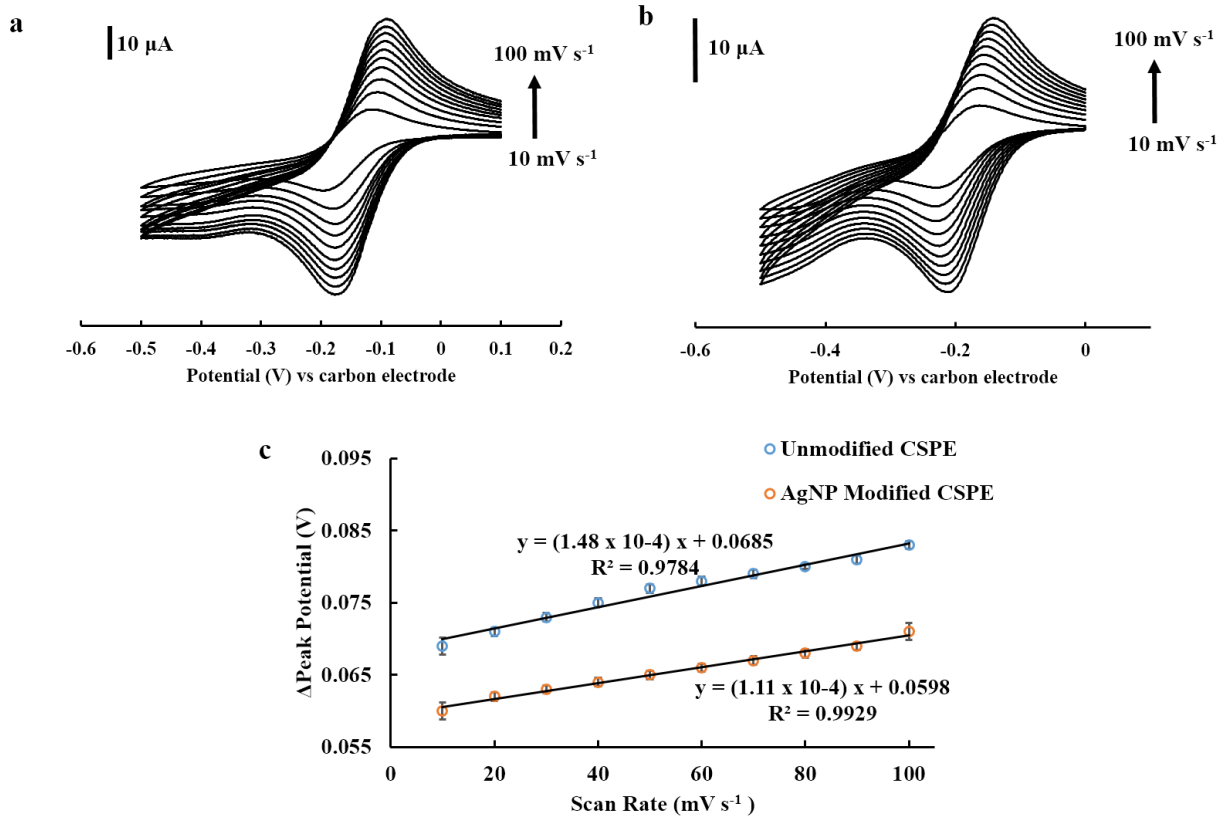

Figure 2.4: Cyclic voltammograms of 1.0 mM $Ru(NH_3)_6Cl_3$ in 0.1 M KNO_3 with varying scan rates from 0.01 V s^{-1} to 0.1 V s^{-1} using an unmodified CSPE (a) or AgNP modified CSPE (b). Relationship between peak potential separation and scan rate of unmodified CSPE and AgNP modified CSPE (c) (n=3).

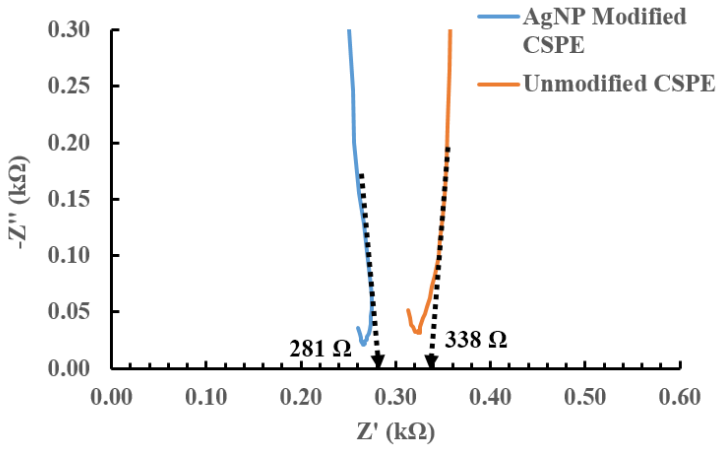

Figure 2.5: Nyquist plots of 1 mM $Ru(NH_3)_6Cl_3$ using unmodified and AgNP modified CSPEs

Zn(II), Cd(II), and Pb(II) determination using unmodified and AgNP/Bi/Nafion-modified CSPEs

AgNP/Bi/Nafion-modified CSPEs were compared to unmodified CSPEs for Zn(II), Cd(II), and Pb(II) detection using SWASV. To enhance signal, bismuth was added to the deposition solution following published protocols.[27] Bismuth has the ability to alloy with metals such as Zn, Cd, and Pb and enabling preconcentration onto the electrode surface.[45] Moreover, the addition of Nafion also enhances the preconcentration process of metal ions as the Nafion sulfonate group has been shown to selectively preconcentrate cations.[46] Figure 2.6 shows voltammograms of the different electrode types using 100 µg L^{-1} each of Zn(II), Cd(II), and Pb(II). The peak heights (n=3) for the AgNP/Bi/Nafion-modified electrodes were also the highest (13.5±1.3 µA for Zn(II), 68.4±2.1 µA for Cd(II), and 21.3±1.8 µA for Pb(II)) compared with those of unmodified CSPEs where there was no measurable peak for Zn(II) (2.07±0.34 µA for Cd(II) and 7.57±2.1 µA for Pb(II)), or Bi/Nafion CSPEs (5.40±0.53 µA for Zn(II), 16.6±1.48 µA for Cd(II), and 16.0±1.25 µA for Pb(II)). The double peaks were occurred in the cadmium region and another in the lead region when using Bi/Nafion CSPE causing from the stripping process of the deposited metals (Cd and Pb) at different sites. One is from bismuth (small peak) and another is from CSPE or Cd/Pb itself.[47] The increase in peak current when using AgNP/Bi/Nafion-modified CSPEs is believed to

result from improved uncompensated resistance and electron transfer and therefore improved efficiency of Zn(II), Cd(II), and Pb(II) detection. An increase in electrode surface may also be responsible for this improvement.

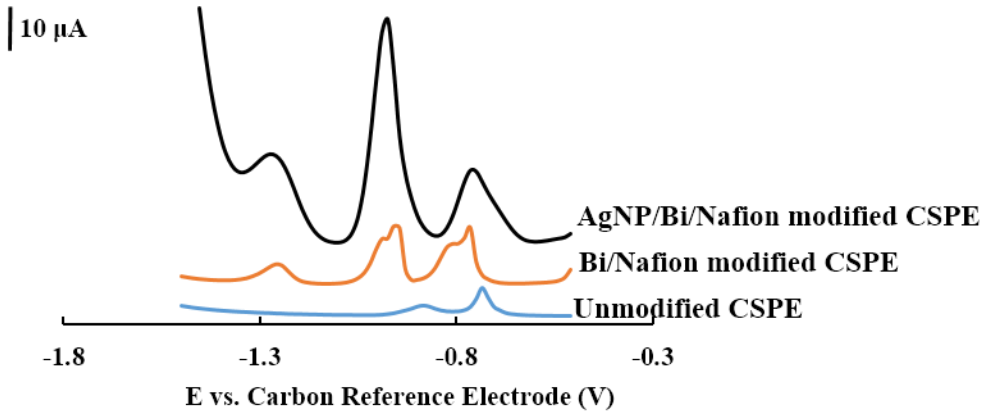

Figure 2.6: Square-wave voltammograms of 100.0 µg L^{-1} Zn(II), Cd(II), and Pb(II) in 0.1 M acetate buffer pH 5 using an unmodified CSPE, Bi/Nafion modified CSPE, and AgNP/Bi/Nafion modified CSPE.

pH and supporting electrolyte optimization

Background current plays an important role when measuring peak currents in anodic stripping voltammetry because the background can obscure the peak of Zn(II) at -1.2 V versus carbon reference electrode. To achieve the lowest LOD, the potential window of 0.1 M KNO_3 in various pH and supporting electrolyte solutions was investigated. Figure 2.7 shows that increasing pH provides a wider potential window and lower interference for Zn detection.[48] The increase in the cathodic potential window (lower than -1.1 V) with increasing pH is due to the decrease in onset of oxygen reduction as shown in the following equation.

$$O_2 + 4H^+ + 4e^- \rightleftharpoons 2H_2O \qquad E^0 = 1.229 \text{ vs. NHE}$$

It is well established that oxygen can more easily react with H^+ with increasing pH, thus contributing to the higher background at lower pH [49]. Oxygen reduction as a source of background

current was confirmed by purging the supporting electrolyte (acetate buffer pH 4.5) with N_2. Figure 2.8 shows a lower background current at -1.1 V in acetate buffer at pH 4.5 when N_2 purging is performed. In case of tartrate buffer, it provided a wider potential window than acetate (Figure 2.7a), it was not suitable for determination of all three species, Zn(II), Cd(II), and Pb(II), as it produced lower peak currents when compared with the acetate buffer (Figure 2.7b and c). While pH 4.5 acetate buffer provided the highest peak current (13.5 µA for Zn(II), 66.1 µA for Cd(II), and 38.2 µA for Pb(II)), the background current at pH 5.0 was lower (Figure 2.7b and c). Therefore, these two conditions were used for determining LODs.

Electrochemical detection of Zn(II), Cd(II), and Pb(II)

Experimental LODs and linear ranges of Zn(II), Cd(II), and Pb(II) were evaluated for both pH 4.5 and 5.0 acetate buffers (Table 2.3). Voltammograms for each condition are shown in Figure 2.9. At low Zn(II), Cd(II), and Pb(II) concentrations (0.1-10.0 µg L^{-1} for acetate buffer pH 4.5 and 0.1-2.5 µg L^{-1} for acetate buffer pH 5.0), the voltammograms are shown in Figure 2.10. At pH 4.5, a lower LOD for Zn(II) (0.5 µg L^{-1}) was obtained than for pH 5.0 (5.0 µg L^{-1}). A pH 5.0 buffer, however, provided a larger linear range for lower concentrations (5.0-400.0 µg L^{-1}). The improvement in linear range was the result of a lower background current at pH 5.0 compared to that obtained at pH 4.5. Therefore, the pH 5.0 acetate buffer was used as the supporting electrolyte for subsequent experiments. Using the optimized conditions, LODs were 5.0, 0.5, and 0.1 µg L^{-1} for Zn(II), Cd(II), and Pb(II), respectively. Linear ranges were 5.0-400, 0.5-400, and 0.1-500 µg L^{-1} for Zn(II), Cd(II), and Pb(II), respectively. LODs and linearity ranges from previous work for Zn(II), Cd(II), and Pb(II) using CSPE are summarized in Table 2.4.

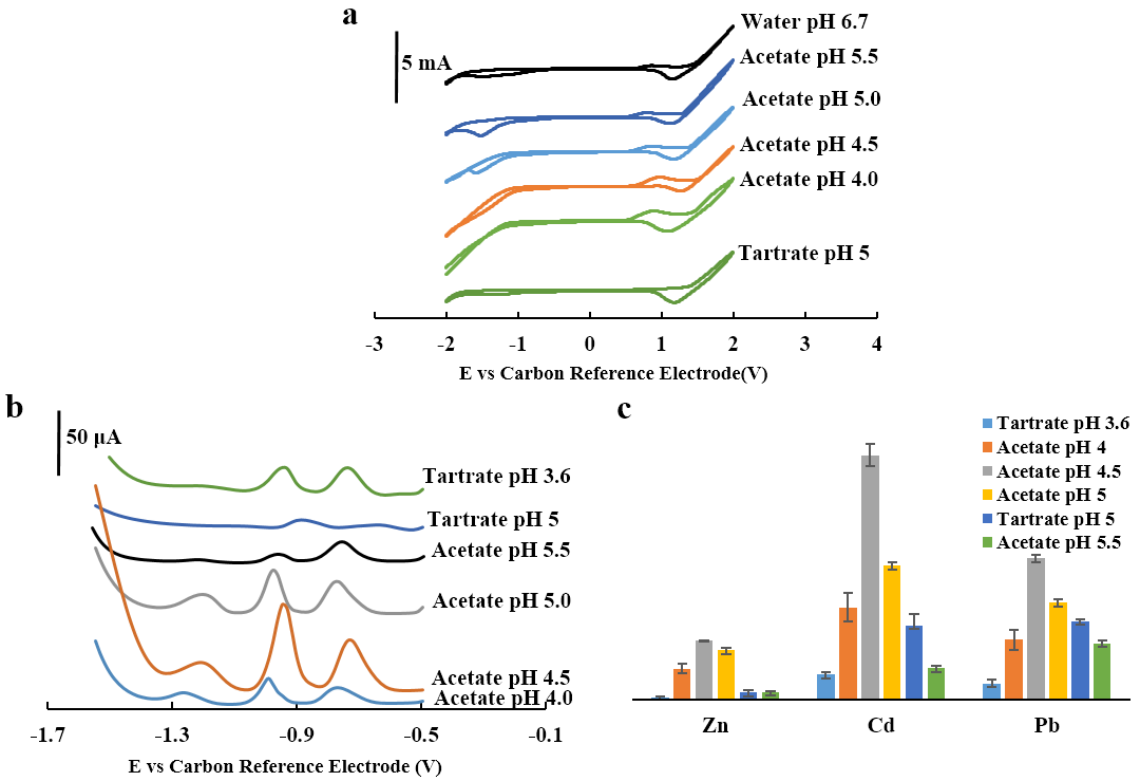

Figure 2.7: Buffer potential windows (a), and SWVs of 100.0 µg L^{-1} of Zn(II), Cd(II), and Pb(II) measured using different buffers (b). Comparison of peak currents for each metal using different buffers (c) (n=3).

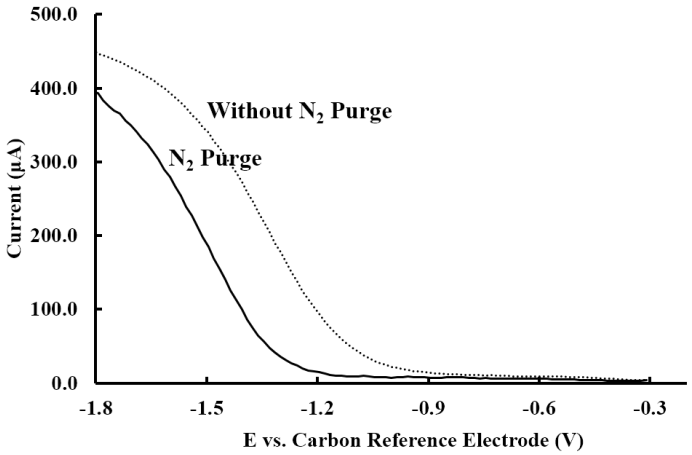

Figure 2.8: Square-wave voltammograms of 7 mL acetate buffer pH 4.5 with N_2 purge for 15 min and without N_2 purge.

Table 2.3: Experimental LODs and linear ranges of different acetate buffer pHs

Metal ions	Experimental LODs (µg L^{-1})		Linearity Range (µg L^{-1})	
	pH 4.5	pH 5.0	pH 4.5	pH 5.0
Zn(II)	0.5	5.0	75.0-500.0	5.0-400.0
Cd(II)	0.5	0.5	0.5-500.0	0.5-400.0
Pb(II)	0.1	0.1	0.1-500.0	0.1-500.0

Table 2.4: Carbon screen-printed electrode comparison for Zn(II), Cd(II), and Pb(II) measurement

Modified Materials	LODs (µg L^{-1})			Linearity Range (µg L^{-1})			Volume	References
	Zn(II)	Cd(II)	Pb(II)	Zn(II)	Cd(II)	Pb(II)		
antimony film	-	3.4	5.0	-	11.5-72.4	16.8-62.6	-	[25]
bismuth film	-	8	10	-	20-300	20-300	100 µL	[20]
bismuth oxide	-	16	8	-	20-300	20-300	100 µL	[50]
Bi-D24C8/Nafion	-	0.27	0.11	-	0.5-60	0.5-60	sequential injection	[37]
G/PANI/PS	-	4.43	3.30	-	10-500	10-500	-	[51]
mercury nanodroplet	-	12 nM	23 nM	-	40-200 nM	40-200 nM	-	[52]
MWCNT	0.3	0.1	0.07	0.5-100	0.5-80	0.5-100	mL level	[19]
Nafion/G/PANI nanocomposite	1	0.1	0.1	1-300	1-300	1-300	50 µL	[28]
Nafion/ionic liquid/graphene	0.09	0.06	0.08	0.1-100	0.1-100	0.1-100	10 mL	[38]
AgNP/Bi/Nafion	5.0	0.5	0.1	5.0-400.0	0.5-400.0	0.1-500.0	50 µL	this work

(Bi-D24C8/Nafion SPCE: Bi film dibenzo-24-crown-8/Nafion; G/PANI/PS: graphene/polyaniline/polystyrene; MWCNT: multiwalled carbon nanotube; G/PANI: graphene polyaniline)

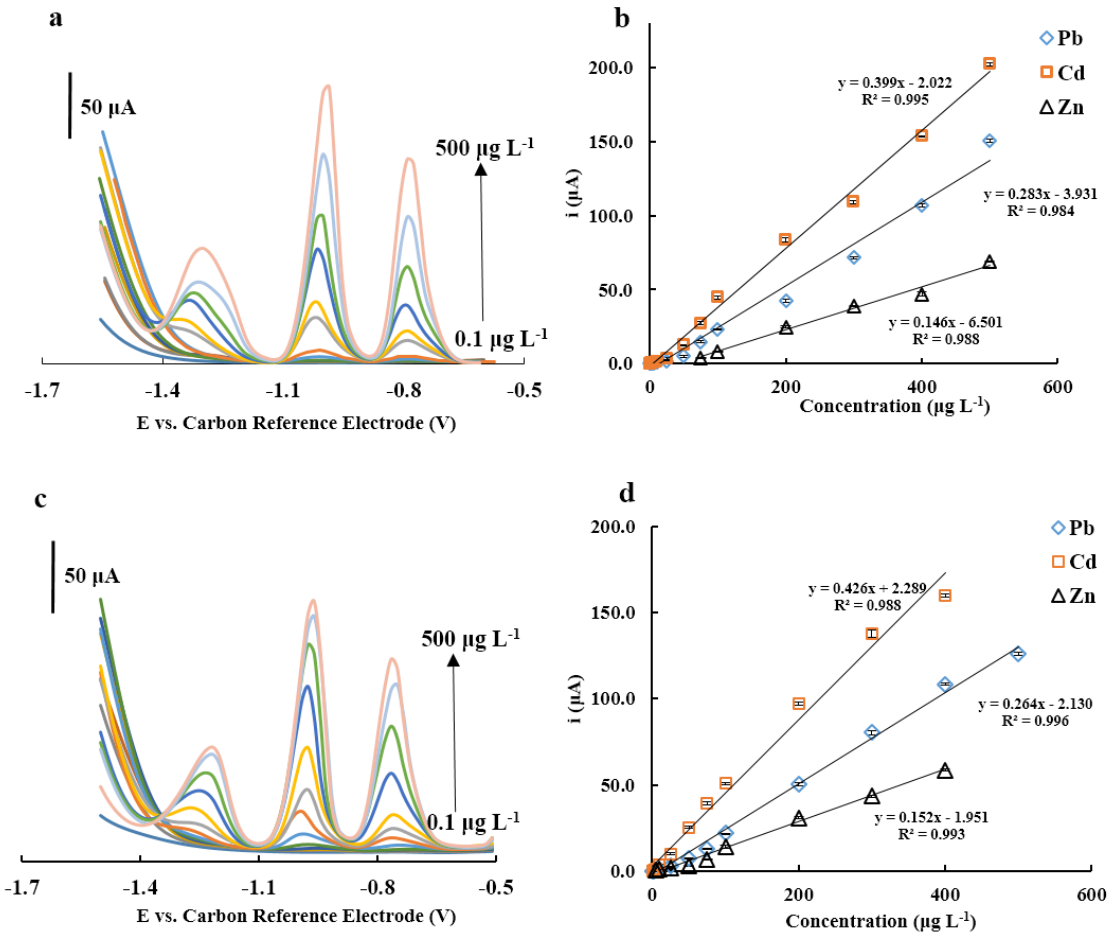

Figure 2.9: Square-wave voltammograms for the simultaneous detection of 0.1 µgL^{-1} – 500.0 µg L^{-1} of Zn(II), Cd(II), and Pb(II) using pH 4.5 acetate buffer (a) or pH 5.0 acetate buffer (c) with their corresponding calibration curves (b) and (d) respectively. (n=3)

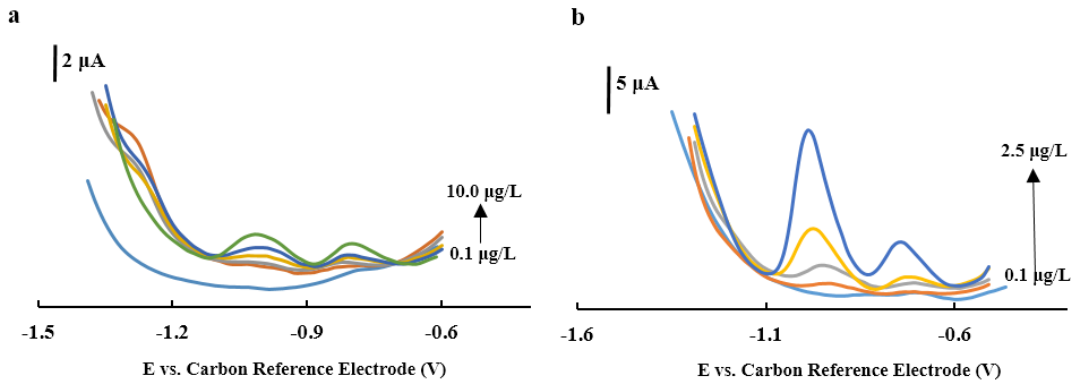

Figure 2.10: Square-wave voltammograms of Zn(II), Cd(II), and Pb(II) simultaneous detection from 0.1 – 10.0 µg L^{-1} using acetate buffer pH 4.5 (a). Square-wave voltammograms of Zn(II), Cd(II), and Pb(II) simultaneous detection from 0.1 µg L^{-1} – 2.5 µg L^{-1} using acetate buffer pH 5.0 (b).

Interference study

Before using the electrodes for real environmental sample analysis, the effects of potentially interfering metals present in aerosol samples were investigated. The interference tolerance ratio, which is defined as the mass ratio of interfering species relative to the target metal that creates a change in peak current of ±5%, was determined for each species.[34] Among all of the tested species (Table 2.5), Cu was the only metal that caused significant interference. To eliminate the Cu interference, ferricyanide was used as a masking agent.[39,53] However, ferricyanide itself was found to suppress the Zn(II), Cd(II), and Pb(II) signal shown as in Figure 2.11. Therefore, the optimum concentration of ferricyanide to eliminate Cu(II) was investigated. From Figure 2.10, the optimum concentration of ferricyanide was determined to be 3 µM. This concentration was able to eliminate the interference of Cu(II) up to 500.0 $\mu g L^{-1}$.

Table 2.5: Interference ratio defining the mass ratio making a change in peak current of ±5% (Concentration of target metals is 50 $\mu g\ L^{-1}$ each.)

Interference	Tolerance Ratio (by mass)		
	Zn	Cd	Pb
Cu(I)	1	10	10
Cu(II)	0.5	1	1
Fe(II)	50	50	50
Fe(III)	100	100	100
Cr(III)	≥500	≥500	≥500
Cr(VI)	10	10	10
Mn(II)	≥500	≥500	≥500
Ni(II)	10	100	100
Co(II)	10	≥500	≥500
V(III)	100	100	100

Zn(II), Cd(II), and Pb(II) determination in PM samples

The AgNP/Bi/Nafion-modified CSPEs were used for Zn(II), Cd(II), and Pb(II) determination in PM samples from known sources including incense, fly ash, cigarette, and solder. Concentrations were validated using ICP-MS. The amount of these metals in each aerosol sample

is shown in Table 2.6. Zn(II) was found to be present in all aerosol samples tested. The concentrations of Zn(II) in incense, fly ash, cigarette, and solder aerosol samples were 22.0, 42.6, 35.8, and 13.1 µg L^{-1}, respectively by ASV and 19.6, 49.6, 29.1, and 17.1 µgL^{-1}, respectively by ICP-MS. ICP-MS analysis detected Cd(II) in fly ash (0.23 µg L^{-1}) and cigarette (0.16 µg L^{-1}) aerosol samples and Pb(II) in fly ash (0.11 µg L^{-1}), but these concentrations were near or below the LOD for the AgNP/Bi/Nafion-modified electrode and were not detected. A paired Student's *t*-test was used to compare results between AgNP/Bi/Nafion-modified electrodes and ICP-MS for Zn detection. Because the t value (-0.165) is less than the critical t value (3.1824, P=0.05) for (n-1=3) degrees freedom when n = 4, the null hypothesis is not rejected. Therefore, the developed method does not provide significantly different results with 95% confidence.

Table 2.6: Concentration of Zn(II), Cd(II), and Pb(II) in samples (n=3)

Samples	Zn(II) (µg L^{-1})		Pb(II) (µg L^{-1})		Cd(II) (µg L^{-1})	
	ePADs	ICP-MS	ePADs	ICP-MS	ePADs	ICP-MS
Incense	22.0 ± 2.4	19.6 ± 1.85	<0.1	<0.05	<0.5	<0.05
Fly ash	42.6 ± 2.7	49.6 ± 1.87	<0.1	0.11± 0.01	<0.5	0.23 ± 0.02
Cigarette	35.8 ± 2.1	29.1 ± 1.64	<0.1	<0.05	<0.5	0.16 ± 0.01
Solder	13.1 ± 2.3	17.1 ± 1.83	<0.1	<0.05	<0.5	<0.05

Conclusion

An AgNP/Bi/Nafion-modified CSPE was developed for Zn(II), Cd(II), and Pb(II) measurement providing LODs of 5.0, 0.5, and 0.1 µg L^{-1}, respectively. An improvement in performance from unmodified CSPE was the result of AgNPs increasing the electrode surface area and improving uncompensated resistance and electron transfer kinetics. Electrospray deposition yielded a uniform dispersion of AgNP. Additionally, pH 5.0 acetate buffer produced wider working linear ranges for Zn(II), Cd(II), and Pb(II) measurements than pH 4.5 acetate buffer due

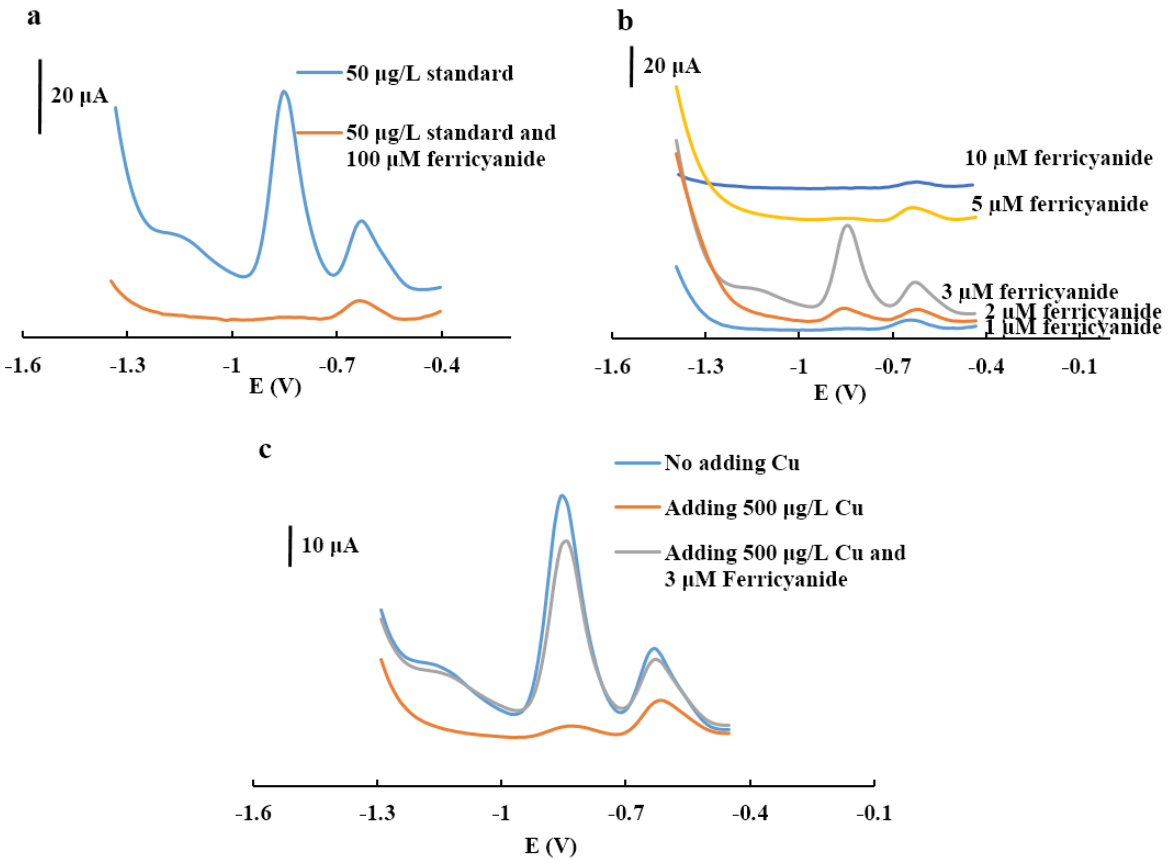

Figure 2.11: Effect of ferricyanide to 50.0 µg L^{-1} Zn(II), Cd(II), and Pb(II) square-wave voltammograms (a). Square-wave voltammograms of 50.0 µg L^{-1} Zn(II), Cd(II), and Pb(II) with adding 500.0 µg L^{-1} Cu(II) and different concentrations of ferricyanide (b). Influence of ferricyanide for elimination of Cu effect in square-wave anodic stripping voltammetric detection of Zn(II), Cd(II) and Pb(II) (c).

to a decrease in background current. An interference study found that only Cu(II) has a major role interfering with detection, and was addressed by adding 3 µM ferricyanide. Metals analysis of collected PM samples found the presence of Zn(II) in all aerosol samples. When compared against ICP-MS, our developed method gave statistically similar results. These results illustrated the capability of AgNP/Bi/Nafion-modified CSPE for sensitive and selective detection of Zn(II), Cd(II), and Pb(II).

REFERENCES

1. J. Mettakoonpitak, J. Mehaffy, J. Volckens and C. S. Henry, *Electroanalysis*, 2017, **29**, 880-889.
2. D. A. Grantz, J. H. B. Garner and D. W. Johnson, *Environment International*, 2003, **29**, 213-239.
3. R. M. Harrison and J. Yin, *Science of The Total Environment*, 2000, **249**, 85-101.
4. N. C. Jones, C. A. Thornton, D. Mark and R. M. Harrison, *Atmospheric Environment*, 2000, **34**, 2603-2612.
5. U. Lohmann and J. Feichter, *Atmos. Chem. Phys.*, 2005, **5**, 715-737.
6. U. Poschl, *Angew Chem Int Ed Engl*, 2005, **44**, 7520-7540.
7. T. Weiss, B. Pesch, A. Lotz, E. Gutwinski, R. Van Gelder, E. Punkenburg, B. Kendzia, K. Gawrych, M. Lehnert, E. Heinze, A. Hartwig, H. U. Kafferlein, J. U. Hahn, T. Bruning and W. Group, *Int J Hyg Environ Health*, 2013, **216**, 175-183.
8. A. A. Yusuf and B. P. Resosudarmo, *Ecological Economics*, 2009, **68**, 1398-1407.
9. A. Faiz, *Transportation Research Part A: Policy and Practice*, 1993, **27**, 167-186.
10. C. L. Wiseman, *Anal Chim Acta*, 2015, **877**, 9-18.
11. D. M. Cate, S. D. Noblitt, J. Volckens and C. S. Henry, *Lab Chip*, 2015, **15**, 2808-2818.
12. S. M. Pyle, J. M. Nocerino, S. N. Deming, J. A. Palasota, J. M. Palasota, E. L. Miller, D. C. Hillman, C. A. Kuharic, W. H. Cole and P. M. Fitzpatrick, *Environmental science & technology*, 1995, **30**, 204-213.
13. A. W. Martinez, S. T. Phillips, M. J. Butte and G. M. Whitesides, *Angew Chem Int Ed Engl*, 2007, **46**, 1318-1320.

14. N. A. Meredith, C. Quinn, D. M. Cate, T. H. Reilly, J. Volckens and C. S. Henry, *Analyst*, 2016, **141**, 1874-1887.

15. J. Mettakoonpitak, K. Boehle, S. Nantaphol, P. Teengam, J. A. Adkins, M. Srisa-Art and C. S. Henry, *Electroanalysis*, 2016, DOI: 10.1002/elan.201501143, n/a-n/a.

16. D. M. Cate, J. A. Adkins, J. Mettakoonpitak and C. S. Henry, *Analytical Chemistry*, 2015, **87**, 19-41.

17. J. Adkins, K. Boehle and C. Henry, *ELECTROPHORESIS*, 2015, **36**, 1811-1824.

18. J.-M. Oh and K.-F. Chow, *Analytical Methods*, 2015, **7**, 7951-7960.

19. L. Fu, X. Li, J. Yu and J. Ye, *Electroanalysis*, 2013, **25**, 567-572.

20. R. O. Kadara and I. E. Tothill, *Anal Bioanal Chem*, 2004, **378**, 770-775.

21. Z. Nie, C. A. Nijhuis, J. Gong, X. Chen, A. Kumachev, A. W. Martinez, M. Narovlyansky and G. M. Whitesides, *Lab Chip*, 2010, **10**, 477-483.

22. A. Maattanen, P. Ihalainen, P. Pulkkinen, S. Wang, H. Tenhu and J. Peltonen, *ACS Appl Mater Interfaces*, 2012, **4**, 955-964.

23. N. Dossi, R. Toniolo, A. Pizzariello, F. Impellizzieri, E. Piccin and G. Bontempelli, *Electrophoresis*, 2013, **34**, 2085-2091.

24. V. Kumar and W. R. Heineman, *Analytical Chemistry*, 1987, **59**, 842-846.

25. V. Sosa, C. Barcelo, N. Serrano, C. Arino, J. M. Diaz-Cruz and M. Esteban, *Anal Chim Acta*, 2015, **855**, 34-40.

26. I. Švancara, C. Prior, S. B. Hočevar and J. Wang, *Electroanalysis*, 2010, **22**, 1405-1420.

27. J. Wang, J. Lu, S. B. Hocevar, P. A. M. Farias and B. Ogorevc, *Analytical Chemistry*, 2000, **72**, 3218-3222.

28. N. Ruecha, N. Rodthongkum, D. M. Cate, J. Volckens, O. Chailapakul and C. S. Henry, *Anal Chim Acta*, 2015, **874**, 40-48.

29. J. Yang, J. Y. Lee, L. X. Chen and H.-P. Too, *The Journal of Physical Chemistry B*, 2005, **109**, 5468-5472.

30. Z. Peng, Z. Jiang, X. Huang and Y. Li, *RSC Adv.*, 2016, **6**, 13742-13748.

31. S. Xing, H. Xu, J. Chen, G. Shi and L. Jin, *Journal of Electroanalytical Chemistry*, 2011, **652**, 60-65.

32. K. Tschulik, C. Batchelor-McAuley, H.-S. Toh, E. J. E. Stuart and R. G. Compton, *Physical Chemistry Chemical Physics*, 2014, **16**, 616-623.

33. B. Ding, M. Wang, X. Wang, J. Yu and G. Sun, *Materials Today*, 2010, **13**, 16-27.

34. S. Chaiyo, O. Chailapakul, T. Sakai, N. Teshima and W. Siangproh, *Talanta*, 2013, **108**, 1-6.

35. J. Volckens, C. Quinn, D. Leith, J. Mehaffy, C. S. Henry and D. Miller-Lionberg, *Indoor Air*, 2016, DOI: 10.1111/ina.12318, n/a-n/a.

36. D. M. Cate, P. Nanthasurasak, P. Riwkulkajorn, C. L'Orange, C. S. Henry and J. Volckens, *Annals of Occupational Hygiene*, 2014, **58**, 413-423.

37. K. Keawkim, S. Chuanuwatanakul, O. Chailapakul and S. Motomizu, *Food Control*, 2013, **31**, 14-21.

38. S. Chaiyo, E. Mehmeti, K. Zagar, W. Siangproh, O. Chailapakul and K. Kalcher, *Anal Chim Acta*, 2016, **918**, 26-34.

39. P. Rattanarat, W. Dungchai, D. Cate, J. Volckens, O. Chailapakul and C. S. Henry, *Anal Chem*, 2014, **86**, 3555-3562.

40. R. B. Channon, M. B. Joseph, E. Bitziou, A. W. Bristow, A. D. Ray and J. V. Macpherson, *Anal Chem*, 2015, **87**, 10064-10071.

41. I. W. Lenggoro, B. Xia, K. Okuyama and J. F. de la Mora, *Langmuir*, 2002, **18**, 4584-4591.

42. P. Chen, M. A. Fryling and R. L. McCreery, *Analytical Chemistry*, 1995, **67**, 3115-3122.

43. R. S. Nicholson, *Analytical Chemistry*, 1965, **37**, 1351-1355.

44. A. Bard and L. Faulkner, *Electrochemical Methods: Fundamentals and Applications*, John Wiley & Sons, Inc, 2001.

45. M. Li, D. W. Li, Y. T. Li, D. K. Xu and Y. T. Long, *Anal Chim Acta*, 2011, **701**, 157-163.

46. T. Wang, D. Zhao, X. Guo, J. Correa, B. L. Riehl and W. R. Heineman, *Anal Chem*, 2014, **86**, 4354-4361.

47. J. Wang, J. Lu, Ü. A. Kirgöz, S. B. Hocevar and B. Ogorevc, *Analytica Chimica Acta*, 2001, **434**, 29-34.

48. K. C. Armstrong, C. E. Tatum, R. N. Dansby-Sparks, J. Q. Chambers and Z.-L. Xue, *Talanta*, 2010, **82**, 675-680.

49. R. J. Taylor and A. A. Humffray, *Journal of Electroanalytical Chemistry and Interfacial Electrochemistry*, 1975, **64**, 85-94.

50. R. O. Kadara and I. E. Tothill, *Anal Chim Acta*, 2008, **623**, 76-81.

51. N. Promphet, P. Rattanarat, R. Rangkupan, O. Chailapakul and N. Rodthongkum, *Sensors and Actuators B: Chemical*, 2015, **207**, 526-534.

52. W. Song, L. Zhang, L. Shi, D.-W. Li, Y. Li and Y.-T. Long, *Microchimica Acta*, 2010, **169**, 321-326.

53. R. O. Kadara and I. E. Tothill, *Talanta*, 2005, **66**, 1089-1093.

CHAPTER 3. LOW-COST REUSABLE SENSOR FOR COBALT AND NICKEL DETECTION IN AEROSOLS USING ADSORPTIVE CATHODIC SQUARE-WAVE STRIPPING VOLTAMMETRY

Chapter Overview

A low-cost electrochemical sensor with Nafion/Bi modification using adsorptive stripping voltammetry for Co and Ni determination in airborne particulate matter and welding fume samples is described. Carbon stencil-printed electrodes (CSPEs) manufactured on low-cost PET films were utilized. Dimethylglyoxime (DMG) was used as a Co(II) and Ni(II) chelator with selective chemical precipitation for trace electrochemical analysis. Electrochemical studies of the Nafion/Bi-modified CSPE indicated a diffusion-controlled redox reaction for Co and Ni measurements. The Nafion coating decreased the background current and enhanced the measured peak current. Repeatability tests based on changes in percent relative standard deviation (RSD) of peak current showed the electrode could be used at least 15 times before the RSD exceeded 15% (the reported value of acceptable repeatability from Association of Official Analytical Chemists (AOAC)) due to deterioration of electrode surface. Limits of detection were 1 $\mu g\ L^{-1}$ and 5 $\mu g\ L^{-1}$ for Co and Ni, respectively, which were comparable to electrochemical sensors requiring more complicated modification procedures. The sensor produced a working range of 1-250 and 5-175 $\mu g\ L^{-1}$ for Co and Ni, respectively. Interference studies showed no other metal species interfered with Co and Ni measurements using the optimized conditions. Finally, the developed sensors were applied for Co and Ni determination in aerosol samples generated from Co rods and a certified welding-fume reference material, respectively. Validation with ICP-MS showed no statistically different results with 95% confidence between sensor and the ICP methods. This work was published in *Journal of Electroanalytical Chemistry*.[1]

Introduction

Co and Ni exposure are detrimental to human health depending on the magnitude and duration of exposure.[2-8] Occupational exposure to Co has been linked to a variety of respiratory tract and skin disorders such as skin lesions from allergy, inflammation of nasopharynx, and bronchial asthma.[5] Mortality from Co exposure can also occur when individuals reach to the final stage at which *cor pulmonale* and cardiorespiratory failure take place.[5] Long-term exposure to Ni has been associated with incidence of nasal cancer.[9] High occupational exposure of Co and Ni occurs primarily in industrial settings.[10] The amount of Co found in industrial areas can exceed 10 ng m^{-3}, which is substantially higher than in remote areas (1×10^{-4} ng m^{-3}).[11] Similarly, Ni can be released from a variety of industrial processes such as welding (e.g., from stainless steel), leading to high occupational exposures.[4,12] Therefore, measurement of Co and Ni in aerosols is important for understanding Co and Ni exposure.

Conventional measurements of Co and Ni measurements are performed using spectrophotometry coupled with flow injection analysis,[13] atomic absorption spectrometry,[14] x-ray fluorescence spectrometry,[15] and inductively coupled plasma spectroscopy.[16] These traditional methods require expensive and/or complicated equipment and long, laboratory-based analysis. Several fast, low-cost sensors have been proposed for metal detection.[17-22] Recently, we have achieved colorimetric detection for Ni in particulate matter (PM) with microfluidic paper-based analytical devices (μPADs).[19,23,24] Here, we describe a low-cost electrochemical sensor (less than $0.1) for Co and Ni with improved sensitivity and selectivity.[17,18,25,26] Several other reports utilized Hg thin film electrodes[27,28] or cation exchanger-modified electrodes[29] for detecting Co and Ni, but these electrodes require relatively complicated preparation procedures. Bi was also introduced to avoid the use of Hg while providing analogous analytical capability of forming metal amalgams

to generate well-defined peaks and reproducible stripping signals.[30-32] For trace Co(II) and Ni(II) analysis, dimethylglyoxime (DMG) has been used as a chelator to selectively complex Co(II) and Ni(II) before detecting these complexes with adsorptive stripping voltammetry that could adsorptively accumulate sub-ppb level of complexes on the working electrode.[33-35]

Here, carbon stencil-printed electrodes (CSPEs) were modified with bismuth, fabricated on polyethylene transparency (PET) sheets, and used to detect Co and Ni in particulate matter and welding fume. In the proposed method, DMG was employed as a chelating agent for complexing with Co and Ni and the complexes were detected by adsorptive cathodic stripping voltammetry. The ability of Bi-modified CSPE (BiCSPEs) to analyze Co(II)DMG and Ni(II)DMG was compared with that of unmodified CSPEs. Electrochemical characterization indicated a diffusion-controlled redox reaction for Co and Ni complexes. Nafion coating of the electrode surface enhanced peak current and lowered background current, improving the detection limit. Sensor precision was within the Association of Official Analytical Chemists (AOAC) relative standard deviation (RSD) limit of 15%.[36] Common metals that might interfere with Co and Ni measurements were analyzed and none of them showed significant interference. Finally, Nafion/BiCSPEs were applied for Co and Ni detection in aerosols and welding fume samples. Samples were validated with inductively coupled plasma mass spectrometry (ICP-MS) and the techniques provided statistically similar results. This work demonstrates the development of a low-cost, portable, and disposable sensor for Co and Ni with detection limits at ppb levels.

Experimental

Materials and methods

Zinc(II) nitrate, chromium(III) chloride, cobalt(II) chloride, aluminum sulfate, bismuth(III) oxide, sodium dodecyl sulfate (SDS), sodium acetate trihydrate, and trimethylsilylated Nafion®

were purchased from Sigma–Aldrich (St. Louis, MO). Potassium dichromate, iron(II) sulfate, iron(III) nitrate, manganese(II) chloride tetrahydrate, sodium nitrate, potassium nitrate, calcium nitrate tetrahydrate, hydrochloric acid, and ammonium chloride were purchased from Fisher Scientific (Waltham, MA). Copper(II) nitrate, ammonium hydroxide, sodium bicarbonate, and nitric acid were purchased from Mallinckrodt (St. Louis, MO). Nickel(II) sulfate hexahydrate was purchased from Acros (Morris, NJ). Dimethylglyoxime was purchased from Fluka (St. Louis, MO). Glacial acetic acid was purchased from EMD Millipore (Billerica, MA). Certified welding fume reference materials (SSWF-1 and MSWF-1) were obtained from Health & Safety Laboratory (Buxton, Derbyshire, UK). Milli-Q water from Millipore ($R \geq 18.2$ MΩ cm) was used for all experiments. All chemicals were used as received without further purification. Carbon Ink purchased from Ercon (Wareham, MA), graphite powder (diameter <20 μm, Sigma–Aldrich, St. Louis, MO), and transparency film PP2200 (3M, St. Paul, MN) were used for electrode fabrication. A 30 W Epilog Zing Laser Cutter and Engraver (Golden, CO) was used to create electrode patterns on a transparency sheet using Corel Draw X4 program for stencil printing. A CHI1242B potentiostat (CH Instruments) was used for all electrochemical measurements. Electrodes were imaged using a JSM-6500F scanning electron microscope (JEOL USA Inc., Peabody, MA).

Fabrication of CSPEs

CSPEs were prepared as previously described.[37-39] Home-made electrode inks were created by adding 0.43 g graphite to 1.00 g of the commercial carbon ink followed by hand mixing until homogeneous. All working, counter, and reference electrodes were stencil printed on a PET sheet through a laser-cut stencil. The circle-shape working electrode had 3 mm diameter. After printing, the electrodes were dried at 65 °C for 1 h. A laser-cut, ring-shaped piece of adhesive tape was used

for confining the solution droplet to the electrodes (Figure 3.1a). A photograph of a representative CSPE is shown in Figure 3.1b.

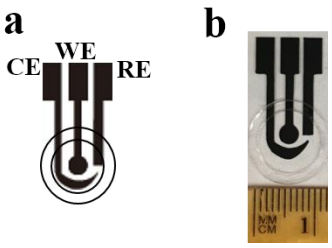

Figure 3.1: (a) Design drawing of a CSPE consisting of a counter electrode (CE), a working electrode (WE), and a reference electrode (RE) with a ring-shape packing tape to confine the sample droplet. (b) Photograph of a completed CSPE.

Electrode modification

Electrode modification of Nafion/Bi CSPE was accomplished by dropcasting 1 µL of 0.5% Nafion dissolved in 50% v/v isopropanol/water onto the CSPE working electrode and allowing it to dry. 50 µL of 10 mg mL^{-1} Bi_2O_3 in 0.1 M acetate buffer pH 4.5 was electroplated on the CSPE surface using an optimum deposition potential of -1.4 V vs. carbon pseudo-reference electrode and deposition time of 20 min. After Bi modification, the CSPE was rinsed with 0.01 M ammonium buffer pH 9.0 prior to use.

Electrochemical measurements

Cyclic voltammetry (CV) of 50 µg L^{-1} Co(II) and Ni(II) in 0.01 M ammonium buffer pH 9.0 (used as supporting electrolyte) containing 2 x 10^{-4} M DMG was performed using Nafion-modified BiCSPE (Nafion/BiCSPE). The potential was swept from -0.85 to -1.30 V versus a carbon pseudo-reference electrode with scan rates of 40-90 mV s^{-1}. Square-wave cathodic stripping voltammetry (SWCSV) was carried out by pipetting 50.0 µL of standard Co(II) and Ni(II) in 0.01 M ammonium buffer pH 9.0 containing 2 x 10^{-4} M DMG onto the electrode. An optimum

deposition potential was -0.85 V and the deposition time was varied from 15 s to 240 s as indicated in experimental details below. SWCSV was performed after a 10-s equilibration time from -0.9 to -1.5 V, and with an optimized step potential of 2 mV, amplitude of 25 mV, and frequency of 60 Hz.

Interference study

An interference study was performed using Cr(III), Cr(VI), Fe(II), Fe(III), Mn(II), Zn(II), Cu(II), Na(I), K(I), Ca(II), and Al(III) and the target metals, Co(II) and Ni(II). The mass ratios between the interfering metals and the target analytes were varied to determine tolerance ratios for potential interfering species. The tolerance ratio is defined as the mass ratio that creates a change in peak current of ±5%.[40]

Sample collection and sample preparation

Cobalt aerosol was generated from a cobalt rod (ESPI Metals, Ashland, OR) using an arc-discharge generator with ultra-pure nitrogen as the flow. Aerosol was collected on 37-mm MCE filters (SKC Limited, Dorset, UK). The mass of the Co aerosol samples is shown in Table 3.1. A 5-mm diameter punch was removed from the 37-mm diameter filter for CSPE analysis. Before quantifying Co(II), punches were digested using a modification to a previously published procedure[23]. The digestion was performed by adding 8 µL of 5% w/v SDS in Milli-Q water to aid in filter wetting and 2 µL of concentrated nitric acid onto the 5-mm diameter punch. The punch was then placed in a microwave on high power for 15 s and repeated twice (i.e., a total of three heated digestions for 45 s total). A 15 µL aliquot of 5% SDS was added to the punch between each heating step. Each punch was then neutralized with 2 M Na_2CO_3 after the last digestion step. Verification that the punch was neutralized was performed with pH paper. A 50 µL of 0.01 M ammonium buffer pH 9.0 containing 2 x 10^{-4} M DMG was used to elute metals from the digested

filter and the digestion container. 50 µL of the eluent was analyzed for Co(II) using the optimal settings described above from three punches of each sample filter to create replicate measurements.

Table 3.1: Mass of cobalt aerosol sampled onto 37mm filters

Cobalt Samples	Weight of Cobalt Aerosols (g)
1	4.361×10^{-5}
2	1.246×10^{-4}
3	6.611×10^{-5}
4	9.736×10^{-5}

Welding fume reference materials (SSWF-1 and MSWF-1) (the preparation was described in HSL report AS/2012/12)[41] were digested using aqua regia (3:1 of hydrochloric acid: nitric acid). The sample masses and volumes of aqua regia solution, water, and 2 M sodium bicarbonate (for neutralization) used are shown in Table 3.2.

Table 3.2: Aqua regia digestion

Sample (Certified Reference Material)	Mass of Samples (g)	Volume of Aqua Regia Solution (mL)	Volume of 2 M Sodium Bicarbonate (mL)	Volume of Water (mL)
SSWF-1	1.4	0.60	0.90	0.60
MSWF-1	1.2	0.46	0.90	0.74

Results and Discussion

Co and Ni determinations using unmodified and Bi modified CSPEs

The analytical behavior of BiCSPEs for measuring Ni(II) and Co(II) DMG complexes was compared to that of the unmodified CSPEs. Ammonium buffer at pH 9.0 was used in this work because it was previously reported to provide a wide potential window for Bi thin-film electrodes generated by electroplating [32]. Figure 3.2a shows a cathodic peak current (23.0 ± 1.1 µA) at -1.16 ± 0.05 V (vs C pseudo-reference) by reducing Co(II)DMG with a BiCSPE; alternatively, no

measurable peak is produced under these conditions with an unmodified CSPE. For detecting Ni(II)DMG with a BiCSPE (Figure 3.2b), the cathodic peak current (12.7 ± 0.8 µA) occurs at -1.07 ± 0.04 V and the peak is not present when using unmodified CSPE. These results demonstrate that BiCSPE can detect Co(II) and Ni(II) when these metals are complexed with DMG.

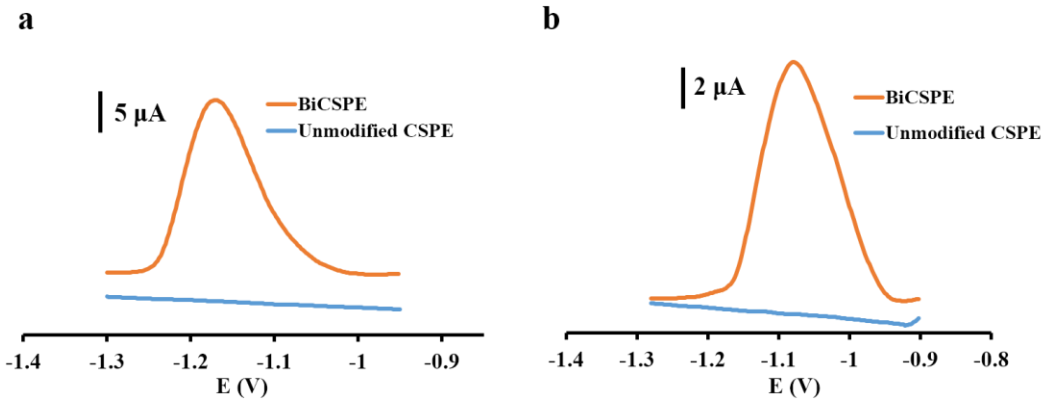

Figure 3.2: (a) Voltammograms of 100 µg L^{-1} Co(II)DMG complex using unmodified CSPE and Bi modified CSPE with 120 s deposition time. (b) Voltammograms of 100 µg L^{-1} Ni(II)DMG complex using unmodified CSPE and Bi modified CSPE with 120 s deposition time.

Electrochemical characterization

The mass transfer process of Co(II) and Ni(II) to BiCSPEs was studied as shown in Figure 3.3. In a diffusion-controlled electrochemical redox reaction, the peak current (i_p) shows a linear relationship with the square root of the scan rate as described by the Randles-Sevcik equation:[42]

$$i_p = (2.69 \times 10^5)\, n^{3/2} A D_0^{1/2} C \upsilon^{1/2},$$

where n is the number of electrons transferred in the redox reaction, A is the effective electrode area in cm^2, D is the diffusion coefficient in $cm^2\ s^{-1}$, C is the concentration in mol cm^{-3} and υ is the scan rate of the cyclic voltammogram in V s^{-1}. Figure 3.3 shows cyclic voltammograms at various scan rates of Co(II)DMG complex (Figure 3.3a) and Ni(II)DMG complex (Figure 3.3c). The peak currents (i_p) at various square roots of scan rate of Co(II)DMG and Ni(II)DMG complexes detection are shown in Figures 3.3b and 3.3d, respectively. The peak current increases

linearly with the square root of the scan rate for both complexes, suggesting that the mass transfer process is diffusion-controlled. Moreover, the adsorption of Co(II)DMG and Ni(II)DMG existed on BiCSPE that was observed from the linear relationship between peak currents and scan rates as shown in Figure 3.4a and 3.4b. However, the correlation coefficients (R^2) of the linear fit from diffusion controlled process (R^2 = 0.994 for Co and 0.965 for Ni) were better than those from the adsorption process (R^2 = 0.982 for Co and 0.943 for Ni). Therefore, the mass transfer process for Co and Ni was predominantly controlled by the diffusion process. Additionally, cyclic voltammograms of both Co(II)DMG (Figure 3.3a) and Ni(II)DMG (Figure 3.3c) show one peak during cathodic scan and no peak during anodic scan, indicating the reduction of the complexes is irreversible. The peak potential appears to shift with increasing scan rate caused by the decrease of electron transfer rate constant.[43] In addition, a CV was recorded in 0.1 M ammonium buffer pH 9.0 containing 2 x 10^{-4} M DMG (Figure 3.5) demonstrated that the appearance of the slopped background in the cyclic voltammograms of Co(II)DMG and Ni(II)DMG was due to the onset of oxygen reduction at -1.25 V.[44]

Effect of Nafion coating and Bi electroplating time

Nafion was utilized to enhance detection current. Nafion, as a cation exchange polymer, is insoluble in water, electrochemically inert, and non-electroactive making it suitable for electrode modification.[45] The sulfonate group in Nafion allows selective preconcentration of cations resulting in improved detection performance.[46] Figure 3.6a shows coating Nafion onto CSPE before Bi-electroplating increased the peak current of Co(II)DMG to 12.2 μA from 4.8 μA without Nafion coating.

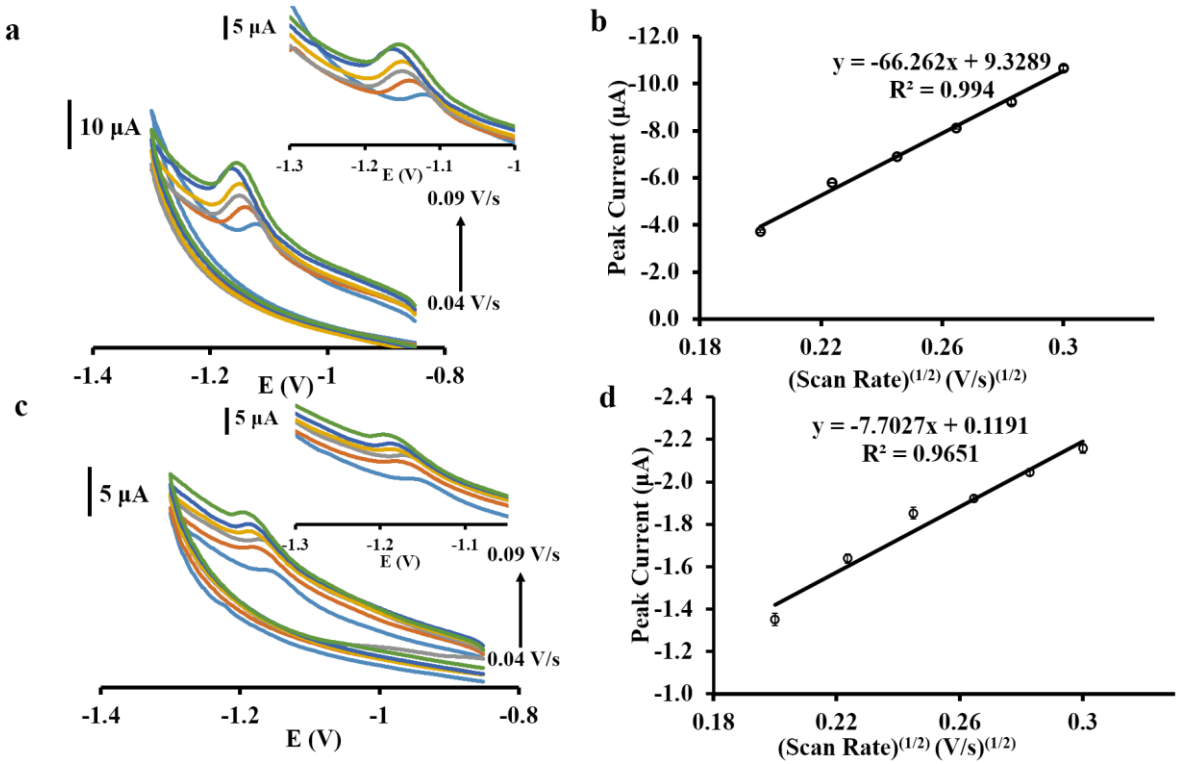

Figure 3.3: (a) Cyclic voltammograms of 50 µg L^{-1} Co(II)DMG complex using Bi modified CSPE with different scan rates (40-90 mV s^{-1}). The expansion of reduction peaks of Co(II)DMG is shown in inset. (b) Relationship between peak current and square root of scan rate from (a) (n=3). (c) Cyclic voltammograms of 50 µg L^{-1} Ni(II)DMG complex using Bi modified CSPE with different scan rates (40-90 mV s^{-1}). The expansion of reduction peaks of Ni(II)DMG is shown in inset. (d) Relationship between peak current and square root of scan rate from (c) (n=3).

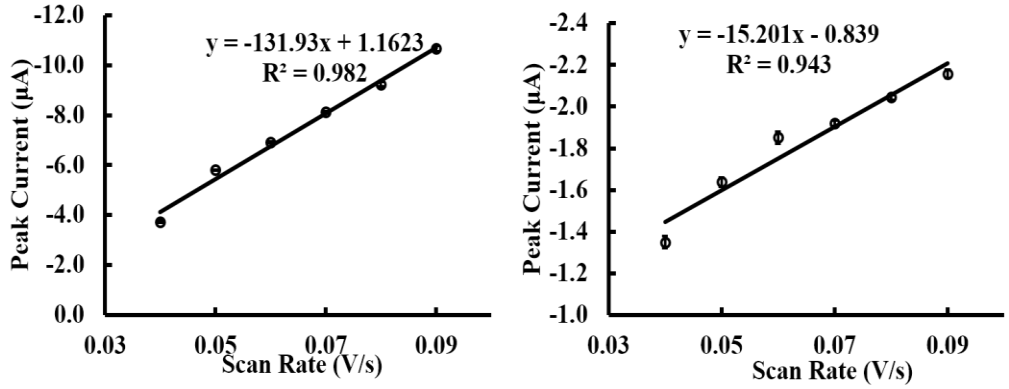

Figure 3.4: (a) Relationship between peak current and scan rate from Figure 3.3a for Co(II)DMG (n=3). (b) Relationship between peak current and scan rate from Figure 3.3c for Ni(II)DMG (n=3).

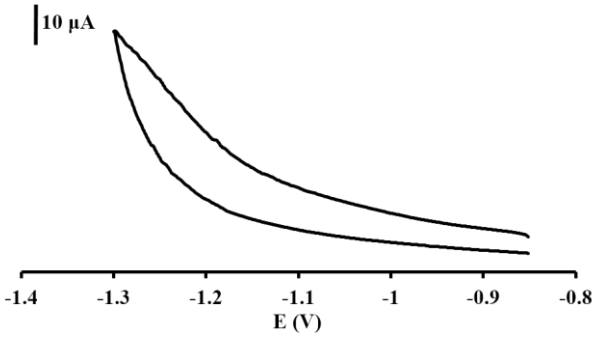

Figure 3.5: Cyclic voltammograms of 0.1 M ammonium buffer pH 9.0 containing 2 x 10^{-4} M DMG using Bi modified CSPE at 0.09 V s^{-1} of scan rate.

We also investigated the influence of electrochemical deposition time for electroplating Bi on CSPEs for Co(II) and Ni(II) detection (Figure 3.6b). As expected, when increasing the deposition time, the current density (defined as the ratio of peak current [µA] to area of the working electrode [28.3 mm^2]) for both Co(II)DMG and Ni(II)DMG increases until reaching a plateau at 20 min. Therefore, 20 min was chosen as an optimum time for electroplating Bi on CSPEs.

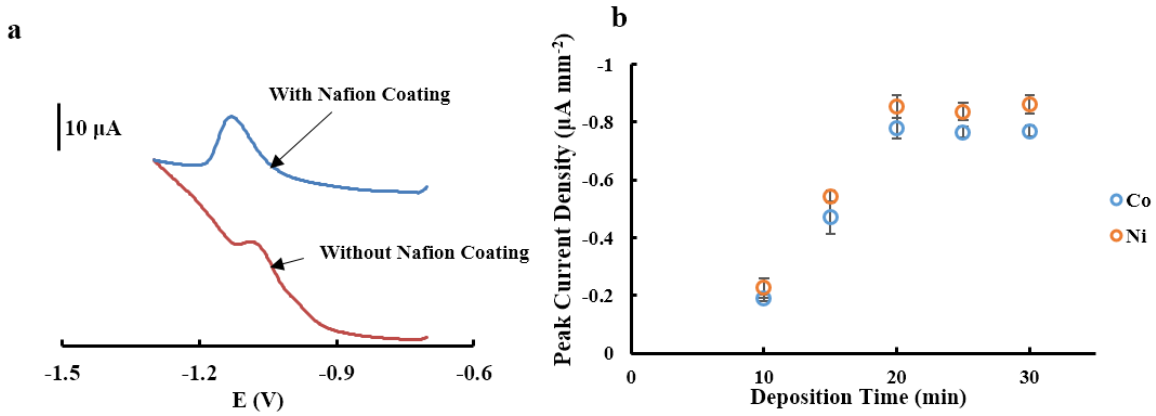

Figure 3.6: (a) Square-wave voltammograms of 100 µg L^{-1} Co(II)DMG complex using Bi modified CSPE with/without Nafion coating using 120 s deposition time. (b) Representative graph for 100 µg L^{-1} Co(II)DMG and 100 µg L^{-1} Ni(II)DMG at various electrodeposition times of Bi (n=3).

Repeatability of Nafion/BiCSPE for Co(II) and Ni(II) detections

After optimizing the detection conditions of Nafion/BiCSPE, the electrode lifetime was tested by determining how many runs could be performed with a single low-cost electrode system.

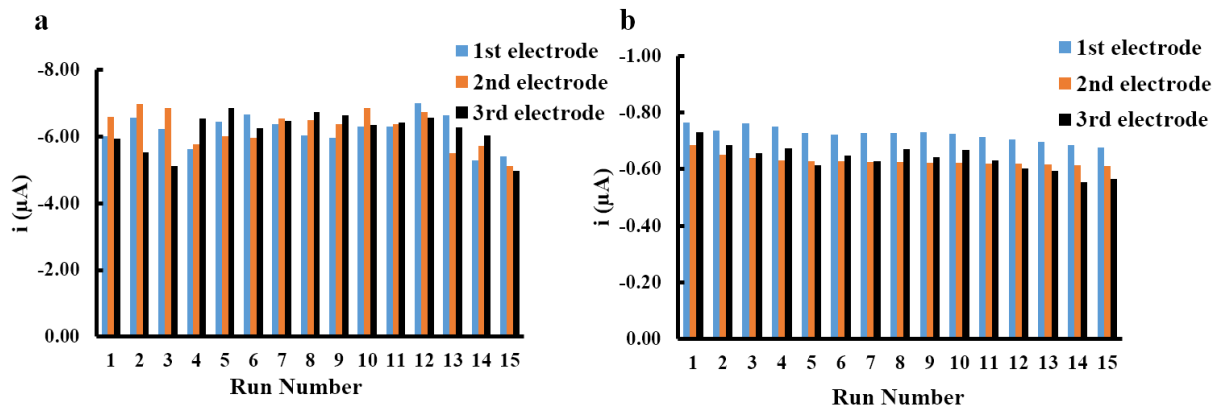

Figure 3.7: (a) Repeatability of three Nafion/BiCSPEs to measure current of 50 µg L^{-1} Co(II)DMG complex using 15 s deposition time. (b) Repeatability of three electrodes to measure current of 50 µg L^{-1} Ni(II)DMG complex using 45 s deposition time.

Repeated runs using the same electrode for standard Co and Ni measurements were performed as shown in Figure 3.6. Three separated Nafion/BiCSPE (n=3) were used to determine repeatability of each metal (labelled in different colors in Figure 3.7). The peak currents were stable for 15 runs as shown in Figure 3.7a (Co(II)) and Figure 3.7b (Ni(II)). The %RSDs (7.3 ± 0.5 % for Co(II) and 9.1 ± 0.6 % for Ni(II)) of 15 runs for Co(II) are less than the reported value from AOAC (for the detection in µg L^{-1} level) (15%) on three separated Nafion/BiCSPEs.[36] The results indicate that Nafion/BiCSPEs can be used for up to 15 times. No attempt was made to extend the system beyond 15 runs given the low-cost of the electrodes. For Ni(II) detection (Figure 3.7b), the modified electrodes also provided acceptable repeatability with %RSDs of 15 runs <15%. However, %RSDs of Nafion/BiCSPEs at run 12 to 15 for Ni(II) detection increased slightly, which is different from Co(II) detection where %RSDs maintained stable for 15 runs. We hypothesized that the deposition time of each metal caused a change in the surface morphology leading to smaller peak currents. This assumption was verified by imaging the surface of the Nafion/BiCSPE with scanning electron microscopy (Figure 3.8). When comparing the surface after measuring Co(II) (Figure 3.8c) and Ni(II) (Figure 3.8d), Nafion (represented as the bright flat sheets) and Bi (represented as the small

crystals) were more deteriorated than those on the surface of the unused CSPE (Figure 3.8b). Moreover, as hypothesized, the electrode morphology when detecting Ni(II) with 45 s deposition time (Figure 3.8d) changed more than that for the Co(II) measurement that required a 15 s deposition time (Figure 3.8c).

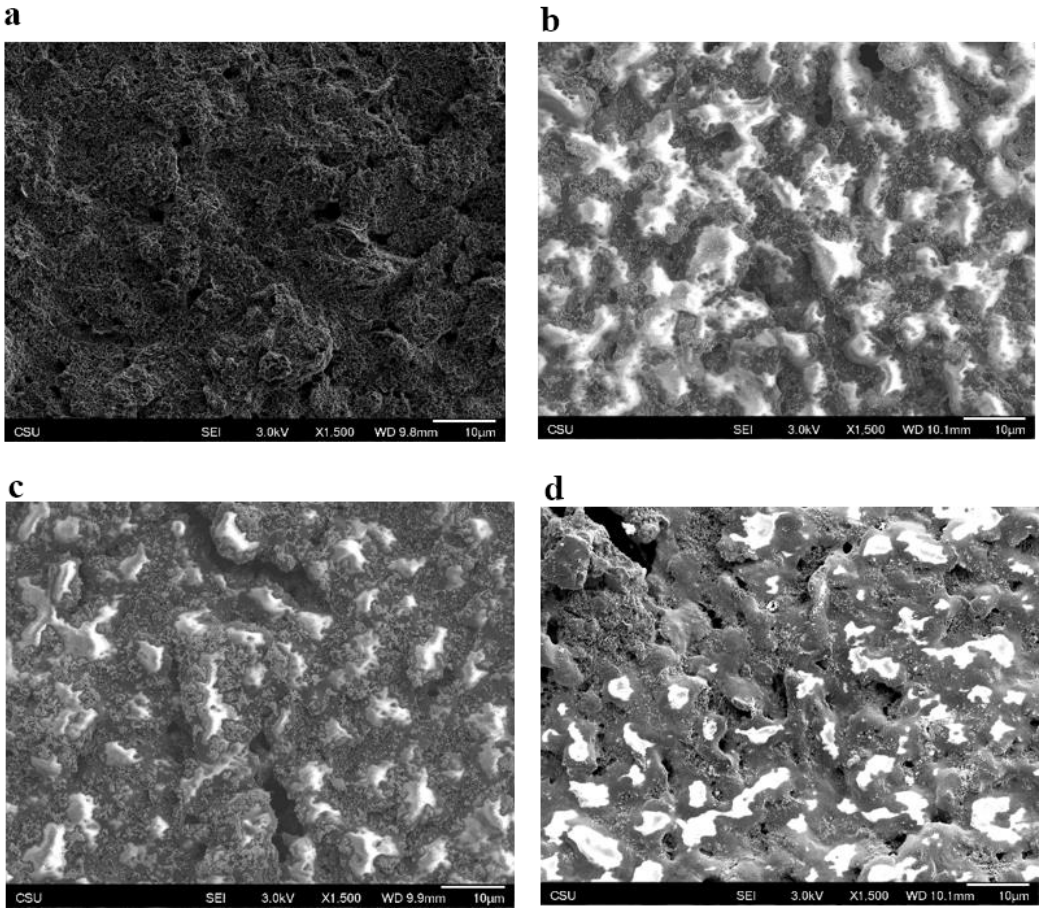

Figure 3.8: (a) SEM images of CSPE. (b) Nafion/BiCSPE. (c) Nafion/BiCSPE after 20 runs of 50 µg L^{-1} Co(II)DMG complex. (d) Nafion/BiCSPE after 20 runs of 50 µg L^{-1} Ni(II)DMG complex.

Electrochemical measurement of Co(II) and Ni(II)

The linear working ranges for measuring Co(II) and Ni(II) at Nafion/BiCSPE are shown in Figure 3.9. The decrease of current density at high concentration of Ni(II)DMG (200 µg L^{-1}) in Figure 3.8d was caused by electrode fouling bringing about incomplete reduction of Ni(II)DMG.[47]

The Bi deposition time significantly influenced the linear ranges of Co(II) and Ni(II) as shown in Table 3.3. The widest linear range was observed when using the deposition time of 15 s and 45 s for Co(II) (20-250 μg L^{-1}) and Ni(II) (50-175 μg L^{-1}), respectively. Longer Bi deposition time allowed detection at lower concentration ranges for Co(II) and Ni(II) (1-50 μg L^{-1} for Co(II)) and 5-50 μg L^{-1} for Ni(II)) at 240 s deposition time). Likewise, a longer deposition time provided lower LODs than a shorter deposition time. LODs for Co(II) and Ni(II) using 240 s deposition time were 1 μg L^{-1} and 5 μg L^{-1}, respectively. The LODs of Co(II) and Ni(II) detection at each deposition time are summarized in Table 3.3. The voltammograms and calibration curves for Co and Ni using 120 s and 240 s deposition time are shown in Figures 3.10 and 3.11, respectively.

Table 3.3: Linearity range with various deposition times

Deposition Time (s)	Co(II) (μg L^{-1})		Ni(II) (μg L^{-1})	
	Linearity range	LOD	Linearity range	LOD
15	20-250	20	-	-
45	-	-	50-175	50
120	20-100	20	20-75	20
240	1-50	1	5-50	5

Interference study

As the goal of this work is to detect Ni and Co in sample matrices such as welding fume, the tolerance ratio for key interferences was determined. The tolerance ratio is defined as the mass ratio of an interfering species relative to the target metal that gives a change in peak current of ±5%.[40] The tolerance ratios between interfering species and Co(II) and Ni(II) are shown in Table 3.4. The results indicated that none of the tested interfering elements affected Co(II) and Ni(II)

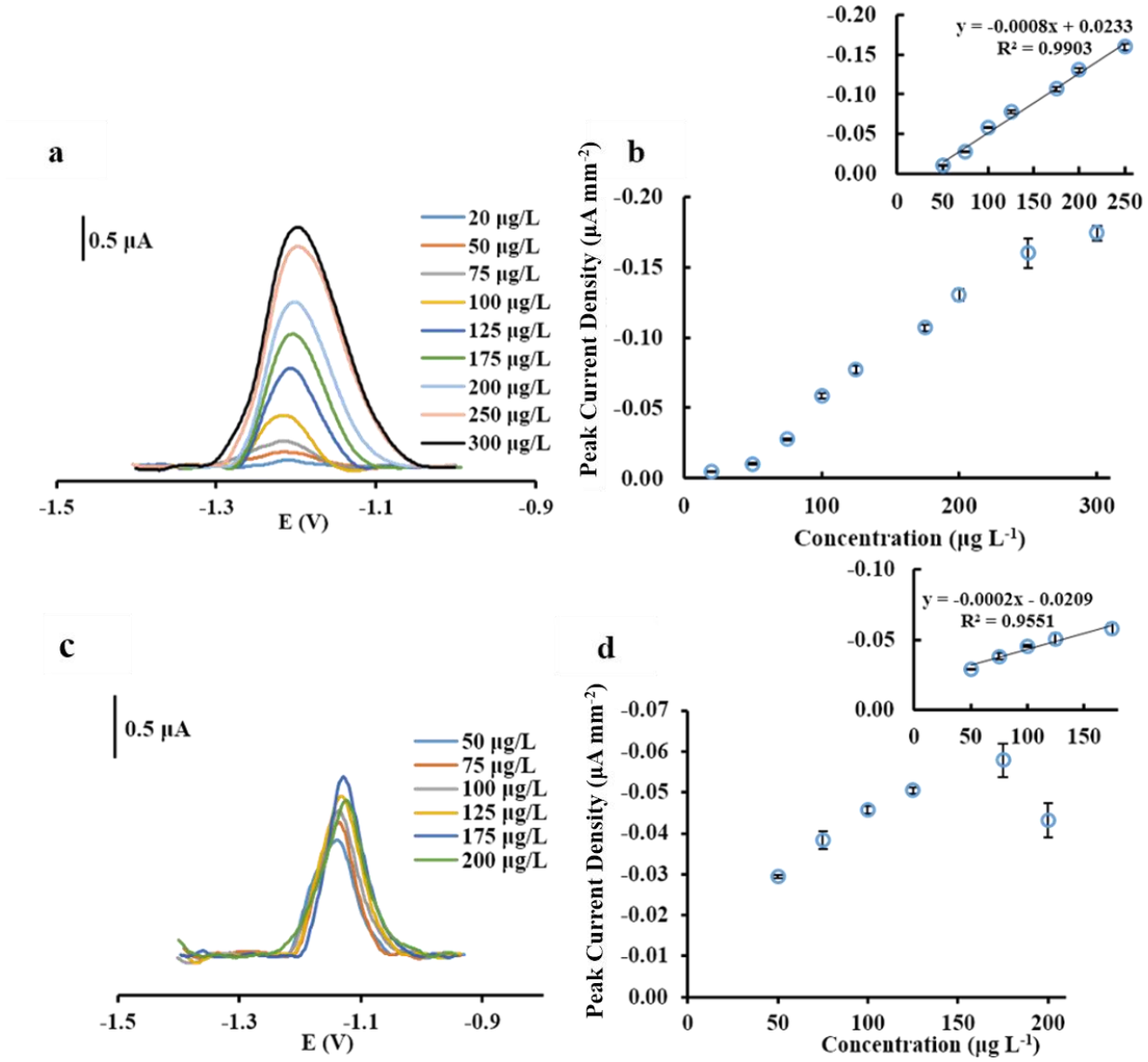

Figure 3.9: (a) Square-wave voltammograms of Co(II)DMG complex from 1-100 µg L^{-1} using 15 s deposition time. (b) Representative calibration graph for Co(II)DMG complex. Linear fit of calibration graph for Co(II)DMG complex (b inset) (n=3). (c) Square-wave voltammograms of Ni(II)DMG complex from 5-100 µg L^{-1} using 45 s deposition time. (d) Representative calibration graph for Ni(II)DMG complex. Linear fit of calibration graph for Co(II)DMG complex (d inset) (n=3).

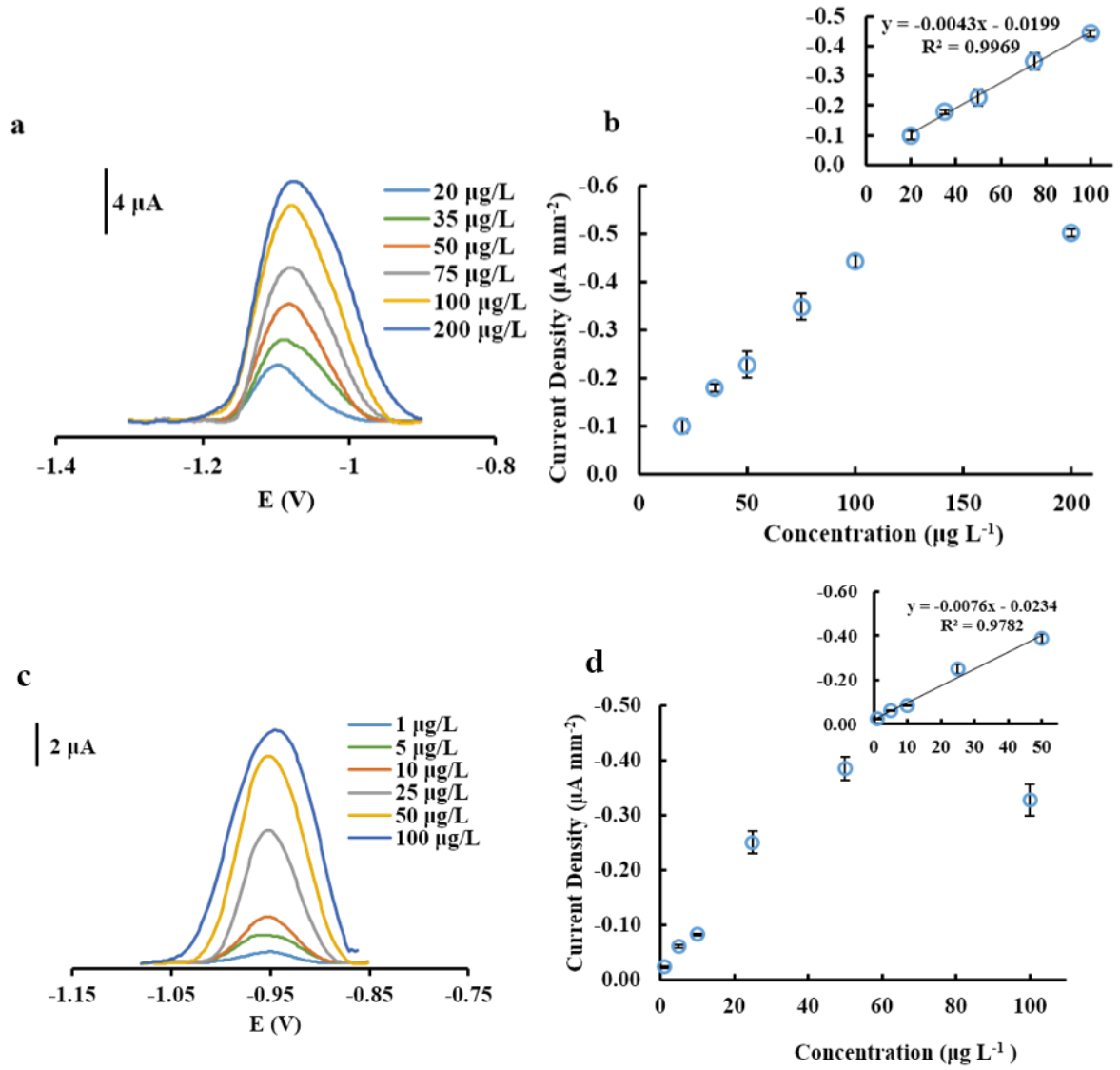

Figure 3.10: (a) Square-wave voltammograms of Co(II)DMG complex from 20-200 µg L^{-1} using 120 s deposition time. (b) Representative calibration graph for Co(II)DMG complex using 120 s deposition time. Linear fit of calibration graph for Co(II)DMG complex using 120 s deposition time (b inset). (c) Square-wave voltammograms of Co(II)DMG complex from 1-100 µg L^{-1} using 240 s deposition time. (d) Representative calibration graph for Co(II)DMG complex using 240 s deposition time. Linear fit of calibration graph for Co(II)DMG complex using 240 s deposition time (d inset).

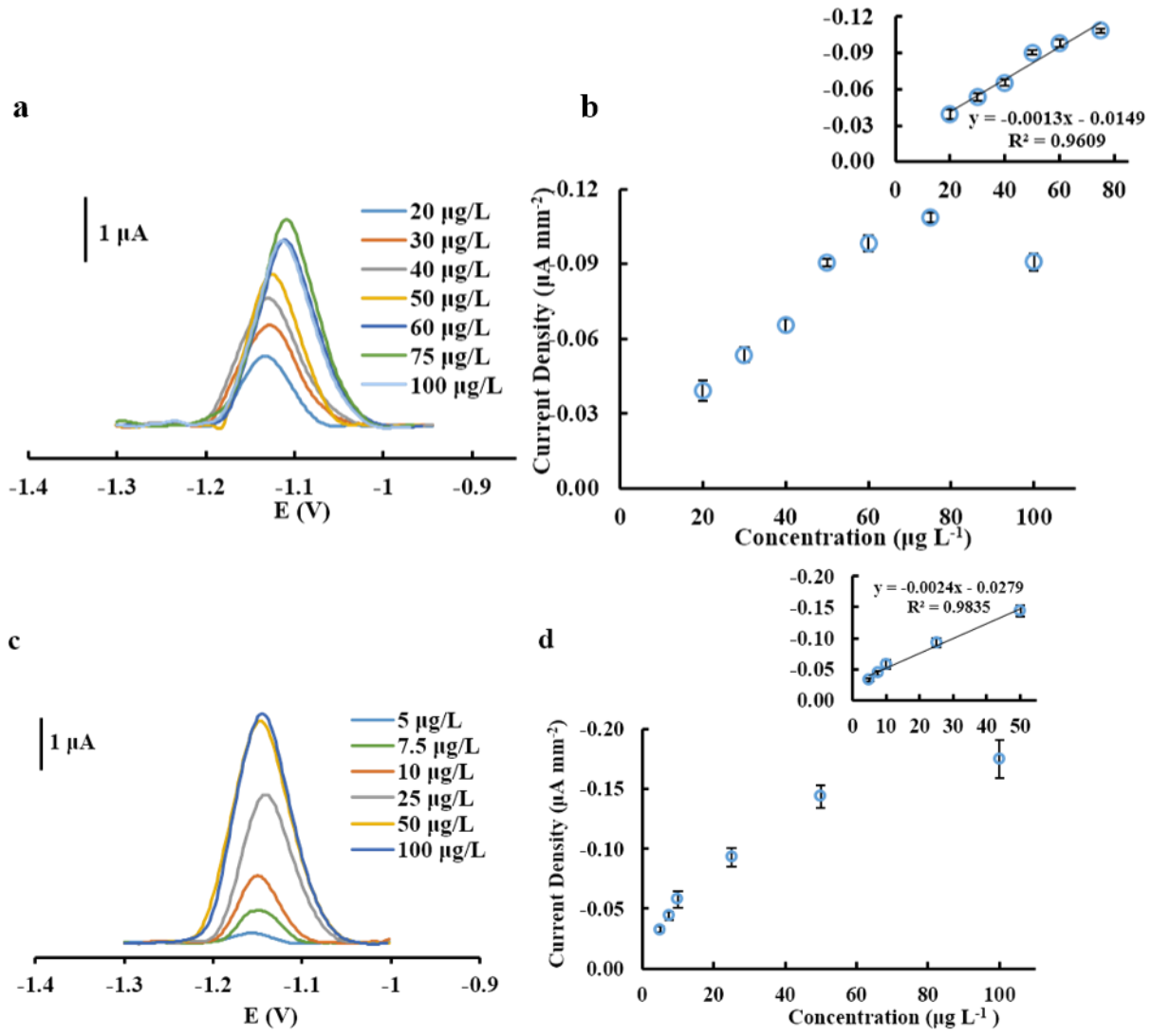

Figure 3.11: (a) Square-wave voltammograms of Ni(II)DMG complex from 20-100 µg L^{-1} using 120 s deposition time. (b) Representative calibration graph for Ni(II)DMG complex using 120 s deposition time. Linear fit of calibration graph for Ni(II)DMG complex using 120 s deposition time (b inset) (c) Square-wave voltammograms of Ni(II)DMG complex from 5-100 µg L^{-1} using 240 s deposition time. (d) Representative calibration graph for Ni(II)DMG complex using 240 s deposition time. Linear fit of calibration graph for Co(II)DMG complex using 240 s deposition time (d inset)

detection at a significant level except Cu(II). The tolerance ratio between Cu(II) and Ni(II) was low because DMG can also chelate with Cu(II).[48] While there are known strategies to address Cu interferences, Cu(II) is present at very low levels in welding fume and related samples making removal of the interference unnecessary. As a result, the proposed method showed selectivity and sensitivity toward Co(II) and Ni(II) to enable analysis of aerosol samples and welding fume samples.

Co(II) and Ni(II) detections in environmental samples

Adsorptive cathodic stripping square-wave voltammetry was applied for detecting Co(II) and Ni(II) through complexing with DMG in Cobalt-generated aerosol and welding fume samples. The voltammograms for Co(II) determination are shown in Figure 3.12a. The amount of Co(II) measured by Nafion/BiCSPE and the validation method (ICP-MS) was summarized in Table 3.5. In the case of Ni(II) determination, the signal of Ni(II)DMG in welding fume reference materials (SSWF-1 and MSWF-1) is shown in Figure 3.12b. The amount of Ni(II) detected in SSWF-1 was

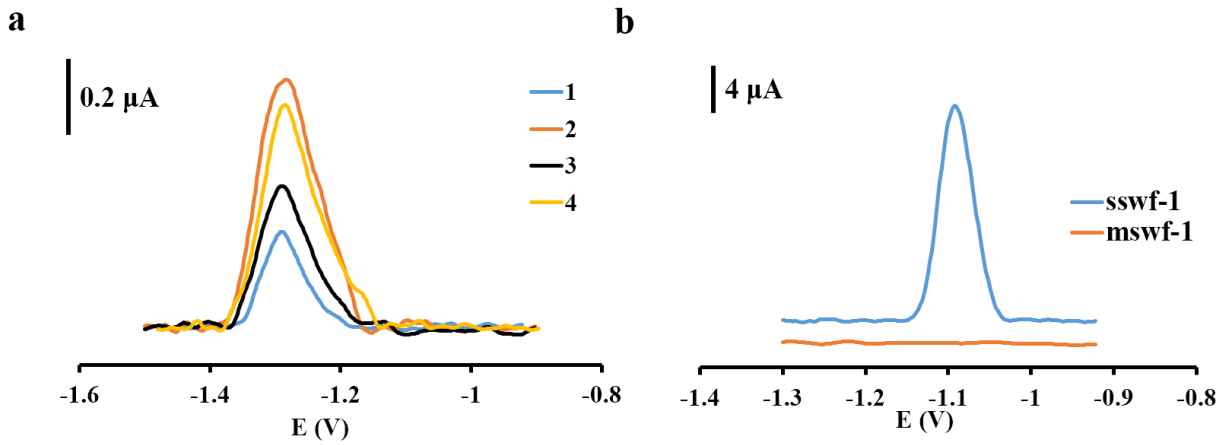

Figure 3.12: (a) Square-wave voltammograms of Co determination in aerosol samples. (b) Ni determination in welding fume samples (sswf-1 and mswf-1 certified reference materials).

Table 3.4: Tolerance ratio of interfering ions in the electrochemical determination of 100 μg L^{-1} of Co(II)DMG complex and Ni(II)DMG complex

Interference	Tolerance Ratio for Co(II)DMG Complex	Tolerance Ratio for Ni(II)DMG Complex
Cr^{3+}	500	500
Cr^{6+}	100	100
Fe^{2+}/Fe^{3+}	500	50
Mn^{2+}	>500	50
Zn^{2+}	100	>500
Cu^{2+}	100	10
Na^{+}	100	500
K^{+}	100	100
Ca^{2+}	100	500
Al^{3+}	>500	>500

3.3 ± 0.2 %, close to the certified value (3.7%) as shown in Table 4. For MSWF-1, the amount of Ni(II) was under detection limit and corresponded to the reference data showing that the sample did not contain Ni(II). Quantitation of Co(II) and Ni(II) in different samples is summarized in Table 3.5 and 3.6, respectively. A paired Student's *t*-test was used to compare measured Co(II) values between Nafion/BiCSPE and ICP-MS. For Co, the t value (-9.00) is less than the critical t value (3.182, P=0.05) for n-1=3 degrees freedom when n = 4 implying that the null hypothesis is not rejected. Therefore, the proposed method does not provide significantly different results with 95% confidence for Co detection.

Conclusion

A home-made Nafion/BiCSPE was fabricated for trace Co(II) and Ni(II) determination by chelating with DMG. The proposed sensors provided LODs of 1 μg L^{-1} and 5 μg L^{-1} for Co(II) and Ni(II), respectively. The key factor leading to improved performance was the electroplating of a

thin film of Bi onto the electrode surface. Nafion coating also enhanced peak current and decreased background current. The resulting electrodes and chemistry allowed for repeated Co(II) and Ni(II) measurements up to 15 times based on changes in %RSD. Furthermore, the Nafion/BiCSPE was selective for Co(II) and Ni(II) against other possible metal interferences. Cu(II) was the only element that caused a significant change in signal but was not a problem with the target samples because of its low concentration. The resulting system was used to measure Co(II) and Ni(II) in aerosol samples and welding fume, respectively. Results from the electroanalytical system were statistically similar with the results from ICP-MS (for Co) and close to certified values (for Ni). The results show that the Nafion/BiCSPEs using adsorptive stripping voltammetry have great potential for selective and sensitive determination of Co(II) and Ni(II) in environmental applications.

Table 3.5: Co(II) Determination in aerosol samples (n=3)

Sample	Concentration of Co (μg)	
	BiCSPE	ICP-MS
1	36 ± 1.4	41 ± 0.9
2	40 ± 1.2	43 ± 1.0
3	37 ± 1.1	42 ± 0.8
4	59 ± 1.9	64 ± 1.3

Table 3.6: Ni(II) Determination in welding fume samples (n=3)

Sample (Certified Reference Material)	%Ni (Experimental value)	%Ni (theoretical value)
SSWF-1	3.3±0.2	3.7
MSWF-1	below LOD	0

REFERENCES

1. J. Mettakoonpitak, D. Miller-Lionberg, T. Reilly, J. Volckens and C. S. Henry, *Journal of Electroanalytical Chemistry*, 2017, **805**, 75-82.
2. A. Léonard and R. Lauwerys, *Mutation Research/Reviews in Genetic Toxicology*, 1990, **239**, 17-27.
3. E. Denkhaus and K. Salnikow, *Critical Reviews in Oncology/Hematology*, 2002, **42**, 35-56.
4. D. Schaumlöffel, *Journal of Trace Elements in Medicine and Biology*, 2012, **26**, 1-6.
5. R. Lauwerys and D. Lison, *Science of The Total Environment*, 1994, **150**, 1-6.
6. M. Goldoni, S. Catalani, G. De Palma, P. Manini, O. Acampa, M. Corradi, R. Bergonzi, P. Apostoli and A. Mutti, *Environmental Health Perspectives*, 2004, **112**, 1293-1298.
7. E. MASTROMATTEO, *Journal of Occupational and Environmental Medicine*, 1967, **9**, 127-136.
8. D. J. Paustenbach, B. E. Tvermoes, K. M. Unice, B. L. Finley and B. D. Kerger, *Critical Reviews in Toxicology*, 2013, **43**, 316-362.
9. M. Costa, T. L. Davidson, H. Chen, Q. Ke, P. Zhang, Y. Yan, C. Huang and T. Kluz, *Mutation Research/Fundamental and Molecular Mechanisms of Mutagenesis*, 2005, **592**, 79-88.
10. G. Scansetti, G. Maina, G. C. Botta, P. Bambace and P. Spinelli, *International Archives of Occupational and Environmental Health*, 1998, **71**, 60-63.

11. D. Lison, in *Handbook on the Toxicology of Metals (Fourth Edition)*, eds. B. A. Fowler and M. Nordberg, Academic Press, San Diego, 2015, DOI: http://dx.doi.org/10.1016/B978-0-444-59453-2.00034-2, pp. 743-763.

12. B. Sjögren, K. S. Hansen, H. Kjuus and P. G. Persson, *Occup Environ Med*, 1994, **51**, 335-336.

13. P. B. Martelli, B. F. Reis, E. A. M. Kronka, H. B. Ƒ, M. Korn, E. A. G. Zagatto, J. F. C. Lima and A. N. Araujo, *Analytica Chimica Acta*, 1995, **308**, 397-405.

14. A. Profumo, G. Spini, L. Cucca and M. Pesavento, *Talanta*, 2003, **61**, 465-472.

15. T. G. Dzubay and R. K. Stevens, *Environmental Science & Technology*, 1975, **9**, 663-668.

16. P. Kulkarni, S. Chellam, J. B. Flanagan and R. K. M. Jayanty, *Analytica Chimica Acta*, 2007, **599**, 170-176.

17. N. A. Meredith, C. Quinn, D. M. Cate, T. H. Reilly, J. Volckens and C. S. Henry, *Analyst*, 2016, **141**, 1874-1887.

18. D. M. Cate, J. A. Adkins, J. Mettakoonpitak and C. S. Henry, *Analytical Chemistry*, 2015, **87**, 19-41.

19. D. M. Cate, S. D. Noblitt, J. Volckens and C. S. Henry, *Lab Chip*, 2015, **15**, 2808-2818.

20. A. W. Martinez, S. T. Phillips, G. M. Whitesides and E. Carrilho, *Analytical Chemistry*, 2010, **82**, 3-10.

21. M. M. Mentele, J. Cunningham, K. Koehler, J. Volckens and C. S. Henry, *Analytical Chemistry*, 2012, **84**, 4474-4480.

22. Y. Lin, D. Gritsenko, S. Feng, Y. C. Teh, X. Lu and J. Xu, *Biosensors and Bioelectronics*, 2016, **83**, 256-266.

23. D. M. Cate, P. Nanthasurasak, P. Riwkulkajorn, C. L'Orange, C. S. Henry and J. Volckens, *Annals of Occupational Hygiene*, 2014, DOI: 10.1093/annhyg/met078.

24. P. Rattanarat, W. Dungchai, D. Cate, J. Volckens, O. Chailapakul and C. S. Henry, *Analytical Chemistry*, 2014, **86**, 3555-3562.

25. J. Adkins, K. Boehle and C. Henry, *ELECTROPHORESIS*, 2015, **36**, 1811-1824.

26. J. Mettakoonpitak, K. Boehle, S. Nantaphol, P. Teengam, J. A. Adkins, M. Srisa-Art and C. S. Henry, *Electroanalysis*, 2016, **28**, 1420-1436.

27. J. M. Zen and M. L. Lee, *Analytical Chemistry*, 1993, **65**, 3238-3243.

28. A. Economou and P. R. Fielden, *Analyst*, 1993, **118**, 1399-1404.

29. P. González, V. A. Cortínez and C. A. Fontán, *Talanta*, 2002, **58**, 679-690.

30. A. Królicka and A. Bobrowski, *Electrochemistry Communications*, 2004, **6**, 99-104.

31. J. Wang, J. Lu, S. B. Hocevar, P. A. M. Farias and B. Ogorevc, *Analytical Chemistry*, 2000, **72**, 3218-3222.

32. E. A. Hutton, B. Ogorevc, S. B. Hočevar, F. Weldon, M. R. Smyth and J. Wang, *Electrochemistry Communications*, 2001, **3**, 707-711.

33. M. Morfobos, A. Economou and A. Voulgaropoulos, *Analytica Chimica Acta*, 2004, **519**, 57-64.

34. F. O. Tartarotti, M. F. de Oliveira, V. R. Balbo and N. R. Stradiotto, *Microchimica Acta*, 2006, **155**, 397-401.

35. R. P. Baldwin, J. K. Christensen and L. Kryger, *Analytical Chemistry*, 1986, **58**, 1790-1798.

36. A. International, *Official methods of analysis of AOAC International*.

37. N. Ruecha, N. Rodthongkum, D. M. Cate, J. Volckens, O. Chailapakul and C. S. Henry, *Analytica Chimica Acta*, 2015, **874**, 40-48.

38. K. E. Berg, J. A. Adkins, S. E. Boyle and C. S. Henry, *Electroanalysis*, 2016, **28**, 679-684.

39. J. Mettakoonpitak, J. Mehaffy, J. Volckens and C. S. Henry, *Electroanalysis*, 2017, **29**, 880-889.

40. S. Chaiyo, O. Chailapakul, T. Sakai, N. Teshima and W. Siangproh, *Talanta*, 2013, **108**, 1-6.

41. .

42. A. J. Bard and L. R. Faulkner, *Electrochemical Methods: Fundamentals and Applications*, Wiley, 2000.

43. R. S. Nicholson, *Analytical Chemistry*, 1965, **37**, 1351-1355.

44. J. Wang and J. Lu, *Electrochemistry Communications*, 2000, **2**, 390-393.

45. F. Torma, A. Grün, I. Bitter and K. Tóth, *Electroanalysis*, 2009, **21**, 1961-1969.

46. T. Wang, D. Zhao, X. Guo, J. Correa, B. L. Riehl and W. R. Heineman, *Anal Chem*, 2014, **86**, 4354-4361.

47. D. G. Davis and E. A. Boudreaux, *Journal of Electroanalytical Chemistry (1959)*, 1964, **8**, 434-441.

48. A. Bobrowski, *Electroanalysis*, 1996, **8**, 79-88.

CHAPTER 4. ENHANCED PAPER ELECTROPHORETIC SEPARATIONS USING PARAFILM-PAPER-BASED ANALYTICAL DEVICES

Chapter Overview

Microfluidic paper-based analytical devices (mPADs) have gained significant attention in recent years for applications ranging from clinical diagnostics to environmental testing. However, separation on mPADs remain challenging to implement, particularly in complex samples. This has revived interest in revisiting paper chromatography and paper electrophoresis in mPADs to address these needs. Here, laminated Parafilm-paper (l-paper) is applied to fabricate electrophoretic devices. This approach yields a free-standing channel, leading to improved peak resolution relative to previous electrophoretic separations in traditional wax-printed mPADs. Major factors influencing the separation, including Joule heating, electroosmotic flow, and electrophoretic mobility, were investigated. As a result of paper's high ratio of surface area (78%) to pore volume (22%) resulting in slow heat dissipation, a usable applied field strength range of 0 - 200 V cm^{-1} was employed to avoid Joule heating. The electroosmotic flow of the system was found to be $2.5 \times 10^{-5} \pm 7.7 \times 10^{-7}$ cm^2 $V^{-1}s^{-1}$ and the electrophoretic mobility of chlorophenol red was $1.2 \times 10^{-4} \pm 7.7 \times 10^{-7}$ cm^2 $V^{-1}s^{-1}$. Basic separation protocols were optimized using colorimetric detection of chlorophenol red and indigo carmine dyes as representative molecules. Paper type, channel width, and applied potential were then used to optimize the separations. Addition of an injection port to the device improved resolution and reduced peak broadening. Finally, the separation of fluorescein isothiocyanate (FITC) and L-glutamic acid (Glu) labeled with FITC, was successfully carried out using the l-paper electrophoretic device. Imaging with a microscope was found to achieve reduced peak broadening and increased resolution relative to imaging with a mobile camera, due to

elimination of background signal, achieving a 72 ± 4% conjugation of Glu and FITC. This work is submitted to *Sensors and Actuators B: Chemical*.[1]

Introduction

Simple, low-cost, portable microfluidic paper-based analytical devices (mPADs) have been widely used for biomedical, environmental, and food and beverage contamination analysis.[2-6] Most mPAD developments aim to improve figures of merit for detection by coupling mPADs with sensitive detection techniques and/or using chemical modification to increase accuracy and extend the detectable concentration range.[7] Moreover, incorporating functionality to mPADs for reducing detection time and improving multiplexed detection has been reported.[2,6,8,9] Despite the recent developments, chemical separations from complex mixtures are limited, hindering analysis of complex samples such as biological, environmental, and clinical samples.[10] Consequently, the integration of chromatographic separation functions into mPADs has been proposed.[11,12] Low separation efficiency is common due to decreasing fluid velocity over time that results in progressively slower migration of the mobile phase. The reduction in flow rate leads to broad peaks and poor resolution.[10] Electrophoresis, which is well-known for providing high resolution separations, can provide constant flow rates in paper due to the presence of electrokinetic forces.[13-19] Paper electrophoresis was established in the 1950s but required extensive instrumentation.[20] Recent reports have demonstrated electrophoretic separations on portable, low-cost mPADs.[10,21-24] The wax-printing method was used for fabricating electrophoretic mPADs for protein,[23] indicator,[10] and amino acid[21] separations. Although the wax-printing method provides fabrication simplicity, the resulting peaks remain broad in general. In 2016, C. Xu *et al*[24] and C. Chagas *et al*[22] made use of the laminated paper for electrophoresis, where small pieces of paper were embedded in plastic. However, these previous works did not report important electrophoretic

factors, such as Joule heating, evaporation effects, and electroosmotic mobility, that play a major role in electrophoretic separations.

Here, a laminated Parafilm-paper (l-paper) fabrication approach is introduced to create mPADs for electrophoretic separations.[25] Parafilm and paper are low cost, light weight, disposable, and regularly found in laboratories. In addition, the l-paper platform can generate free-standing channels that should theoretically give narrower separation peaks, while requiring very low sample volumes (0.3 μL). Key parameters including Joule heating (causing poor separation), electroosmotic flow (EOF), and electrophoretic mobility were studied to achieve significant improvement of electrophoretic resolution on l-paper mPADs. The porosity of the paper channel was calculated to explore the paper characteristic that contributes to the generation of Joule heating at low applied field strength. System viability was illustrated using colorimetric and fluorescence detection. For colorimetry, chlorophenol red and indigo carmine were used as representative analytes. Paper types, channel width, and separation potential affected the peak broadening on the separation. An additional injection arm was investigated to achieve narrower separation peaks. For fluorescence, the electrophoretic separation of fluorescein isothiocyanate (FITC) and FITC-labeled L-glutamic acid (FITC-Glu) was accomplished on the l-paper using a low-cost home-made fluorescent detector and % conjugation of FITC-Glu was determined.

Experimental

Materials and methods

Chlorophenol red was purchased from Alfa Aesar (Haverhill, MA). Indigo carmine, L-glutamic acid (Glu), tris(hydroxymethyl)aminomethane (Tris), 4-(2-hydroxyethyl)-1-piperazineethanesulfonic acid (HEPES), and sodium tetraborate were purchased from Sigma–Aldrich (St. Louis, MO). Fluorescein isothiocyanate (FITC) and boric acid were purchased from

Thermo Fisher Scientific (Waltham, MA). Dimethyl sulfoxide (DMSO) was purchased from EMD Millipore (Billerica, MA). Milli-Q water from Millipore (R ≥ 18.2 MΩ·cm) was used for all experiments. All chemicals were used as received without further purification.

A custom-built, floating high-voltage power supply (HVPS) was utilized as previously described.[26] DC-DC converters were obtained from Ultravolt and controlled by a Measurement Computing USB-3103 DAQ. DAQ communication was accomplished using LabView software, and the HVPS was electronically isolated from computer control through an Opticis M2-100 optical USB cable. Power for the HVPS was provided by a series of AA batteries.

Fabrication of a l-paper-based electrophoretic device

The l-paper was prepared by thermal bonding of paper and Parafilm™ (Bemis Company, INC., Neenah, WI) according to published methods.[25] Whatman qualitative filter paper, Grade 1 and Whatman 1 chromatography paper (GE Healthcare Bio-Sciences, Marlborough, MA) were used for chlorophenol red and indigo carmine and FITC and FITC-Glu separations, respectively. The thermal bonding procedure was performed by first inserting a paper sheet and a Parafilm sheet between two transparency sheets and then sandwiching the stack between stainless steel plates. The l-paper device was created using a heated press (Carver, Inc, Wabash, IN) by applying heat at 60 °C and pressure at 0.1 MPa for 20 seconds. The channel was generated using a 30 W Epilog Zing Laser Cutter and Engraver (Golden, CO) to remove paper and create the Parafilm barrier using the raster mode (95% speed, 25% power, and 2500 Hz) twice. The l-paper device was covered with a thermal laminating pouch sheet (Scotch, St. Paul, MN) except at the reservoirs to minimize evaporation. The designs of the l-paper device without and with the injection arms are shown in Figures 4.1a and 4.1c, respectively. The photographs of the device without and with the injection arms are shown in Figures 4.1b and 4.1d, respectively.

Joule heating study

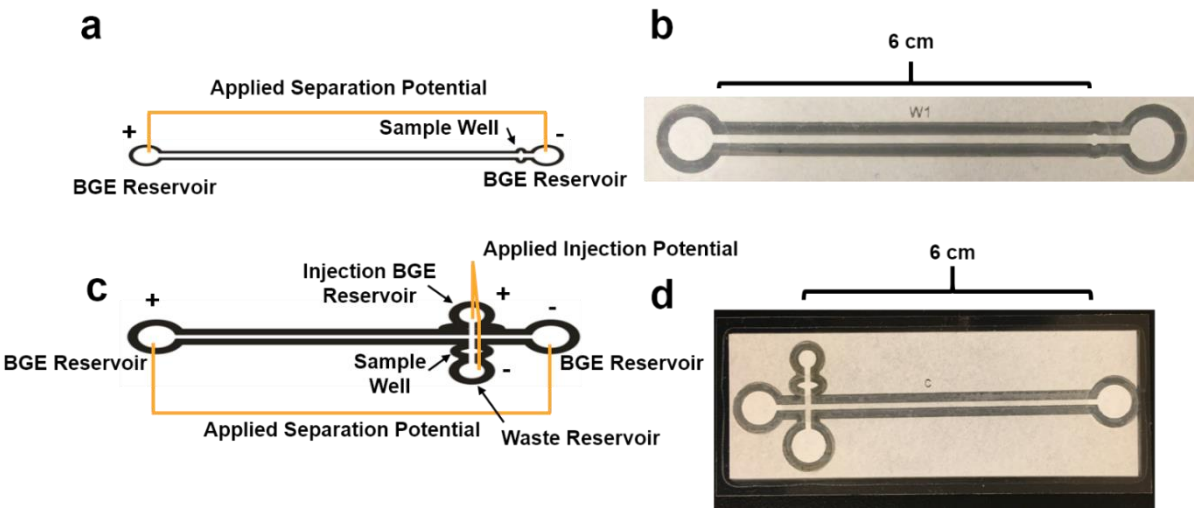

Figure 4.1: (a) Design of the mPAD without the injection port. (b) A photograph of an l-paper device without the injection port. (c) Design of an mPAD for electrophoresis with the injection port. (d) A photograph of a l-paper device with the injection port.

The mixture of 20 mM tris(hydroxymethyl)aminomethane (Tris) and 20 mM 4-(2-hydroxyethyl)-1-piperazineethanesulfonic acid (HEPES) pH 7.8 was used as the BGE. 20 µL were introduced into each reservoir of the device (1 cm channel length) as shown in Figure 4.1a. Voltage (25-400 V) was applied between two BGE reservoirs after a 4 min pre-wetting time. The circuit consisted of a l-paper device and an additional resistor of 26.9 kΩ. The potential difference of the system was measured using a 26.9 kΩ resistor.

Electroosmotic flow (EOF) and electrophoretic mobility measurement

The EOF was measured using the current monitoring method.[27] 10 µL of the BGE between 10 mM Tris and 10 mM HEPES pH 7.8 were introduced into each reservoir of the l-paper device (1 cm channel length and 1 mm channel width, Figure 4.1a). The electrical current was measured while applying 50 V between two reservoirs after a 4 min pre-wetting time.

Ion mobility was calculated by measuring the velocity of chlorophenol red along the l-device (1 cm channel length) when applying a potential of 50 V. A mixture of 20 mM Tris and 20 mM HEPES at pH 7.8 was used as the BGE.

Chlorophenol Red and Indigo Carmine Separation

100 μL (50 μL in each reservoir) of BGE composed of 20 mM Tris and 20 mM HEPES pH 7.8 were introduced into the l-paper device (6 cm channel length and 1 mm channel width) as shown in Figure 4.1b. For the design with the injection arm (Figure 4.1d), 50 μL were additionally added into the injection BGE reservoir and 20 μL were added into the waste reservoir. 0.3 μL of a mixture of 3.5 mM chlorophenol red and 3.5 mM indigo carmine dissolved in the BGE was introduced into the injection well after 4 min pre-wetting time. The optimum separation potential of -600 V (-100 V cm^{-1} field strength) was applied across the BGE reservoir, as shown in Figure 4.1a and 4.1c). The injection time was varied from 20 to 50 s using the optimum injection potential of -150 V. The data analysis was performed using ImageJ via a profile plot obtained from a line scan along the paper channel.

Comparison between electrophoretic separations using the l-paper device and the wax-printed mPAD

The l-paper device (6 cm channel length and 1 mm channel width) and the wax-printed mPAD with the injection port (Figure 4.1c) were used for the comparison. For the wax-printed mPAD fabrication, a wax printer (Xerox ColorQube 8870, Norwalk, CT) was used for creating the device. 150 °C was applied for 90 s with a hot plate (Thermo Fisher Scientific (Waltham, MA)) to melt the wax. The channel width of a wax-printed mPAD was varied from 0.3 mm to 4.3 mm. Chlorophenol red and indigo carmine separation as described in section 2.5 using the l-paper and

the wax-printed mPAD were compared. An optical microscope (Olympus Optical, Waltham, MA) was used for imaging a cross-sectional view of the l-paper device and the wax-printed mPAD.

FITC and FITC-Glu separation

FITC-Glu labeling

FITC-Glu labeling was synthesized as previously described.[28] 0.1 mg of FITC was dissolved in 1 mL of anhydrous DMSO. 8.6 mg of Glu were dissolved in 1 mL of 5 mM borate buffer at pH 9.0. 50 μL of FITC solution were added into Glu solution, very slowly in 5 μL aliquots while gently and continuously stirring the Glu solution. The reaction was incubated in the dark for 8 hours at 4 °C.

FITC and FITC-Glu separation

A total 170 μL of the optimum BGE, 10 mM borate buffer pH 11.35, was introduced into the l-paper device via the injection port. The volume of BGE filled in each reservoir was previously described in the section 2.6. The separation of 0.3 μL FITC-Glu solution was carried out using the l-paper device with the optimized injection potential, separation potential, and time of -150 V, -450 V, and 30 s, respectively. The fluorescent signal was excited using 40 mA of a built-in 480 nm LED used as a custom-made fluorescent detector in a black box, and the video was recorded by an iPhone 7 covered with a yellow filter (Kodak, Rochester, NY) to eliminate light scattering from the paper. The phone put on the black box was oriented perpendicularly to the LED light. The data analysis was performed with ImageJ via a profile plot obtained from a line scan along the paper channel.

To obtain narrower peaks, an inexpensive, USB microscope (Dino-Lite, Torrance, CA) was used. The l-paper device was covered with a sheet of black paper, except for an opening at the detection position (1x1 mm). The detection position was varied from 1 to 4 cm from the T-junction

of the l-paper device. The data was processed by selecting the images from a video record every 10 s. Fluorescent intensity of each selected image was analyzed using ImageJ. The fluorescent intensity was plotted as a function of separation time. FITC calibration was also carried out using a microscope detection method.

Results and Discussion

Joule heating on the l-paper device

In electrophoresis, Joule heating (or resistive heating) causes poor separation efficiency because temperature variation increases peak broadening through temperature-dependent diffusion coefficients, dynamic viscosity, and electrical conductivity.[29] Joule heating is problematic when the heat, which increases proportionally with the square of the applied potential[30], is not sufficiently dissipated from the electrophoretic system.[13] Resistance of the wet l-paper plays a crucial role in the consistency of current response in the Joule heating experiment; hence, determining pre-wetting time to obtain a constant resistance was determined. The equilibration time for pre-wetting paper with BGE was investigated first to make the paper resistance low and constant. Wetting the channel with 20 μL cm^{-1} of BGE provided longer, lower, and more constant resistance than using 10 μL cm^{-1} as shown in Figure 4.2. 7 min after introducing 10 μL cm^{-1} of BGE and 21 min after introducing 20 μL cm^{-1} of BGE, the resistance increased as a result of evaporation. Therefore, the paper needed to be pre-wetted with at least 20 μL cm^{-1} for 4 min before performing electrophoresis. We hypothesized that the pre-wetting causes the fibers to swell, reducing the pore diameter between fibers. Long-term, the impact of evaporation can be addressed by covering the device.

After determining the optimum pre-wetting BGE amount for the l-paper device, the applied voltage range to avoid Joule heating in the l-paper device was determined. An Ohm's plot was

used to determine the optimum applied voltage (Figure 4.3), where deviations from a linear current-voltage relationship indicate Joule heating.[31] The curve deviated from the linear relationship when applying a field strength higher than 200 V cm^{-1} as shown in Figure 4.3.

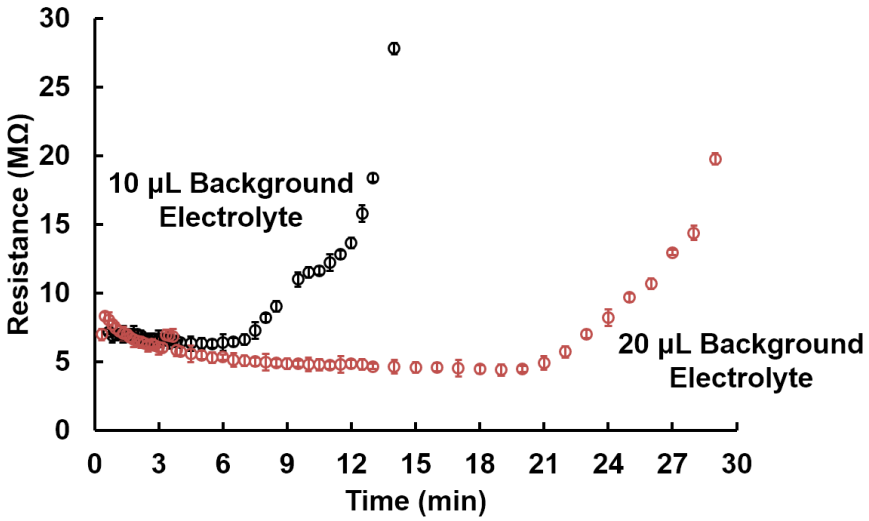

Figure 4.2: Representative curve of measured resistance of the paper channel versus time using different volume of BGE (n=3). Error bars represent ± 1 standard deviation.

Therefore, the optimized applied electric field strength range for the l-paper device was 0-200 V cm^{-1}. We hypothesized that the range for the l-paper device is limited relative to traditional electrophoresis capillaries because heat dissipation in the paper channels is difficult due to the large capillary size of the paper giving rise to large ratios of surface area to pore volume.[32] This assumption was verified by determining porosity of the l-paper device. The I-V plot could also be used for determining the porosity of the paper channel. The porosity was calculated from the equation [1]:[33]

$$\text{Porosity (\%)} = \frac{\text{Volume of Void}}{\text{Total Volume}} \times 100$$

$$\text{Porosity (\%)} = \frac{\text{Effective Area} \times \text{Length of Channel}}{\text{Total Area} \times \text{Length of Channel}} \times 100 \qquad [1]$$

Effective area of the paper channel was calculated from the electrical resistance of the paper channel following equation [2]:[34]

$$R = \frac{L \times \rho}{A_{eff}} \qquad [2]$$

where L is the channel length (0.01 m), ρ is resistivity of BGE (16.60 Ω m), and A_{eff} is cross-sectional effective area of the paper channel (m^2). The resistance of the device determined using

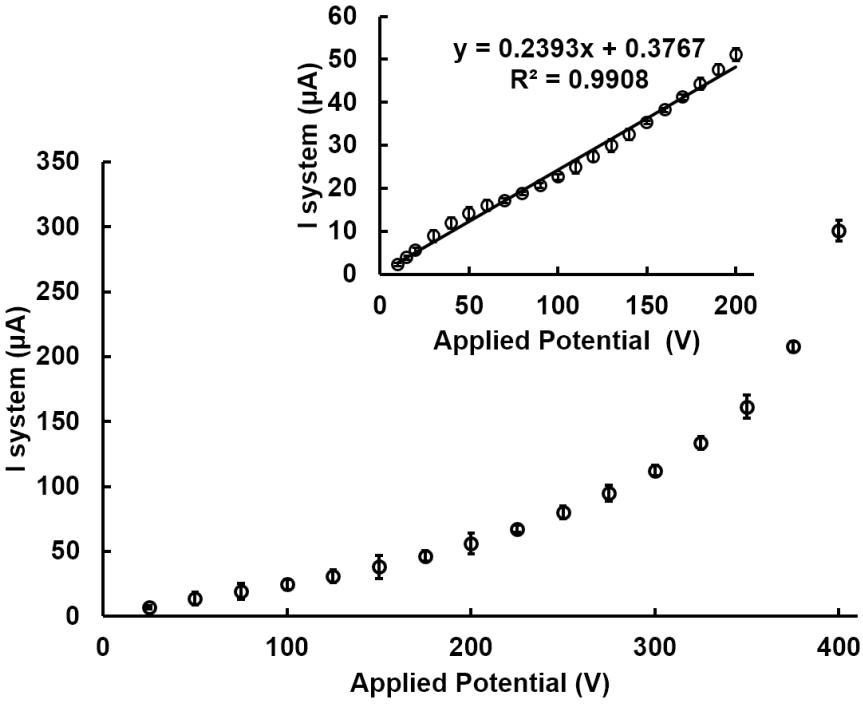

Figure 4.3: Graph of measured current as a function of applied potential (25 – 400 V) using 1 cm channel length and 1 mm channel width (n = 3) and graph of measured current as a function of applied potential (10 – 200 V) using 1 cm channel length and 1 mm channel width (n = 3) (inset). Error bars represent ± 1 standard deviation.

the inverse slope of the I-V plot (the inset of Figure 4.3) was 0.24 MΩ. The calculated effective area of the paper channel was 6.94 x 10^5 μm^2. Porosity of the paper channel calculated from equation [2] was 22%. Therefore, the paper channel consists of 22% BGE and 78% paper. As expected, the paper channel has a high surface area to pore volume ratio resulting in the narrow applied potential range.

EOF and electrophoretic flow measurements

Next, the EOF generated within the channel was studied.[35] The current monitoring method was used to determine EOF.[27,36] The resulting change in current is measured to determine when the BGE in the channel is replaced with the new BGE. For these experiments, BGE concentrations of 10 mM and 20 mM were used. As the low concentration replaces the high concentration in the channel, the current decreases until plateauing. The time of the electroosmotic flow to completely replace the high concentration of BGE was 803.7 ± 25.0 s (n=3) as shown in Figure 4.4. Electroosmotic flow was calculated at 2.5 x 10^{-5} ± 7.7 x 10^{-7} cm^2 V^{-1} s^{-1} (n=3), which is roughly an order of magnitude slower than found in glass and polymer channels.[37,38]

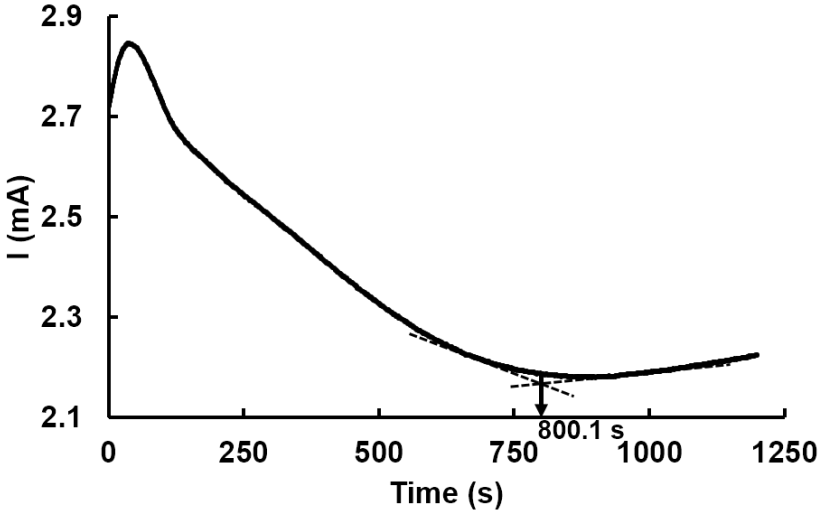

Figure 4.4: Current-time trace showing the measurement of the electroosmotic flow rate. The representative curve shows measured current versus time for 10 mM each of Tris and HEPES buffer pH 7.8 replacing 20 mM each of Tris and HEPES buffer pH 7.8 in a 1 cm l-paper channel. Two dotted lines touching the curve are drawn for determining the time of the electroosmotic flow to completely replace the high concentration of BGE.

The electrophoretic mobility of a dye was determined next, where electrophoretic mobility was calculated from equation [3]:[13]

$$v = (\mu_{EP} + \mu_{EOF})E \qquad [3]$$

where ν is the velocity of the ion (m s^{-1}), μ_{EP} is electrophoretic flow (m^2 V^{-1} s^{-1}), and E is the electric field (V m^{-1}). The velocity of chlorophenol red, a representative ion, was experimentally measured. The velocity of chlorophenol red was 7.2 x 10^{-3} cm s^{-1}, and the electrophoretic mobility calculated from equation [3] was 1.2 x 10^{-4} ± 7.7 x 10^{-7} cm^2 V^{-1} s^{-1}. The apparent mobility (sum of electrophoretic mobility and EOF) of chlorophenol red using l-paper was close to the reported value (2.2 x 10^{-4} cm^2 V^{-1} s^{-1})[39] using fused-silica capillaries. The minimal difference between the experimental and the reported values was contributed from using different BGE and pH.

Chlorophenol red and indigo carmine separation

Chlorophenol red and indigo carmine were used as the model analytes for electrophoretic separations using colorimetric detection. The optimum BGE was a mixture of 20 mM Tris and 20 mM HEPES, pH 7.8. Each compound could be detected via the color of which chlorophenol red (pKa = 6.25) and indigo carmine (pKa = 12.2) appear red and blue, respectively when dissolved in BGE pH 7.8.[40] Negatively charged chlorophenol red travelled faster than neutral indigo carmine. The parameters including paper types, channel width, and applied potential were optimized as shown in Figure 4.5. Whatman qualitative filter paper, Grade 1, 1 mm channel width, and -600 V of applied potential (-100 V cm^{-1} field strength) provided the narrowest peaks at 10% peak maximum for chlorophenol red and indigo carmine separation. However, the peak was still broad. To further reduce peak width, an injection arm was added to the design (Figure 4.1c and 4.1d). Addition of the injection port aims to control the sample volume by controlling injection times as shown in Figure 4.6. When adding the injection port, the peak was narrower than that using the device without the injection port. We first studied injection time. An injection time of 20 s was not long enough for the sample to travel into the separation channel, resulting in no separation peak (Figure 4.6a). At longer injection times (40 s and 50 s), too much sample volume was introduced

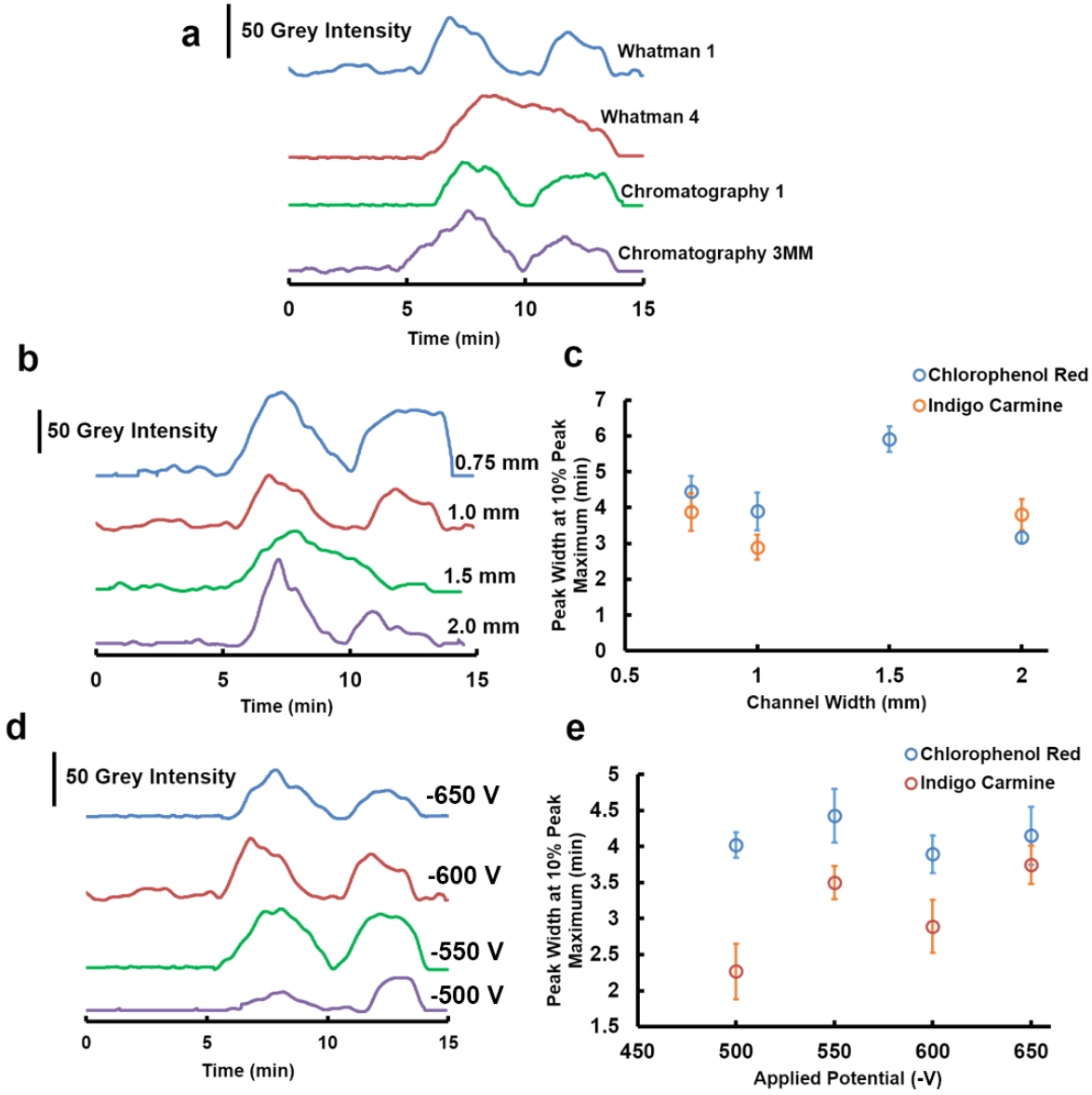

Figure 4.5: (a) Electropherograms of chlorophenol red and indigo carmine separation using different types of paper. (b) Electropherograms of chlorophenol red and indigo carmine separation using different channel width. (c) Relationship of 10% peak width of the separated peaks from (b) at different channel width (n=3). (d) Electropherograms of chlorophenol red and indigo carmine separation using different applied negative voltages. (e) Relationship of 10% peak width of the separated peaks from (d) at different applied negative voltages (n=3). Error bars represent ± 1 standard deviation.

resulted in the separation channel leading to broad peaks as shown in Figure 4.6b. An injection time of 30 s provided the narrowest peak width (Figure 4.6b). The separation bands of indicators

using the injection port pattern (Figure 4.6d) were much narrower that those using the l-paper without the injection port (Figure 4.6c).

Comparison of electrophoretic separations using the l-paper device and the wax-printed mPAD

We next compared separations performed on devices made using the two fabrication methods. It was hypothesized that the interaction between the sample and the hydrophobic channel barriers leads to band broadening due to variations on the zeta potential.[41] The absence of barriers on the side with l-paper would reduce the zeta potential variability relative to wax-printed

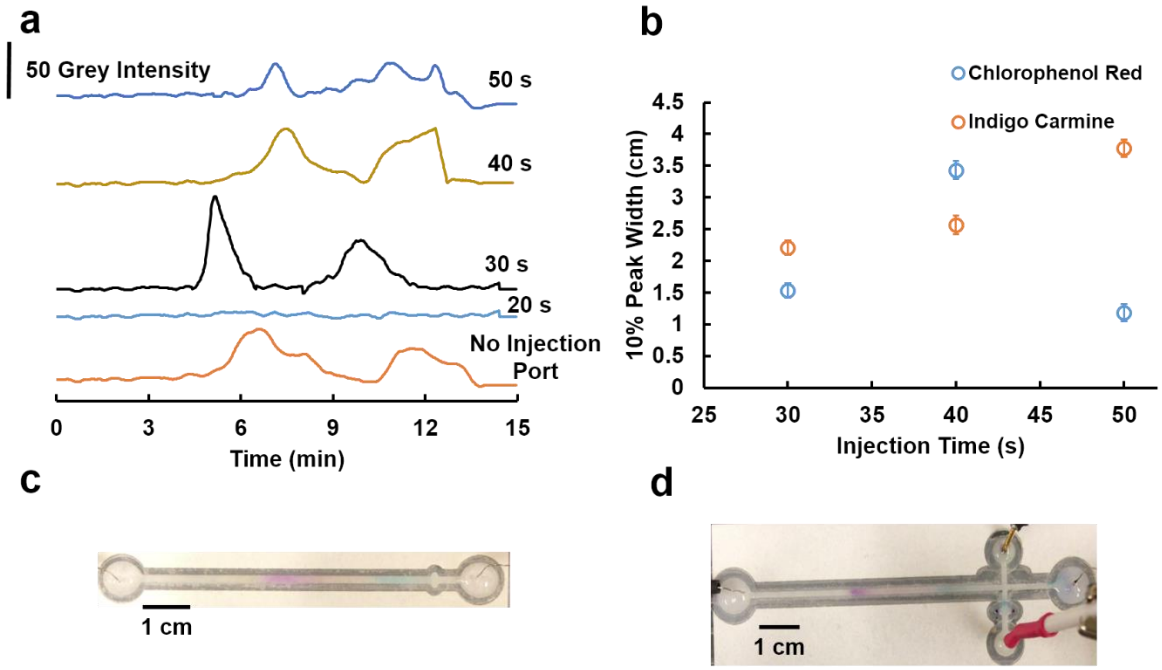

Figure 4.6: (a) Electropherograms of chlorophenol red and indigo carmine separation using the l-paper device without the injection port and with the injection port at different injection times. (b) Relationship of 10% peak width of the separated peaks from (a) at different injection times (n = 3). Error bars represent ± 1 standard deviation. (c) A photograph of chlorophenol red and indigo carmine separation using the l-paper device without the injection port. (d) A photograph of chlorophenol red and indigo carmine separation using the l-paper device with the injection port.

channels. Chlorophenol red and indigo carmine separations from the l-paper and the traditional wax-printed devices were compared. The l-paper electropherogram shows narrower peaks than electropherograms from the wax-printed mPAD (Figure 4.7a) at different channel widths. The

electropherogram from the wax-printed mPAD with a 0.3 mm channel width did not produce peaks due to lack of flow. To further understand why the fabrication method used affects peak width, the l-paper device and the wax-printed mPAD cross-sections were imaged. The l-paper device gave a free-standing channel with a precise edge as shown in Figure 4.7b, while the wax-printing mPAD produced a rough channel edge as shown in Figure 4.7c. It is likely that some of the wax dispersed into the paper channel impacting both flow and zeta potential, resulting in broader peaks.

FITC and FITC-Glu Separation

For demonstrating system viability for fluorescent applications, a FITC and FITC-labeled amino acid separation was performed. FITC is commonly used for labeling proteins and amino acids.[42,43] Conventional capillary electrophoresis was previously proposed to separate FITC labeling proteins and amino acid.[44-46] However, large, expensive, and complicated instrumentation is required for performing the capillary electrophoresis. Here, the l-paper device separated

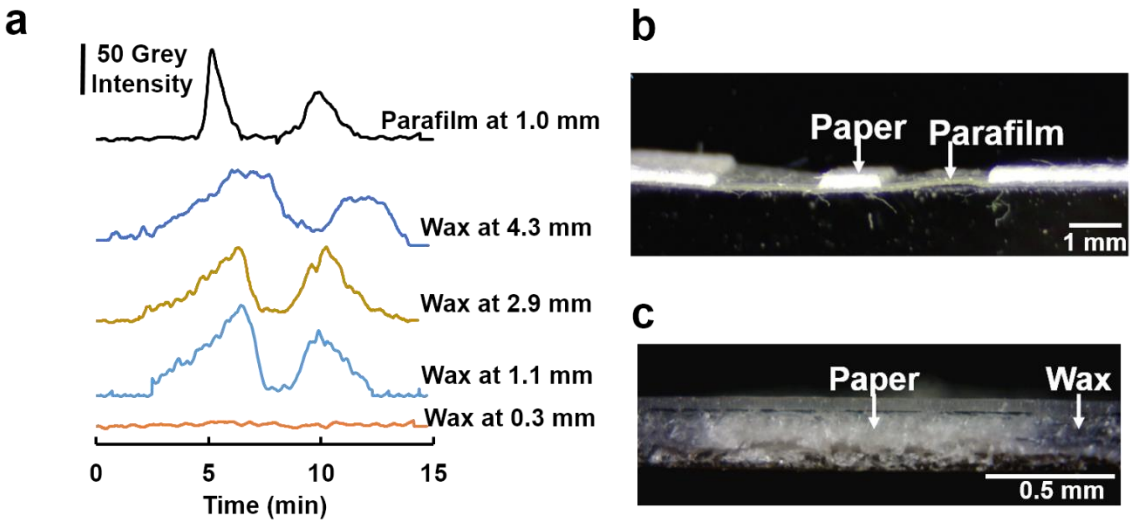

Figure 4.7: (a) Electropherograms of chlorophenol red and indigo carmine separation using the l-paper device (1 mm channel width) and the wax-printed mPAD at different channel widths. (b) A photograph of the cross-sectional l-paper device using optical microscope at 40x magnification. (c) A photograph of the cross-sectional wax-printed mPAD using optical microscope at 100x magnification.

unreacted FITC from a FITC-labeled amino acid to determine conjugation percentage. Glu was used as the representative amino acid. Unbound FITC and FITC-labeled Glu were successfully

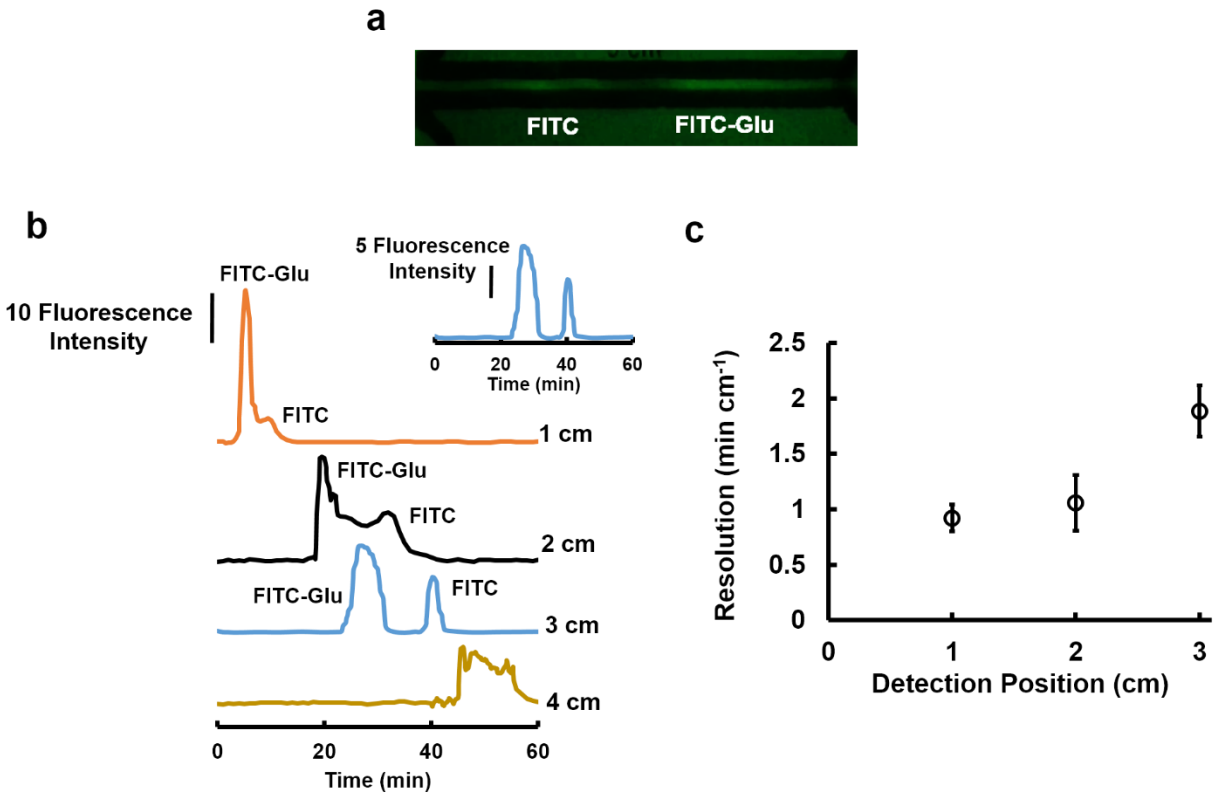

Figure 4.8: (a) A photograph of FITC and FITC-Glu separation. (b) Electropherograms of FITC and FITC-Glu separation using a microscope to present time-dependent measurement at different detection positions and expansion of the electrophorogram using the detection position at 3 cm (inset). (c) Resolution of FITC and FITC-Glu separation from (c) (n = 3). Error bars represent ± 1 standard deviation.

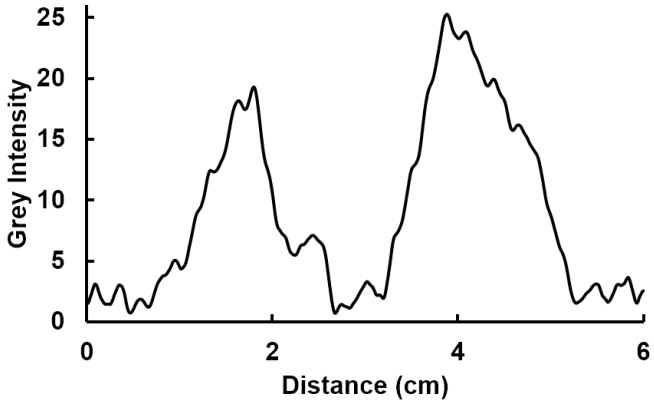

Figure 4.9: Electropherograms of FITC and FITC-Glu separation using a mobile camera for collecting signal.

separated using the proposed method as shown in Figure 4.8a. FITC-labeled Glu ($pKa_3 = 9.67$)[47], which has a negative three charge, was eluted earlier than unbound FITC ($pKa = 6.4$)[48], which has a negative charge, when using a pH 11.35 BGE. An electrophorogram showing the separation is included in Figure 4.9. While the separation was successful, the peaks were broad. Therefore, the detection method was improved to reduce peak width. A time-dependent plot was used to reduce peak width by imaging the fluorescent signal from a narrow window using an inexpensive microscope in a manner analogous to traditional capillary electrophoresis. The microscope set-up allowed for the collection of a higher fluorescent intensity due to eliminating background interference when compared to that using a mobile camera to image the entire device. The detection area (1 x 1 mm) was fixed at various positions along the paper channel. The fluorescent signal was analyzed every 10 s. The electrophorograms obtained at various positions are shown in Figure 4.8b. The optimum detection position which provided the best resolution (1.9 ± 0.2 min cm^{-1}) was 3 cm from the T-junction of the injection arm (Figure 4.8c). The separation peaks obtained with a microscope were better resolved than those obtained with a mobile camera. The closer detection positions (1 and 2 cm) provided lower resolution (0.9 ± 0.1 min cm^{-1} and 1.1 ± 0.1 min cm^{-1}, respectively) due to incomplete separation. When using 4 cm as the detection position, the two peaks merged due to the dispersion of the compounds with the increased distance. The time-dependent method was applied for colorimetric separation as well (Figure 4.10). Finally, percent conjugation of FITC and Glu was calculated by generating a FITC calibration, as shown in Figure 4.11a and 4.11b. Percent conjugation of FITC and Glu calculated from peak area was $72 \pm 4\%$.

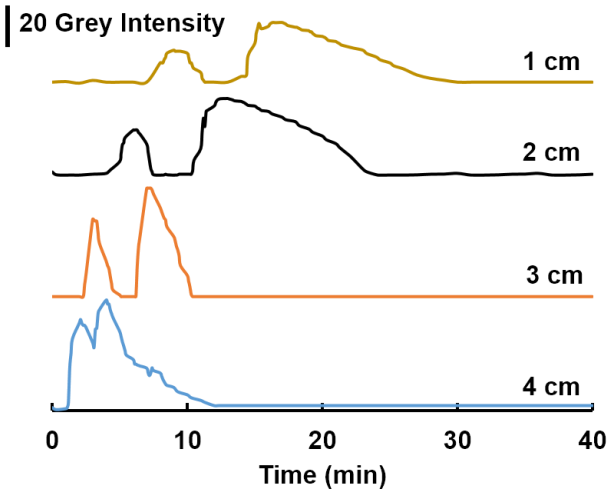

Figure 4.10: Electropherograms of chlorophenol red and indigo carmine separation using a microscope to present time-dependent measurement at different detection positions.

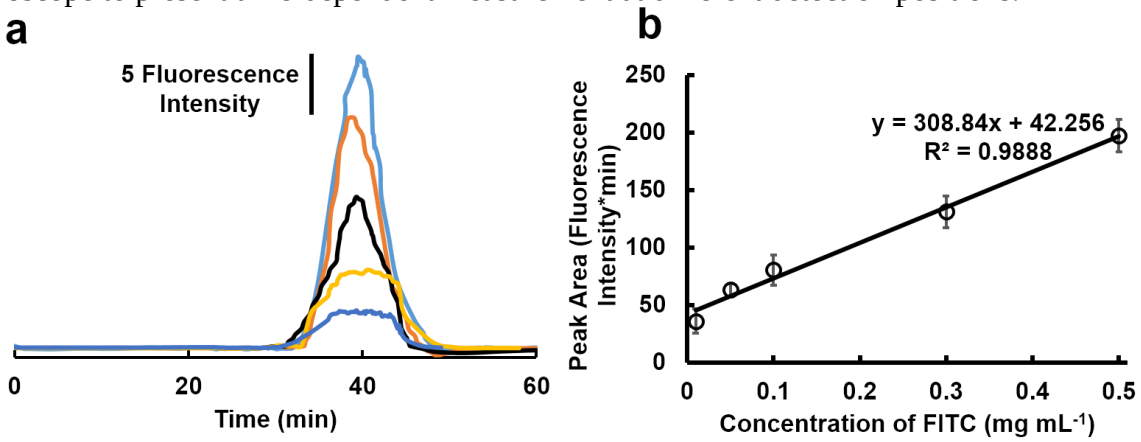

Figure 4.11: (a) Electropherograms of FITC movement at 3 cm from the injection arm. (b) A calibration plot of FITC at varied concentrations (n = 3). Error bars represent ± 1 standard deviation.

Conclusion

Electrophoresis on l-paper devices demonstrates an improved electrophoretic separation in paper relative to other methods. The essential characterization of the electrophoretic separation on paper included Joule heating, EOF, and electrophoretic flow. Joule heating was generated due to large ratio of surface area (78%) to pore volume (22%) of the paper leading to the narrow working applied electric field range (0-200 V cm^{-1}). In the case of EOF and electrophoretic mobility, the EOF was 2.5 x 10^{-5} cm^2 V^{-1} s^{-1} when using a Tris/HEPES buffer pH 7.8 as the BGE, and the

electrophoretic mobility of chlorophenol red was 1.2 x 10^{-4} cm^2 V^{-1} s^{-1}. For demonstrating device usability, electrophoresis on the l-paper device was carried out with both colorimetric and fluorescent separations. Paper types, channel width, and applied potential significantly influenced separation resolution. For colorimetric detection, chlorophenol red and indigo carmine were separated. Addition of the injection port helped to significantly reduce peak broadening. This work also made the successful separation of FITC-labeled Glu from unbound FITC using a low-cost l-paper electrophoresis device. Using a time-dependent measurement with an inexpensive microscope significantly improved resolution. Percent conjugation of FITC and Glu was 72 ± 4 %. Moreover, the laminated-Parafilm method materialized the goal of producing a free-standing channel resulting in reducing separation peak width. The proposed electrophoretic l-paper device could pave a way to analyze complicated samples using low-cost, portable, and simple mPADs.

REFERENCES

1. J. Mettakoonpitak and C. S. Henry *(Submitted)* 2018.
2. D. M. Cate, J. A. Adkins, J. Mettakoonpitak and C. S. Henry, *Analytical Chemistry*, 2015, **87**, 19-41.
3. N. A. Meredith, C. Quinn, D. M. Cate, T. H. Reilly, J. Volckens and C. S. Henry, *Analyst*, 2016, **141**, 1874-1887.
4. J. Mettakoonpitak, K. Boehle, S. Nantaphol, P. Teengam, J. A. Adkins, M. Srisa-Art and C. S. Henry, *Electroanalysis*, 2016, **28**, 1420-1436.
5. M. I. G. S. Almeida, B. M. Jayawardane, S. D. Kolev and I. D. McKelvie, *Talanta*, 2018, **177**, 176-190.
6. J. Adkins, K. Boehle and C. Henry, *ELECTROPHORESIS*, 2015, **36**, 1811-1824.
7. Y. Yang, E. Noviana, M. P. Nguyen, B. J. Geiss, D. S. Dandy and C. S. Henry, *Analytical Chemistry*, 2017, **89**, 71-91.
8. X. Li, P. Zwanenburg and X. Liu, *Lab on a Chip*, 2013, **13**, 2609-2614.
9. P. Rattanarat, W. Dungchai, D. Cate, J. Volckens, O. Chailapakul and C. S. Henry, *Analytical Chemistry*, 2014, **86**, 3555-3562.
10. C. Xu, W. Lin and L. Cai, *Journal of Chemical Education*, 2016, **93**, 903-905.
11. T. Songjaroen, W. Dungchai, O. Chailapakul, C. S. Henry and W. Laiwattanapaisal, *Lab on a Chip*, 2012, **12**, 3392-3398.
12. L. Y. Shiroma, M. Santhiago, A. L. Gobbi and L. T. Kubota, *Analytica Chimica Acta*, 2012, **725**, 44-50.

13. D. A. Skoog, F. J. Holler and S. R. Crouch, *Principles of Instrumental Analysis*, Thomson Brooks/Cole, 2007.

14. N. H. Martin and G. T. Franglen, *Journal of Clinical Pathology*, 1954, **7**, 87-105.

15. L. F. J. Parker, *Analyst*, 1955, **80**, 638-651.

16. G. Hanrahan, R. Montes and F. A. Gomez, *Analytical and Bioanalytical Chemistry*, 2008, **390**, 169-179.

17. A. Tiselius, *Discussions of the Faraday Society*, 1953, **13**, 29-33.

18. W. L. Dunn and R. H. Pearce, *Canadian Medical Association Journal*, 1961, **84**, 272-280.

19. A. A. Benson, *Journal of the American Chemical Society*, 1958, **80**, 5010-5010.

20. C. Wunderly, *Principles and applications of paper electrophoresis*, 1961.

21. L. Ge, S. Wang, S. Ge, J. Yu, M. Yan, N. Li and J. Huang, *Chemical Communications*, 2014, **50**, 5699-5702.

22. C. L. S. Chagas, F. R. de Souza, T. M. G. Cardoso, R. C. Moreira, J. A. F. da Silva, D. P. de Jesus and W. K. T. Coltro, *Analytical Methods*, 2016, **8**, 6682-6686.

23. L. Luo, X. Li and R. M. Crooks, *Analytical Chemistry*, 2014, **86**, 12390-12397.

24. C. Xu, M. Zhong, L. Cai, Q. Zheng and X. Zhang, *ELECTROPHORESIS*, 2016, **37**, 476-481.

25. Y. S. Kim, Y. Yang and C. S. Henry, *Sensors and Actuators B: Chemical*, 2018, **255**, 3654-3661.

26. S. D. Noblitt and C. S. Henry, *Analytical Chemistry*, 2008, **80**, 7624-7630.

27. W. Wang, F. Zhou, L. Zhao, J.-R. Zhang and J.-J. Zhu, *Journal of Chromatography A*, 2007, **1170**, 1-8.

28. Y. Cheng and N. Dovichi, *Science*, 1988, **242**, 562-564.

29. X. Xuan and D. Li, *Journal of Micromechanics and Microengineering*, 2004, **14**, 1171.

30. N. J. Petersen, R. P. H. Nikolajsen, K. B. Mogensen and J. P. Kutter, *ELECTROPHORESIS*, 2004, **25**, 253-269.

31. M. S. Bello, M. Chiari, M. Nesi, P. G. Righetti and M. Saracchi, *Journal of Chromatography A*, 1992, **625**, 323-330.

32. Y. Xu, *The Chemical Educator*, 1996, **1**, 1-14.

33. J. Bear, *Dynamics of fluids in porous media / Jacob Bear*, American Elsevier, New York, 1972.

34. A. W. Adamson, *A textbook of physical chemistry*, Academic Press, 1973.

35. A. E. Kaifer, *Journal of Chemical Education*, 1992, **69**, A305.

36. X. Huang, M. J. Gordon and R. N. Zare, *Analytical Chemistry*, 1988, **60**, 1837-1838.

37. D. J. Harrison, A. Manz, Z. Fan, H. Luedi and H. M. Widmer, *Analytical chemistry*, 1992, **64**, 1926-1932.

38. D. Ross, T. J. Johnson and L. E. Locascio, *Analytical Chemistry*, 2001, **73**, 2509-2515.

39. K. G. Hopper, H. LeClair and B. R. McCord, *Talanta*, 2005, **67**, 304-312.

40. E. Pungor and E. Schulek, in *Indicators*, Pergamon, 1972, vol. 51, pp. 437-468.

41. A. E. Herr, J. I. Molho, J. G. Santiago, M. G. Mungal, T. W. Kenny and M. G. Garguilo, *Analytical Chemistry*, 2000, **72**, 1053-1057.

42. H. Maeda, N. Ishida, H. Kawauchi and K. Tuzimura, *The Journal of Biochemistry*, 1969, **65**, 777-783.

43. G. T. Hermanson, in *Bioconjugate Techniques (Third edition)*, Academic Press, Boston, 2013, DOI: https://doi.org/10.1016/B978-0-12-382239-0.00010-8, pp. 395-463.

44. J. Mattusch and K. Dittrich, *Journal of Chromatography A*, 1994, **680**, 279-285.

45. F. Dang and Y. Chen, *Science in China Series B: Chemistry*, 1999, **42**, 663-669.

46. K. Takizawa and H. Nakamura, *Analytical Sciences*, 1998, **14**, 925-928.

47. C. N. Pace, G. R. Grimsley and J. M. Scholtz, *Journal of Biological Chemistry*, 2009, **284**, 13285-13289.

48. S. Smith and W. Pretorius, *Water Sa*, 2002, **28**, 395-402.

CHAPTER 5. CONCLUSION

Particulate matter (PM) has a significant influence on human health, visual air quality, and damage to materials. The concentration, size, and chemical composition of PM are directly linked to harmful effects on human health. Chemical composition of PM is commonly analyzed using large, expensive, and complicated laboratory instruments, such as ICP-MS and atomic absorption spectrometry. These instruments are inappropriate for use in fieldwork and remote areas, due to the large size and expense of these systems. Moreover, collection time, storage of samples, and sample transportation from the field to a centralized laboratory cause can result in changes in the PM composition because of chemical reactions.[1-3] Trace metals are a critical component of PM that contributes to serious health problems and quantitatively change via chemical reactions. My dissertation focused on developing low-cost, portable, disposable analytical tools that would enable people to perform rapid and real-time analysis of trace metals in PM. Additionally, electrophoretic microfluidic paper-based analytical devices (mPADs) were prepared towards separations and analysis of PM components.

The first part of this dissertation sought to develop low-cost, portable, and disposable electrochemical analytical devices for trace detection of Zn, Cd, Pb, Co, and Ni. Electrochemistry integrated into electrochemical paper-based analytical devices (ePADs) offers sensitive and selective measurements.[4] Stencil-printed electrodes were fabricated on a polyethylene transparency (PET) sheet, aimed at improving detection performance of trace metals relative to a paper platform and reducing device costs. For simultaneous Zn, Cd, and Pb detection,[5] silver nanoparticles (AgNPs) were used to modify the electrode surface using an electrospraying technique. Aside from their simple synthesis and electrode modification, the AgNPs increased

electrode surface area and provided low uncompensated resistance and fast electron transfer kinetics. Electrospraying provided more homogeneous AgNPs spread on the surface relative to the drop-casting method. LODs for Zn, Cd, and Pb were 5.0, 0.5, and 0.1 μg L^{-1}, respectively, which were low enough to measure these metals in PM. For Co and Ni measurement,[6] Nafion/Bi modified electrochemical analytical sensors were proposed. The sulfonate group in Nafion allows selective preconcentration of cations resulting in improved detection performance. Bi was introduced to form metal amalgam to generate well-defined peaks and reproducible stripping signals. Dimethylglyoxime (DMG) was used as a chelator to selectively complex Co(II) and Ni(II) before detecting these complexes with adsorptive cathodic stripping voltammetry. This work represented high repeatability of the low-cost devices for Co and Ni measurements that could be used up to 15 times with acceptable %RSD. LODs of 1 μg L^{-1} and 5 μg L^{-1} for Co and Ni, respectively were obtained. The electrochemical sensors for Zn, Cd, Pb, Co, and Ni were applied for determination of those metals in aerosol samples. The validation with ICP-MS showed no statistically different results with 95% confidence between the proposed devices and the ICP-MS method.

This dissertation has also extended mPADs towards the separation and analysis of compounds in complex samples such as PM. Electrophoretic laminated Parafilm paper (l-paper) was proposed to improve peak broadening in paper separation. The l-paper yielded a free-standing channel, resulting in significantly reduced peak broadening relative to wax-printing mPADs. Electrophoretic parameters such as Joule heating, electroosmotic flow (EOF), and electrophoretic mobility were determined. The results indicated that applied potential range proceeded on the electrophoretic l-paper was narrow, due to generation of Joule heating at low applied potential. The electrophoretic l-paper was applied for colorimetric separation of chlorophenol red and indigo carmine and fluorescent separation of fluorescein isothiocyanate (FITC) and FITC labeling

glutamic acid (FITC-Glu). Addition of an injection arm to the device to control sample volume and the use of a low-cost handheld microscope to enhance collected fluorescence intensity were suggested to reduce peak broadening. This work will ultimately be used to analyze complex samples.

Future Directions

This dissertation focused on the development of sensitive, low-cost, portable electrochemical analytical devices for trace metal analysis in PM,[5,6] as well as a simple electrophoretic l-paper prepared for complicated sample analysis in future work. Additional suggestions about device development could also be proposed that would further improve our ability to analyze PM composition. In the case of electrochemical analytical devices, other trace metals such as Fe and Cu play an important role in chemical properties of PM. Voltammetric stripping for determining concentration of Fe and Cu is limited, due to poor reversibility of the $Fe^{2+/3+}$ and the $Cu^{+/2+}$ couple at a bare electrode.[7,8] Specific adsorption of the complex of these metals with the chelator allows the selective electrochemical measurement to occur. Thus, electrochemical methods for detecting these metals should be explored.[7,9] Next, simultaneous electrochemical detection of trace metals in PM would represent a major step forward because it would minimize the required sample amounts and reduce overall analysis time. In fact, different electrochemical conditions are required for each metal detection. A paper-based platform can be utilized for on line adjustment of the sample conditions for each metal, before performing electrochemical detection. A paper-based device is suggested to combine all electrochemical devices to achieve simultaneous metal detection as shown in Figure 5.1a. A shared counter electrode (CE) and a shared reference electrode (RE) for two electrochemical detection zones are fabricated in the paper-based device. A bipotentiostat with a 4-electrode configuration including

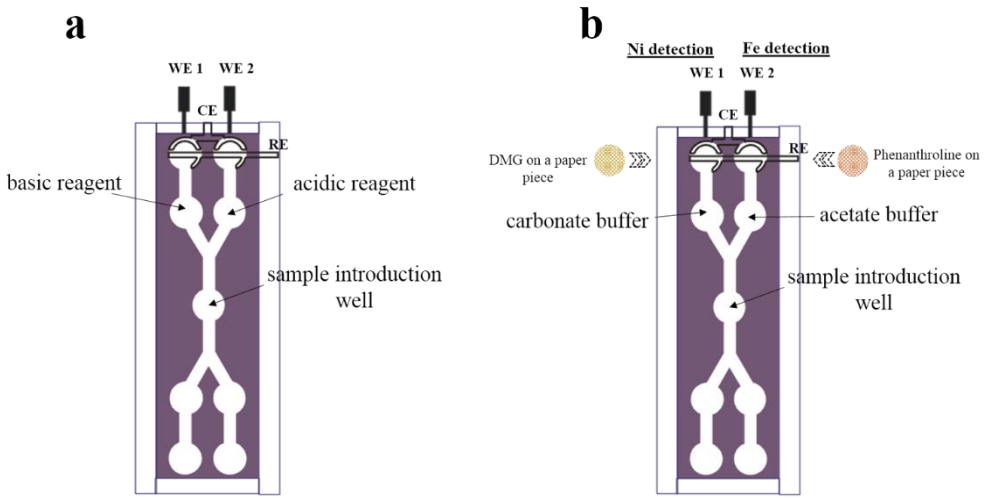

Figure 5.1: (a) A proposed design of a paper-based analytical device for simultaneously electrochemically detecting metals. (b) A proposed electrochemical paper-based analytical device for simultaneously detecting Ni and Fe.

two working electrodes, a CE, and a RE, is required for simultaneously detecting metals. The proposed concept was preliminarily tested for simultaneously detecting Ni and Fe, which required different pH conditions and electrode modification methods. 11 µL of 1 M carbonate buffer pH 9.0 was deposited onto one device arm for preconditioning the sample solution for the electrochemical detection of Ni as shown in Figure 5.1b. For chelating Ni(II), DMG, which was used as a Ni(II) chelator, was dried on a piece of paper, and placed between layers of a paper device and a Bi modified working electrode (WE1) as shown in Figure 5.1b. In the case of Fe detection, 11 µL of 2.5 M acetate buffer pH 4.5 was deposited onto the other device arm as shown in Figure 5.1b. 1,10-Phenanthroline, which was used as a Fe(II) chelator, dried on a piece of paper was inserted between layers of a paper device and a 1,10-phenanthroline modified working electrode (WE2). Adsorptive cathodic stripping voltammetry was performed to simultaneously measure Ni and Fe. Preliminary results using the proposed paper-based device for the electrochemical detection of Ni and Fe are shown in Figure 5.2.

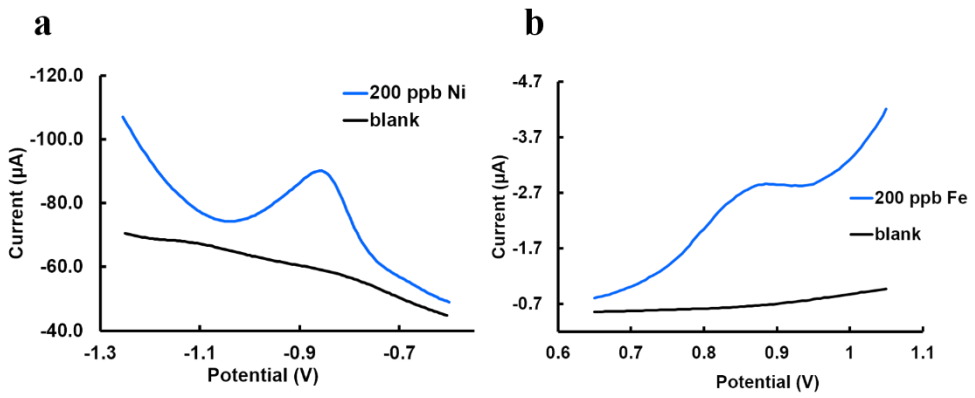

Figure 5.2: Voltammograms of Ni (a) and Fe (b) simultaneous detection using adsorptive cathodic stripping voltammetry. The electrodeposition was performed at the deposition potential of 1.3 V for 240 s. The electrochemical measurement was performed after a 10-s equilibration time from 1.05 to −1.25 V, and with an optimized step potential of 5 mV, amplitude of 75 mV, and frequency of 5 Hz.

Aside from trace metals, there are other compounds in PM, such as radical-generating species, volatile organic compounds, and pathogenic bacteria,[10] which can cause significant health problems. Proper sample preparation and efficient compositional extraction procedures need to be explored. Moreover, methods using low-cost mPADs for quantitatively monitoring Fe, Cu and reactive oxygen species (ROS) should be developed, because Fe and Cu kinetically produce ROS via the Fenton reaction. This study would reveal relevant chemical reactions of PM components that impact human health.

In electrophoretic mPADs, the electroosmotic flow (EOF) is a critical factor to improve the separation resolution. EOF countering electromigration increases sample focusing, which brings about reduced band broadening.[11] Thus, approaches to increase EOF should be investigated. Chemical modification of paper or/and changing device substrates would be suggested to increase EOF. Besides enhancing separation resolution, sensitive detection methods for the electrophoretic separation should be investigated. For example, in the case of multiplexed metal analysis, an electrochemical device could be integrated into electrophoretic mPADs to lower the LODs.[11,12] Amperometry could be used for simultaneous detection of trace metals, using carbon stencil-

printed electrodes as a portable, disposable and simple electrochemical device. The proposed design is shown in Figure 5.3. Low-cost electrochemical sensors coupled with the electrophoretic

Figure 5.3: The integration of carbon stencil-printed electrode into electrophoretic mPAD

mPAD would facilitate separation and analysis of other components in PM, such as organic compounds.

The proposed low-cost electrochemical analytical devices for simultaneous detecting trace metals in PM and the proposed electrophoretic l-paper for improving separation resolution would extend the ability of low-cost analytical tools for the analysis of complex components in PM. These innovations represent an important step towards the assessment and control of PM exposure, air pollution and air quality management.

REFERENCES

1. R. M. Harrison and J. Yin, *Science of the total environment*, 2000, **249**, 85-101.
2. R. P. Schins, J. H. Lightbody, P. J. Borm, T. Shi, K. Donaldson and V. Stone, *Toxicology and applied pharmacology*, 2004, **195**, 1-11.
3. N. Li, T. Xia and A. E. Nel, *Free Radical Biology and Medicine*, 2008, **44**, 1689-1699.
4. J. Mettakoonpitak, K. Boehle, S. Nantaphol, P. Teengam, J. A. Adkins, M. Srisa-Art and C. S. Henry, *Electroanalysis*, 2016, **28**, 1420-1436.
5. J. Mettakoonpitak, J. Mehaffy, J. Volckens and C. S. Henry, *Electroanalysis*, 2017, **29**, 880-889.
6. J. Mettakoonpitak, D. Miller-Lionberg, T. Reilly, J. Volckens and C. S. Henry, *Journal of Electroanalytical Chemistry*, 2017, **805**, 75-82.
7. M. Lu, N. V. Rees, A. S. Kabakaev and R. G. Compton, *Electroanalysis*, 2012, **24**, 1693-1702.
8. M. B. Gumpu, S. Sethuraman, U. M. Krishnan and J. B. B. Rayappan, *Sensors and actuators B: chemical*, 2015, **213**, 515-533.
9. S. Chaiyo, O. Chailapakul, T. Sakai, N. Teshima and W. Siangproh, *Talanta*, 2013, **108**, 1-6.
10. J. A. Araujo and A. E. Nel, *Particle and fibre toxicology*, 2009, **6**, 24.
11. T. Rosenfeld and M. Bercovici, *Lab on a Chip*, 2018.
12. P. D. Voegel and R. P. Baldwin, *Electrophoresis*, 1997, **18**, 2267-2278.

APPENDIX 1. ELECTROCHEMISTRY ON PAPER-BASED ANALYTICAL DEVICES: A REVIEW

Chapter Overview

Even though they were introduced less than a decade ago, electrochemical paper-based devices (ePADs) have attracted widespread attention because of their inherent advantages in many applications. ePADs combine the advantages of microfluidic paper-based devices (low cost, ease of use, equipment free pumping, etc.) for sample handling and processing with the advantages of sensitive, selective detection provided by electrochemistry. As a result, ePADs provide simplicity, portability, reproducibility, low cost and high selectivity and sensitivity for analytical measurements in a variety of applications ranging from clinical diagnostics to environmental sensing. Herein, recent advances in ePAD development and application are reviewed, focusing on electrode fabrication techniques and examples of applications specially focused on environmental monitoring, biological applications and clinical assays. Finally, a summary and prospective directions for ePAD research are also provided. This review was published in *Electroanalysis*.[1]

Introduction

While paper has been used as a substrate for chemical analysis for centuries, the concept of microfluidic paper-based analytical devices (mPADs) was only recently introduced by Whitesides and co-workers in 2007 when paper was patterned using photolithography to perform multiplexed chemical assays.[2] Subsequently, mPADs have been used for various applications, including environmental monitoring, biomedical applications,[3] food and beverage analysis and point-of-care (POC) clinical diagnostics.[3,4] The popularity of μPADs is due to several advantages, which include low cost, simplicity of operation, portability, and disposability. Multiple fabrication techniques have been demonstrated to expedite adaptation of this technology in real world

applications, especially in POC diagnostics and on-site measurements. Detection is also a key aspect of mPAD development, and colorimetric detection has been the dominant technique given its inherent simplicity and potential for instrument free quantification.[5] Color changes caused by reactions on paper can be observed by the naked eye, providing semi-quantitative results that are sufficient for some assays. Quantitative results are obtained by using an imaging tool combined with image processing software to integrate color intensity. Colorimetric detection; however, is limited by the need for low background surfaces, a limited dynamic range, low sensitivity, and variability in environmental illumination.[6] Electrochemical sensing offers a quantitative alternative detection system for mPADs. Electrochemical detection can also improve the performance of mPADs in terms of sensitivity and selectivity while providing low detection limits.

Electrochemical paper-based analytical devices (ePADs) were first published by Duangchai et al. in 2009. Electrochemical sensing is a good match for mPADs because; (i) electrodes can be miniaturized and easily fabricated onto paper, (ii) electrochemistry does not require complicated equipment, (iii) portable potentiostats are already available for on-site measurements and (iv) a wide range of electrochemical methods are known, extending the application space across many fields of interest. Therefore, ePADs have been employed for a variety of applications as discussed in recent review articles.[3,4,7] This review covers recent developments of ePADs, starting with a chronological summary of electrode fabrication. Next, applications of ePADs, including environmental analysis, biomedical applications and clinical assays are summarized. μPAD fabrication is not discussed in this review and the authors refer readers to recent review articles for further device fabrication.[3,5]

Electrode Fabrication-The development

Electrodes are of paramount importance for ePAD performance, as they are for all electrochemical methods. There are a variety of electrode materials (e.g. carbon, metals and nanoparticles) and fabrication techniques (e.g. screen/stencil-printing, pencil/pen drawing, inkjet-printing and wire placement) that have been demonstrated for ePADs. In this review, the development of electrode fabrication methods for ePADs is presented in chronological order, starting from the beginning stage (2009-2010), followed by the growing stage (2011-2013) and ending with the present state-of-the-art (2014-2015). This review approach emphasizes the significant advances that ePAD technology has gone through in less than a decade.

The Early Stages (2009-2010)

During the early stages of ePAD development, electrode materials and fabrication methods were adapted from traditional microfluidic and biosensor systems.[8] Screen-printing was the first electrode fabrication method employed for ePADs and is still commonly used to make carbon electrodes. The popularity of screen-printing is due to the advantages of easy fabrication, low cost, possibility for large scale production and reasonable electrode-to-electrode reproducibility, as previously reviewed.[9] In addition to screen-printing, methods such as inkjet printing and pencil drawing were also demonstrated during this time frame.

Screen/Stencil-printing

The first ePAD report by Dungchai *et al.*[6] relied on screen-printing to generate carbon electrodes for enzymatic detection of glucose, lactate, and uric acid (UA). Electrochemistry was used to improve the sensitivity and selectivity of mPADs relative to colorimetric detection techniques.[2] For screen-printed electrodes (SPEs), the electrode geometry, which can be designed using drawing software, such as Adobe Freehand®, CorelDraw® or Adobe Illustrator®, is

carefully considered to achieve high performance. For example, in Dungchai's work the geometry of the counter electrode was designed to be larger than the working and reference electrodes to minimize current resistance in the circuit. The electrode dimensions and geometry are shown in Figure A1.1A. Electrodes were screen-printed on Whatman®Grade 1 filter paper with the working and counter electrodes made from carbon ink containing Prussian Blue (PB) to increase the selectivity for H_2O_2 detection, and Ag/AgCl ink screen-printed as the reference electrode. Additionally, the conductive pads of all electrodes were painted using Ag/AgCl ink to reduce connection resistance. This electrochemical detection system was tested for the simultaneous determination of glucose, lactate and UA from undiluted serum samples (Figure A1.1B).

Similar to screen-printing, stencil-printing uses an open mask or stencil to fabricate carbon electrodes. Stencils are easily made from solid films, including adhesive tape and transparent film, using craft or laser cutters. Key advantages of this fabrication technique are facile mask generation for rapid prototyping and low cost. A complementary ePAD study to the work presented by Dungchai was presented by Nie et al.[10] In this work, the flow of solution across stencil-printed electrodes was first introduced to produce convection and increase signal. The electrodes (carbon ink for working and counter electrodes and Ag/AgCl as a reference electrode) were stencil-printed on a piece of paper (Whatman® Grade 1 chromatography paper) or polyester–cellulose blend paper (VWR®Spec-Wip) and a hydrophilic channel was created on the second piece of paper using photolithography. The two paper pieces were attached using double-sided adhesive tape to achieve conformal contact between the paper channel and the electrodes (Figure A1.1C). The platform was also applied for glucose determination in urine and selective measurement of Pb^{2+} in an aqueous solution.

Apart from stand-alone analysis, the integration of ePADs with other techniques for dual detection was reported to increase the versatility for other applications. Apilux et al.[11] proposed an ePAD with colorimetric detection for simultaneous detection of Au and Fe. Three electrodes were

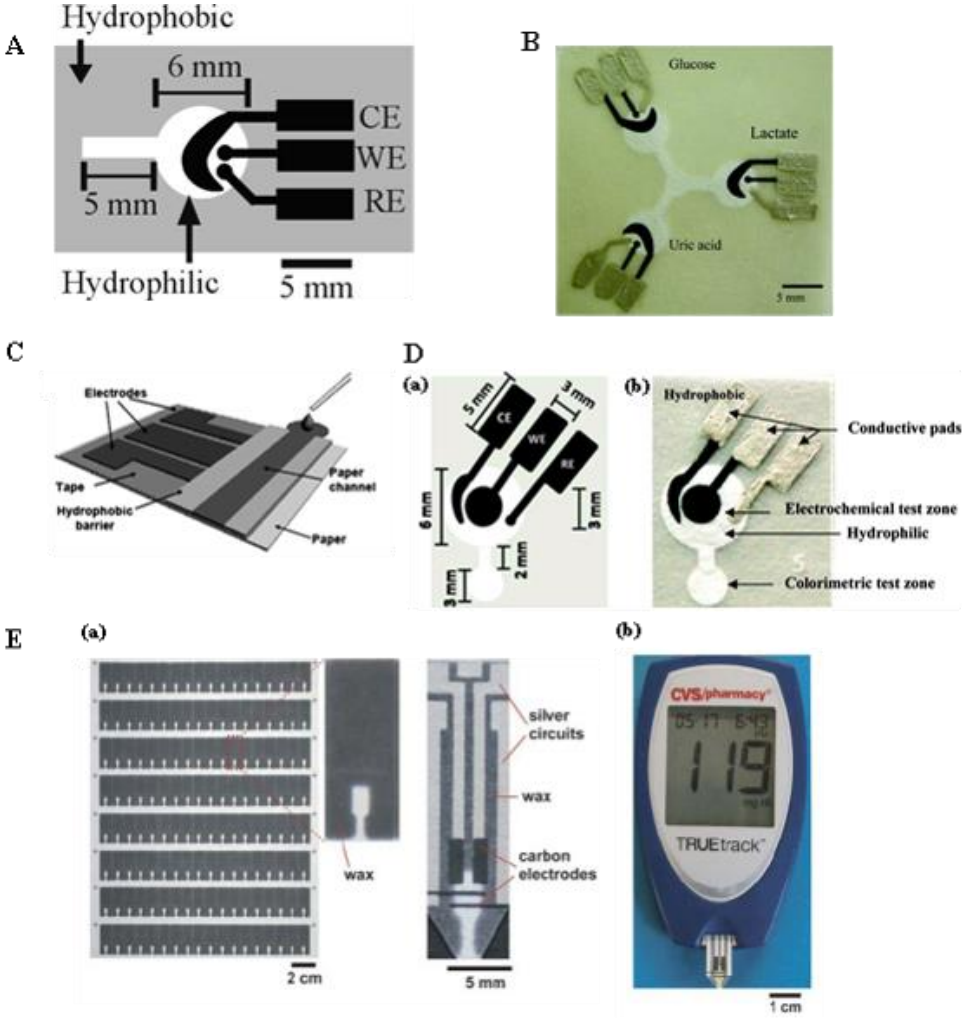

Figure A1.1: Screen-printing for electrode fabrication of ePADs. (A) Layout and (B) an image of electrode configuration of ePAD for simultaneous determination of glucose, lactate, and UA using enzymatic assays. WE, RE and CE stand for working, reference and counter electrodes, respectively. Reprinted with permission from [7]. Copyright 2010 American Chemical Society. (C) SPEs on paper substrate and a paper channel for the analysis of glucose. These two paper pieces were held inplace using double-sided adhesive tape surrounding the electrodes. Reprinted with permission from [10] with permission of The Royal Society of Chemistry. (D) Schematic (a) and an image (b) of μPAD consisting of dual electrochemical and colorimetric detection. Reprinted with permission from [11]. Copyright 2010 American Chemical Society. (E) An ePAD integrated with a commercial glucometer. (a) Arrays of wax-printed electrodes for determination of biological compounds. (b) A commercial glucometer used as an electrochemical reader. Reprinted with permission from [14] with permission of The Royal Society of Chemistry.

screen-printed onto the hydrophilic area of a paper device, which was defined using photolithography (Figure A1.1D). Carbon was screen-printed as working and counter electrodes, while Ag/AgCl ink was screen-printed as a reference electrode and conductive pads for each electrode. For dual detection, the hydrophilic zone for electrochemical detection was designed to connect with a colorimetric detection zone. The device was able to simultaneously determine Au and Fe in water samples from electronic processing waste. Fe is a common byproduct in electronic waste and can interfere with the electrochemical detection of Au above a threshold. The dual detection mode ensured measurement accuracy.

Another technique integrated sputtered gold electrode ePADs with paper separations.[12] Gold electrodes were deposited onto a polyester film and a three electrode design was patterned using photolithography. A chromatography strip of paper was placed on top of a three electrode system, and acted as a separation channel. After spotting sample onto the paper channel 10-mm away from the electrodes, the analytes were separated in the paper channel and detected when they crossed the electrodes using amperometric detection. This work was applied for the chromatographic separation and detection of ascorbic acid (AA) and UA from a mixed sample with detection limits of 20 μM for both species.

Towards the end of this period, commercial SPEs were employed for ePAD measurements. A new method using a paper disk impregnated with reagents and coupled with commercial SPEs was introduced for trace metal detection.[13] An internal standard was stored on the paper disk and employed to improve measurement accuracy. Using this approach, simultaneous determination of Zn^{2+} and Pb^{2+} was carried out, using Zn^{2+}as the internal standard. In addition to commercially available electrodes, a commercial glucometer was also integrated with ePADs for determination of glucose, cholesterol, lactate, and alcohol in blood samples, as shown in Figure A1.1E.[14] Using

portable glucometers along with ePADs is a user friendly and convenient method of detection for a number of assays.

The growing stage (2011-2013)

During this period, the publication of ePADs grew rapidly. A variety of new electrode fabrication methods, including inkjet-printing, stencil-printing and pencil-drawing were introduced for ePADs. However, SPEs remained the most popular fabrication technique and were further developed with more complicated and multiplexed ePAD designs reported.

Inkjet-printing

Fabrication of electrodes using inkjet-printing can be achieved using a commercial inkjet printer. Hu *et al.*[15] used inkjet-printing to fabricate gold electrode arrays made of gold nanoparticles (AuNPs) on mixed cellulose ester membranes for use as a novel paper-based electrochemical oxygen sensor (Figure A1.2A). Additionally, AuNPs were also inkjet-printed on paper and then IR sintered to produce conductive electrodes that were inert, resistant to oxidation and acids (Figure A1.2B).[16] The electrodes were further functionalized using self-assembled octadecanethiol monolayers. The functionalized electrodes have the potential for applications inprinted diagnostics, specifically for molecular recognition detection. Moreover, inkjet-printing of silver nanoparticle ink was used to fabricate electrodes for a bioelectric system-on-chip (SoC) sensor.[17] This SoC sensor was created as a Bio-Patch prototype which was attached on human body to measure bioelectric signals from electrocardiogram and electromyogram measurements.

Pencil-drawing and pencil lead electrodes

Incorporating pencil lead into ePADs is perhaps the easiest and simplest way to fabricate electrodes for ePADs because only an inexpensive, commercially available pencil lead is needed.

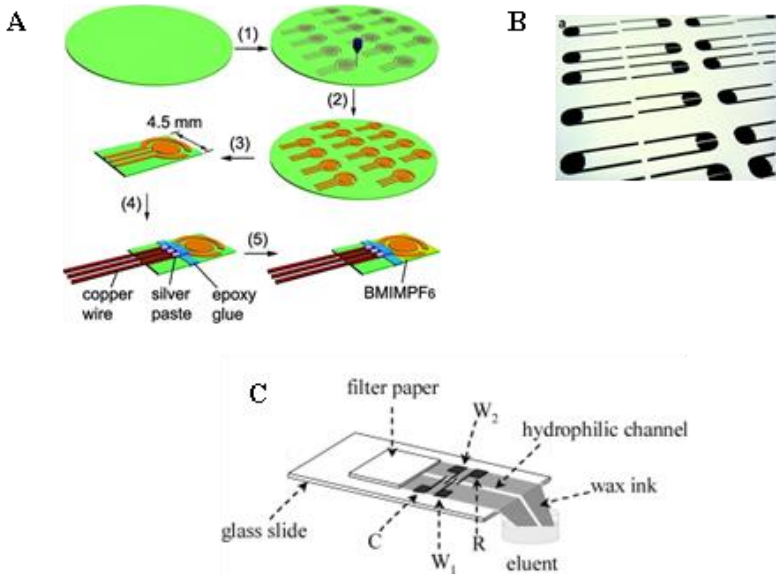

Figure A1.2: (A) Fabrication of gold electrodes on mixed cellulose membrane using inkjet printing. Reprinted with permission from [15]. Copyright 2012 American Chemical Society. (B) AuNPs inkjet-printed on paper (a) and IR sintered to be conductive (b). Reprinted with permission from [16]. Copyright 2012 American Chemical Society. (C) An ePAD consisting pencil-drawn electrodes. R and C stand for reference and counter electrodes, respectively. W, W_1 and W_2 are working electrodes. Reprinted with permission from [19]. Copyright 2013 Wiley-VCH Verlag GmbH & Co. KGaA, Weinheim.

Two separate groups reported the use of pencils for ePAD fabrication almost simultaneously. Dossi *et al.*[18] introduced a simple ePAD consisting of a hand-drawn, graphite three electrode system. This device was applied for electrochemical detection of AA and sunset yellow dye within an ePAD separation device. A similar device presented by Dossi *et al.*[19] included the use of a dual working electrode system for the simultaneous detection of dopamine (DA) and AA at different working electrode potentials (as shown in Figure A1.2C). The second system demonstrated by Santhiago *et al.*[20] showed the integration between using graphite pencils as electrodes and mPADs for glucose biosensing. The electrical performance of pencil-drawing on paper was studied extensively.[21] Although pencil-drawing possesses the advantages of fabrication simplicity and resistance to chemicals and heat, the moisture in the paper can affect the electrical properties of the pencil-traces by raising ionic currents.

Screen-printing

The development of SPEs in this period was adapted to three dimensional (3D) and/or multiplexed ePAD designs. Wang *et al*.[22] proposed 3D ePADs fabricated on two layers of paper with dual working electrodes sharing the same counter and reference electrodes (Figure A1.3A). The top layer consisted of a hydrophilic circular middle zone connected to two circular working zones, where carbon electrodes were screen-printed on the bottom layer. In this example, the two working electrodes were coated with a multi-walled carbon nanotubes/chitosan (MWCNTs/chitosan) mixture. The working electrodes were aligned with the circular middle zone that contained the reference and counter electrodes. The MWCNTs/chitosan coating improved device sensitivity, allowing for simultaneous detection of two tumor markers in serum samples. Moreover, later work used a variation to this system to fabricate eight working zones with eight working electrodes sharing the same reference and counter electrodes (Figure A1.3B).[23] With this improved design, a sensitive point-of-care immunoassay was demonstrated for high-throughput assays. In addition, another 3D ePAD with screen-printed conductive carbon ink was also integrated in a self-powered origami PAD (oPAD) that self-generating an electrical signal from the reaction of glucose oxidase and glucose for the conversion of $[Fe(CN)_6]^{3-}$ to $[Fe(CN)_6]^{4-}$ giving a voltage difference from a control and test zone that was charged in a capacitor and read using a digital multimeter.[24] The charge on the capacitor, while directly proportional to the amount of glucose in the sample, also provided a 17 fold amplification in signal from a direct current measurement.

The modification of screen-printed carbon electrodes (SPCEs) has attracted considerable attention as a way to improve ePAD sensitivity, selectivity and versatility. Modifiers previously reported for SPCEs include ionic liquids,[25] nanoparticles,[26,27] molecular imprinting polymers,[28,29]

conducting polymers,[28] cobalt phthalocyanine,[30] enzymes[31] and graphene.[32] Besides electrode modification, substrate materials were also studied to determine the most suitable paper-based material for reproducible, robust and low-cost sensors.[33] It was found that between inkjet, ruled notepad, and filter paper, inkjet paper provided results most similar to ideal behavior and commercially available SPCEs on polymer substrates, while maintaining flexibility.

In addition to homemade SPCEs, commercial SPCEs were coupled with ePADs for determination of Cd and Pb in soda water and ground water,[34] glucose detection[35-37] and protein assays.[38] Modification of commercial SPEs using sodium dodecyl sulfate was demonstrated to solve the overlapping peaks between DA, AA, and UA in serum samples.[39]

Other electrode fabrication techniques

The use of stencil-printing was further studied by fabricating carbon electrodes onto wax-printed paper and combining this layer with cut polymer layers to form a fluidic channel over the surface of the paper-based electrodes.[40] This device was further studied using amperometric detection of ferrocyanide. Additionally, thin-film sputtering through a mask was used as an electrode fabrication method. Gold was sputtered onto a paper chromatography channel to create gold electrodes for electrochemical detection of paracetamol and 4-aminophenol following separation in a paper channel (Figure A1.3C).[41] Carbon nanotubes (CNTs) have also been used to coat cellulose fibers with conductive material. ACNT-ink was painted to make conductive paper and a specific ion selective membrane was subsequently drop-casted via a stencil onto the conductive paper.[42] The conducting paper was used as an ion selective electrode for measurements of K^+, NH^{4+} and pH. CNTs were also used to make electrodes by vacuuming a CNT mixture into the paper through a metal mask for pH sensing. Polypyrrole, another conductive material which can be used as a supercapacitor, was synthesized on cellulose fibers to be used as alternative paper-

based electrodes.[43] The electrodes were fabricated by dipping the paper into a pyrrole solution and polymerized onto the paper fibers using a chemical oxidant. The electrochemical properties of the

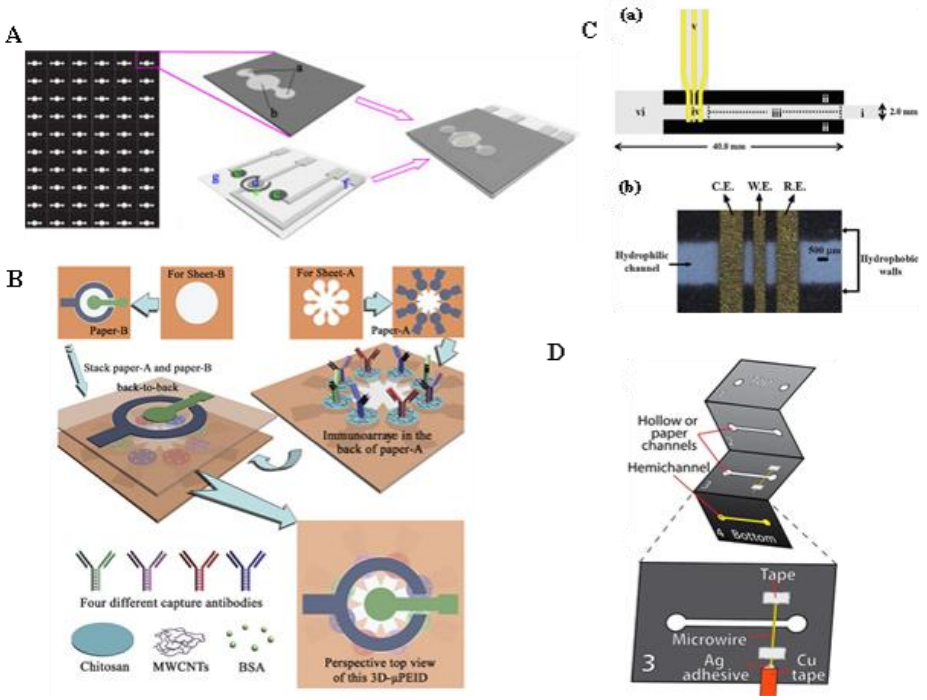

Figure A1.3: (A) Ascreen-printed 3D ePAD. (1) Arrays of wax-printed devices. (2) A top layer of 3D ePAD consisting of (a) working zones and (b) a circular middle zone. (3) SPEs on paper; (c) carbon working electrodes, (d) a Ag/AgCl reference electrode, (e) a carbon counter electrode, (f) silver conductive channel and pad and (g) a transparent polyethylene terephathalate substrate. (4) A complete device having the working zones aligned to the two working electrodes and the circular middle zone aligned to the reference and counter electrodes. Reprinted with permission from [22]. Copyright 2012 Elsevier. (B) An improvement of the ePAD in (A). This new 3D ePAD is composed of eight circular working zones with eight working electrodes sharing the same reference and counter electrodes for high-throughput immunoassays. Reprinted with permission from [23] with permission of The Royal Society of Chemistry. (C) Schematic (top) and a photograph (bottom) of an ePAD for electrochemical separation. C.E., W.E. and R.E. are counter, working and reference electrodes, respectively, fabricated from gold using a sputtering technique. Reprinted with permission from. Copyright 2012 Elsevier. (D) An origami-PAD (oPAD) incorporated with a gold microwire electrode. Reprinted with permission from [41]. Copyright 2014 American Chemical Society. (E) Fabrication of microwire electrodes on wax-printed paper. (a and b) Overview of a three PAD device. (c) A complete device having silver paint applied to the end of the electrodes to secure the electrodes. (d) Device connection to the potentiostat. Reprinted with permission from [44]. Copyright 2015 Elsevier.

polypyrrole paper-based electrode showed an increase in the charge capacity, indicating the possibility to use this system for energy storage.

The present state-of-the-art (2014-2015)

Recent developments in electrode fabrication methods have worked to improve ePADs for specific applications and detection schemes. While known fabrication methods (e.g. screen-printing, pencil-drawing and inkjet-printing) have been widely used for ePADs, a few new fabrication methods have been introduced. One such method is based on microwire placement.

Microwires

Fosdick *et al.*[44] were the first to incorporate prefabricated microwires as electrodes in an oPAD, as shown in Figure A1.3D. This paper showed that gold microwires within a hollow channel provided much lower resistance than carbon paste electrodes and could be easily cleaned and modified prior to device incorporation without contaminating the PAD. Since microwires can be fabricated with many different materials, this also gives the user flexibility in electrode composition. As proof-of-concept gold microwires were modified using self-assembling monolayers to selectively block or promote certain redox couples through electrostatic interactions, such as the blocking of anionic species $Fe(CN)_6^{3-}$. Moreover, metallic mesh electrodes were incorporated, which showed comparable results to single microwires. Apart from gold single-wire electrodes, different types of microwires, including solid gold, solid platinum, platinum with 8% tungsten, and platinum with 20% iridium, have been studied in ePADs and results were compared to traditional carbon SPEs by the author's group.[45] Microwire ePADs showed an overall increase in current density compared to carbon electrode ePADs, though having the wires in contact with the paper decreases the effective electroactive area. The study also demonstrated that cleaning the microwires with 50 mM KOH and 25% H_2O_2 significantly increased signal while

decreasing peak splitting, something that the clean wires maintained over time in storage. This chemical cleaning cannot be done with SPCEs. Although microwires are more expensive than carbon paste, another advantage of using pre-fabricated microwires is that the application can be more consistent than carbon screen-printing, which can vary based on each fabricator's technique.

Other fabrication techniques

Although graphite-based electrodes drawn on paper are not a new concept, Dossi *et al.*[46] introduced a new strategy to fabricate homemade pencils by "doping" the carbon used to make the pencil leads. The pencil leads were made using carbon powder as a conductive agent, sodium bentonite as a binding agent and sodium silicate as a hardening agent. The "doped" pencil leads contained these elements along with either 1% decamethylferrocene or 8% cobalt (II) phthalocyanine as the "dopant". Doping the pencil lead proved successful with the former dopant demonstrating a reversible redox reaction and the latter showing electrocatalytic activity toward cysteine and hydrogen peroxide.

Although incorporating hollow channels into oPADs was reported in 2013,[47] Renault *et al.*[48] demonstrated a hollow channel device with electrochemical detection in 2014. The incorporation of hollow channels into paper exhibited similar electrochemical results to those of traditional hollow-channel glass or plastic-based electrochemical microfluidic devices, but without the need of an external pump. The hollow channels were fabricated using a laser-cutter to create channel-shaped holes in filter paper, which were then folded into the proper configuration allowing SPEs to come into contact with the open channel. While fundamental studies for stencil-printed electrodes in ePADs have been done, these ePADs have also been used for applications in batteries and fuel cells.[49]

Modifying electrodes with nanoparticles as a way to enhance the electrochemical signal is a common practice for ePADs, and researchers are still developing new methods for electrode modification to enhance signal and obtain lower limits of detection. Nantophol *et al.*,[50] for example, fabricated a device for detection of cholesterol through a boron-doped diamond (BDD) working electrode modified with silver nanoparticles (AgNPs). A BDD working electrode was chosen due to its history with low background currents, a wide electrochemical potential window, and resistance to fouling. Although BDD electrodes have been previously used in other electrochemical devices, this was the first time it has been modified with AgNPs and applied to a PAD format. Modification with AgNPs was necessary to detect cholesterol because bare BDD has a low sensitivity for H_2O_2.

Throughout the years of development in electrode fabrication, various electrode materials and fabrication methods have been created and applied in ePADs. SPEs have gained popularity for ePADs due to their simplicity of fabrication, ease of modification, and possibility for large-scale production with reproducible electrodes. However, other electrode types have been proposed for particular applications. Therefore, current and future development of electrode fabrication techniques has put strong emphasis on the fabrication of ePADs for various fields of applications.

ePAD Applications

ePADs have been extensively used for a variety of applications; some key examples of applications are reviewed here to demonstrate the potential of ePADs in a variety of fields. The simple, sensitive, portable, disposable and cost-effective advantages to using ePADs over conventional or traditional methods has led to important advances in monitoring environmental contaminants as well as developing biomedical analysis devices and clinical assays.

Environmental Analysis

Normally, the analyses of environmental contaminants are performed using complicated and expensive equipment in centralized laboratories. Traditional field-based methods also remain complicated and/or require expensive portable spectrometers and/or fluorimeters for testing. ePADs have many features that make them highly desirable for applications in environmental monitoring. Current advances in environmental ePAD applications include the determination of heavy metals and toxic contaminants released or left-over from insecticides or pesticides.

Heavy metals

Due to their toxicity and prevalence in the environment, both Pb^{2+} and Cd^{2+} have gained considerable attention for ePAD detection.[29] Anodic stripping voltammetry (ASV) has been used to determine these metals due to the technique's high sensitivity and reproducibility. The first work demonstrating the use of ePADs for selective determination of $Pb^{2+}$was presented by Nie *et al.*[10] This ePAD system achieved an LOD for $Pb^{2+}$of 1 μg L^{-1}. This detection limit is lower than the guideline value (<10 μg L^{-1} for Pb^{2+} in drinking water) set by the World Health Organization (WHO). In separate work, the simultaneous detection of Cd^{2+} and Pb^{2+}in salty soda water and dirty ground water samples was performed using a paper channel with flow and commercial SPCEs.[51] This device provided detection limits of 2.3 μg L^{-1} and 2.0 μg L^{-1} for Cd^{2+} and Pb^{2+}, respectively. Furthermore, a potentiometric detection method that coupled paper as a sampling method with ion selective electrodes was used for measuring pH, Pb^{2+}, Cd^{2+} and Cl^{-}.[52] In addition, simultaneous detection of $Zn^{2+}$with Pb^{2+} was reported using SPCEs and square wave (SW) anodic stripping voltammetry (SWASV).[13] Bi^{3+}, Zn^{2+}, and buffer reagents were stored dry within a paper disk until time for analysis. The Zn^{2+} served as an internal standard while the $Bi^{3+}$was co-deposited during the preconcentration step to improve sensitivity.

Dual detection using electrochemical and colorimetric methods was also demonstrated for metals determination. Rattanarat *et al.*[53] developed a multilayer paper-based analytical device (as shown in Figure A1.4A) for the colorimetric and electrochemical quantitation of six metals. While Cd^{2+} and Pb^{2+} were electrochemically determined on a layer of the device using SWASV, simultaneous colorimetric detection of Ni, Fe, Cu, and Cr was performed on another layer. This unique configuration had detection limits of 0.75 μg for Fe, Ni and Cu, 0.12 μg for Cr and 0.25 ng for $Cd^{2+}$and $Pb^{2+}$when eluted from filter paper punches. The device effectively determined metals in re-suspended baghouse dust samples. Measured values were not statistically different from validated levels, indicating the system accuracy in complex matrices. Dual detection has also been employed for the electrochemical and colorimetric determination of Au^{3+} and Fe^{3+} respectively in gold-refining waste solutions (Figure A1.1D).[11]

More recently, modification to SPCEs using a graphene–polyaniline (G/PANI) nanocomposite was applied for the simultaneous determination of Zn^{2+}, Cd^{2+} and Pb^{2+} in human serum using SWASV.[54] As shown in Figure A1.4B, electrospraying was employed for electrode modification using G/PANI, producing a high surface area electrode. This resulted in higher sensitivity detection and faster electron transfer from unmodified electrodes. The detection limits were found to be 1.0 μg L^{-1} for Zn^{2+} and 0.1 μg L^{-1} for both Cd^{2+} and Pb^{2+} and were successfully detected from human serum samples.

Other contaminants

ePADs were also reported for determination of toxic compounds released from insecticides/pesticides or byproducts from the degradation process. p-Nitrophenol, is a product from biodegradation of parathion and methyl parathion and can be found in wastewater and agricultural run-off. Quantitative determination of p-nitrophenol was reported using an ePAD that

incorporated a quick response (QR) code for rapid assessment of p-nitrophenol information from a cell phone, as shown in Figure A1.4C.[55] This ePAD had a detection limit of 1.1 µM for p-nitrophenol. Other compounds such as some water soluble and insoluble organic species found in edible oil, including phenols, ortho-diphenols, and tocopherol, were determined with ePADs using cyclic voltammetry.[34] ePADs have also been applied for halide determination in a wide range of concentrations in water samples and food supplements.[56] The device incorporated a cation-exchange membrane between two silver-foil electrodes, each covered with thin cellulose paper. This fabrication was able to coulometrically determine halides, while reducing analysis time and cost of halide measurements when compared with conventional methods such as ion chromatography or volumetric titration. This approach was able to determine bromide and iodide in the concentration ranges of $10^{-4.8}$ to 0.1 M and $10^{-4.5}$ to 0.6 M for chloride, respectively.

Biological Applications

mPADs were originally developed for medical POC diagnostics in developing countries and resource-limited areas, where low-cost, rapid, simple, portable, disposable, and reliable tools are necessary. Accordingly, ePADs have followed this path for biomedical applications. This review highlights ePAD applications for protein, DNA, neurotransmitter, and biomarker determination.

Proteins and DNA

Proteins determined using immunoassays

Enzyme-linked immunosorbent assays (ELISAs) have been a common laboratory technique for decades in biochemical analyses. They have historically been carried out using 96-well microtiter plates and require use of an expensive plate reader for quantitative detection. Cheng *et al.*[57] introduced mPAD-based ELISA detection in 2010 for POC diagnostics using colorimetric

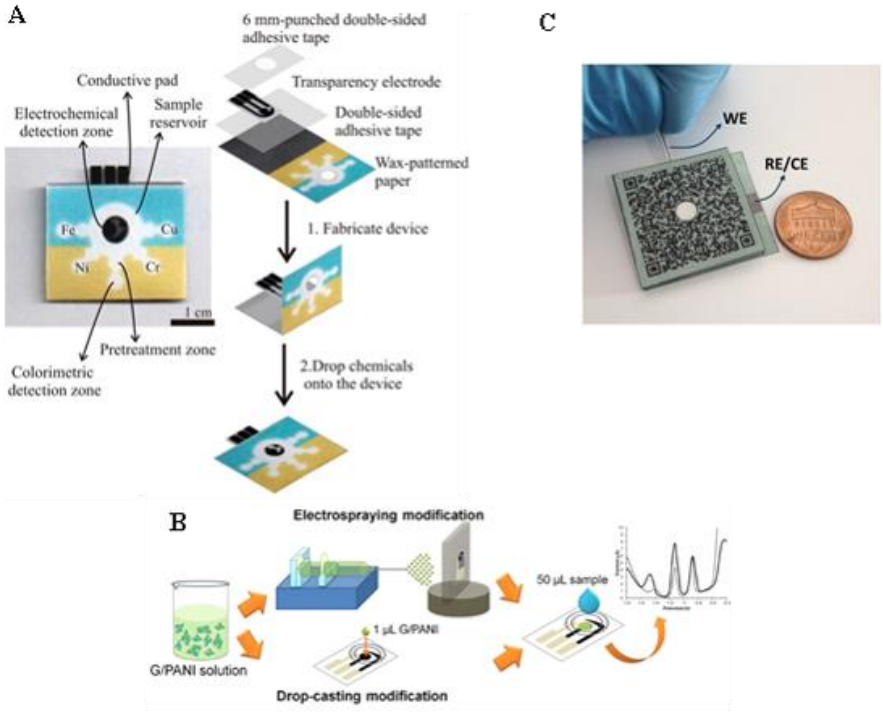

Figure A1.4: Applications of ePAD for environmental monitoring. (A) (left) An image of multilayer mPAD with dual colorimetric and electrochemical detection for simultaneous determination of $Cd^{2+}$and Pb^{2+} using electrochemical detection and Ni, Fe, Cu and Cr using colorimetric measurements. (right) A fabrication procedure for the device. Reprinted with permission from [53]. Copyright 2014 American Chemical Society. (B) A fabrication process of ePAD with commercial SPEs modified with graphene–polyaniline (G/PANI) by means of electrospraying. This device was applied for sensitive and simultaneous determination of Zn^{2+}, Cd^{2+} and Pb^{2+} in human serum. Reprinted with permission from [54]. Copyright 2015 Elsevier. (C) An ePAD with a quick response (QR) code for rapid assessment of p-nitrophenol; WE, RE and CE stand for working, reference and counter electrodes. Reprinted with permission from [55]. Copyright 2014 Elsevier.

detection. It yielded the same high specificity as a microtiter plate, but with faster results (more than an hour per step versus less than one hour total on paper) and cheaper analysis equipment (a desktop scanner versus a plate reader). While Li *et al.*[58] first introduced the concept of electrochemical ELISA's in 2010, it was not until 2012 when Zang *et al.*[23] introduced the first ePAD ELISA capable of detecting multiple analytes from real samples. The device detected multiple cancer biomarkers with a multiplexed format. There are two models of ELISA that have been incorporated into paper, indirect immunoassays and sandwich immunoassays. An indirect

immunoassay, utilized by Cheng et al.,[57] involved applying the desired antigen (most often a biomarker) directly onto the paper first, followed by a blocking agent, which is often bovine serum albumin (BSA) and finished with a primary (and sometimes secondary) enzyme conjugated antibody. The more antigen present, the more antibody that will bind, resulting in a higher signal from the conjugated enzyme. The purpose of the blocking agent is to prevent antibodies from non-specifically binding to the paper when no antigen is present, and prevent false positives from occurring. The sandwich ELISA model (Figure 5A) starts with a primary antibody, followed by the blocking agent, antigen, and enzyme-conjugated secondary antibody.[23,59] Between each step of the ELISA method, the paper is washed, typically with phosphate buffered saline (PBS) containing Tween 20, to wash away unbound substrates. Common enzymes conjugated as tags have include alkaline phosphatase and horseradish peroxidase (HRP).[23,59-61]

The immunoassay format has also been used not only to modify paper, but the electrodes themselves.[62,63] Recently, Montrose *et al.*[63] fabricated an electrochemical immunosensor for the detection of bovine viral diarrhea antibodies. They first modified a gold working electrode with a polymer layer of o-aminobenzoic acid before adding the capture antigen. Antibodies from the sample were detected electrochemically using cyclic voltammetry and impedance Nyquist plots. If BSA-antibodies were present in the solution, a decrease in cyclic voltammetry current intensity occurred from the antibodies blocking the electronic transfer of ferrocene monocarboxylic to the electrode surface. Since ELISA was first incorporated onto paper, several groups have introduced new ways to modify the paper or electrodes to increase sensitivity or stability of the ELISA, including modifying the paper with chitosan[60] or graphene[32] and modifying electrodes with dithiobis(succinimidyl propionate) self-assembled monolayer.[62] One group was able to achieve a detection limit of 0.03 ng mL^{-1} by first modifying the paper with chitosan and then incorporating

a ring-oven washing technique to eliminate nonspecific binding proteins (Figure A1.5A).[64] Modifying the paper with chitosan first was done to covalently immobilize antibodies on the surface. Several different electrode fabrication methods for ELISA detection have also been used including gold nano- and microwires[62] or CDs,[59] carbon nanotubes[61] and SPCEs.[57]

Proteins determined using other methods

Other papers have been published on detecting proteins without the use of immunoassays. Cunningham *et al.*[65] used a conformational switching assay to fabricate a biosensor for detection of DNA and thrombin. The absence of the target analyte (thrombin or DNA) resulted in the redox reporter (in this case, methylene blue) being in close proximity to the electrode surface for electron transfer or in the "off" position (Figure A1.5B). If the analyte is present, it binds to the redox reporter, causing a conformational change so that methylene blue is further away from the electrode surface and a decrease in electron transfer current is measured. This conformational switching model demonstrated a low detection limit of 30 nM and 16 nM for DNA and thrombin respectively. Another similar sensor was fabricated by Mahshid *et al.*[66] using a DNA probe. The DNA probe contained both a capture region for target proteins and a redox label. A complimentary DNA strand was used to capture the DNA probe, bring the redox label close to the electrode surface, resulting in an increase in signal. The presence of target protein binding to the DNA probe caused steric hindrance and reduced the binding of the two DNA strands. The sensor detected proteins as low as 100 nM in blood based on whether steric hindrance prevented the capture probe from binding and resulting in a decrease in electrochemical signal output.

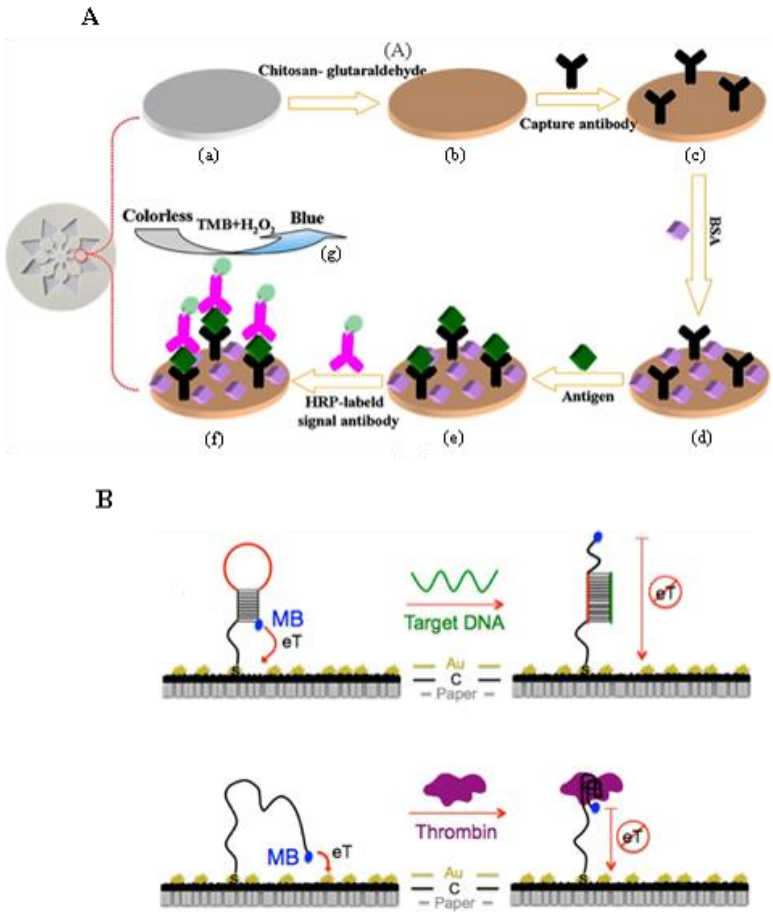

Figure A1.5: (A) A schematic of a typical sandwich enzyme-linked immunosorbent assay (ELISA). For this specific device, the paper (a) was first modified with chitosan (b) before putting down the capture antibody (c). Bovine serum albumin (BSA) was then applied to block non-specific binding (d) before applying the specific antigen (protein or other biomarker) (e) and HRP-labeled detection antibody that catalyzes the reaction (f). The concentration of product from the catalyzed reaction is proportional to the amount of specific antigen in the sample. Reprinted with permission from [65]. Copyright 2015 American Chemical Society. (B) The concept of an "off" sensor based on paper electrochemical device for detection of (a) DNA and (b) thrombin. Reprinted with permission from [66]. Copyright 2014 American Chemical Society.

DNA

Immobilization of a suitable probe on the electrode surface is key to improving sensitivity, selectivity, accuracy, and reproducibility of ePADs for DNA analysis. Lu *et al.*[67] first introduced a three-dimensional folding ePAD device for DNA detection using AuNP/graphene modified SPCEs. The ssDNA was immobilized on the surface of the AuNPs and used to capture nanoporous

gold nanoparticles bioconjugated with thionine and double-stranded DNA (dsDNA) as signal tags and the complementary ssDNA. This resulted in an excellent amplification with a LOD for the target DNA as low as 2nM. More recently, Li *et al.*[68] used a slip origami device (*o*Slip) with magnetic microbeads (MμBs) functionalized with capture DNA and a AgNP modified electrode to detect Hepatitis B virus (HBV). The device relied on the detection of Ag^+ resulting from the rapid oxidation of the AgNP labels by $KMnO_4$ pre-dispensed onto the paper in the final step and yielded the detection limit of 85 pM of HBV.

Clinical Assays

As the demand for rapid detection in on-site clinical analyses and personal health monitoring has increased, several laboratories have investigated the use of ePADs for detecting clinically significant biomarkers. Compounds such as DA, glucose, lactate, UA, cholesterol and cancer cells/biomarkers, provide key diagnostic indicators for health and disease states for individuals and have been quickly integrated into ePADs.

Dopamine

The development of analytical methodologies to accurately detect neurotransmitters is of interest for brain research and understanding neurodegenerative diseases. Rattanarat *et al.*[39] demonstrated a novel ePAD for the selective determination of DA in serum. Using SDS, the electrostatic interaction between cationic DA and anionic SDS resulted in a peak potential shift for the oxidative detection of the DA peak towards a more negative potential. This rendered the DA peak clearly distinguishable from the more positive potentials for AA and UA oxidation with a detection limit of 0.37 μM for DA. In a separate work, the simultaneous detection of DA or paracetamol mixed with AA was achieved using dual pencil-drawn working electrodes on a paper-based device.[19] Since AA oxidation is nonreversible, it is only oxidized at the first electrode.

Therefore, DA and paracetamol which are reversible electroactive species were reduced at the second electrode. This simultaneous detection was achieved without the need for separation and yielded detection limits of 5 μM and 6 μM for DA and paracetamol, respectively. Alternatively, carbon nanotubes and Nafion were used to modify a carbon tape working electrode for DA detection.[69] The working electrode was a double-sided conductive carbon tape supported on ITO glass. The modification of carbon tape electrodes with Nafion improved selectivity for DA detection by stopping AA from reaching the electrode surface. In addition, the Nafion modified electrode enhanced electrochemical signals of DA because Nafion had negative charges which enhance the adsorption of DA. This device provided electrochemical detection of DA with volumes of only10 μL and a detection limit of 0.01 μM.

Glucose/lactate/uric acid/ascorbic acid

Dungchai *et al.*[6] developed a novel ePAD for the simultaneous detection of glucose, lactate and UA, which are critical health markers in serum, using PB modified SPCEs (PB-SPCEs) (Figures A1.1A and A1.1B). The PB in the electrodes acted as a mediator for the amperometric detection of hydrogen peroxide formed from the oxidase reactions of each species. By spotting one enzyme for each analyte into individual detection zones (as shown in Figure A1.1B) and adding liquid samples into the hydrophilic center of the ePAD, the sample was then wicked outward along the channels and into three separate detection zones. Analytes in the sample then reacted with specific enzymes, and resulted in electrochemical signal from H_2O_2 generated from the oxidase enzyme reactions. The levels of glucose and lactate measured from neat and serum samples using ePADs were in good agreement with amounts obtained from traditional tests. Limits of detection for glucose, lactate, and UA were 0.21, 0.36, and 1.38 mM respectively. The success of this first mPAD integrated with electrochemical detection paved the way for the use of ePADs

for POC monitoring and clinical diagnostics. As a method to improve the analytical performance of ePADs, PANI was also used to modify SPCEs using an inkjet-printing technique for ascorbic acid (AA) detection.[70] The analytical performance was improved by optimizing the printed layer of PANI which affected the peak shape and current due to high electrochemical catalytic properties of PANI towards AA. Under optimal conditions using 5 layers of printed PANI, a detection limit as low as 30 μM of AA of this PANI modified sensor was obtained with no interference from UA; however, acetaminophen was found to interfere at concentrations above 140 μM. The simultaneous electrochemical detection of AA and UA was also reported within a paper-based separation device.[12] Although the analysis time for this device was slightly longer than that obtained from HPLC analysis of both species, no expensive equipment was required.

Glucose has been an analyte of significant research using ePADs. Therefore, new techniques to improve the efficiency of ePADs for glucose determination have been developed. A method for quantitative analysis of glucose in artificial urine was demonstrated using ePADs with a LOD of 0.22 mM.[10] In addition, a dumbbell-shaped ePAD design was created for glucose determination in blood samples.[37] With this ePAD platform, blood separation was achieved and only serum was electrochemically measured for glucose. In a similar work, a cellulose paper disc was used to immobilize glucose oxidase (GOX) via a simple physical adsorption method and for glucose measurements.[71] This immobilization method was simple and biocompatible, giving high enzyme activity. For electrochemical detection, the paper disc immobilized with GOX was placed on top of PB-SPCEs and a standard/sample solution was then added onto the paper (Figure A1.6B). This approach required 15μLsamples for electrochemical detection of glucose with a detection limit of 0.01 mM. Another feature of paper devices is the ability to incorporate layers with different functionalities. Accordingly, Santhiago et al. developed an ePAD glucose sensor with three

hydrophilic regions within a wax patterned device. The device was folded into three layers for different functions, including filtration, reaction with GOX, and subsequent reaction with redox mediator within a detection zone. The detection zone also contained two electrodes fabricated from silver ink and graphite pencil (Figure. A1.6C). This device provided a detection limit of 0.38 μM for glucose, sample consumption of 40 μL and analysis time <5 min.

To enhance the analytical performance of ePADs for glucose detection, a commercial instrument was also integrated with ePADs. Nie *at el.*[14] presented the use of a commercial glucometer as an electrochemical reader for ePAD devices to detect glucose, cholesterol, lactate, and alcohol (Figure 1E). This study showed the feasibility of ePADs for real world POC diagnostics utilizing existing glucometer technology. Aside from this works novel integration between an ePAD device with a commercial electrochemical reader, Liu and Crooks[36] proposed an all-in-one battery-powered ePAD device without the need for an external power source for glucose detection. This device was highly promising for POC clinical diagnosis in resource-limited areas and provided a 0.1 mM limit of detection for glucose in artificial urine samples.

Cholesterol

Cholesterol is another key health marker successfully implemented into ePADs. One device incorporated an electrosprayed nanocomposite graphene (G), polyvinylpyrrolidone (PVP) and PANI on SPCEs to increase the electrode surface area and enhance the sensitivity for cholesterol detection.[72] Interference from AA was eliminated using electrostatic repulsion from an anionic SDS coating on the G/PVP/PANI-modified working electrode. The LOD for cholesterol was found to be as low as 1 μM. More recently, Nantaphol *et al.*[73] improved the analytical performance of ePADs for cholesterol determination using a silver nanoparticle modified boron-

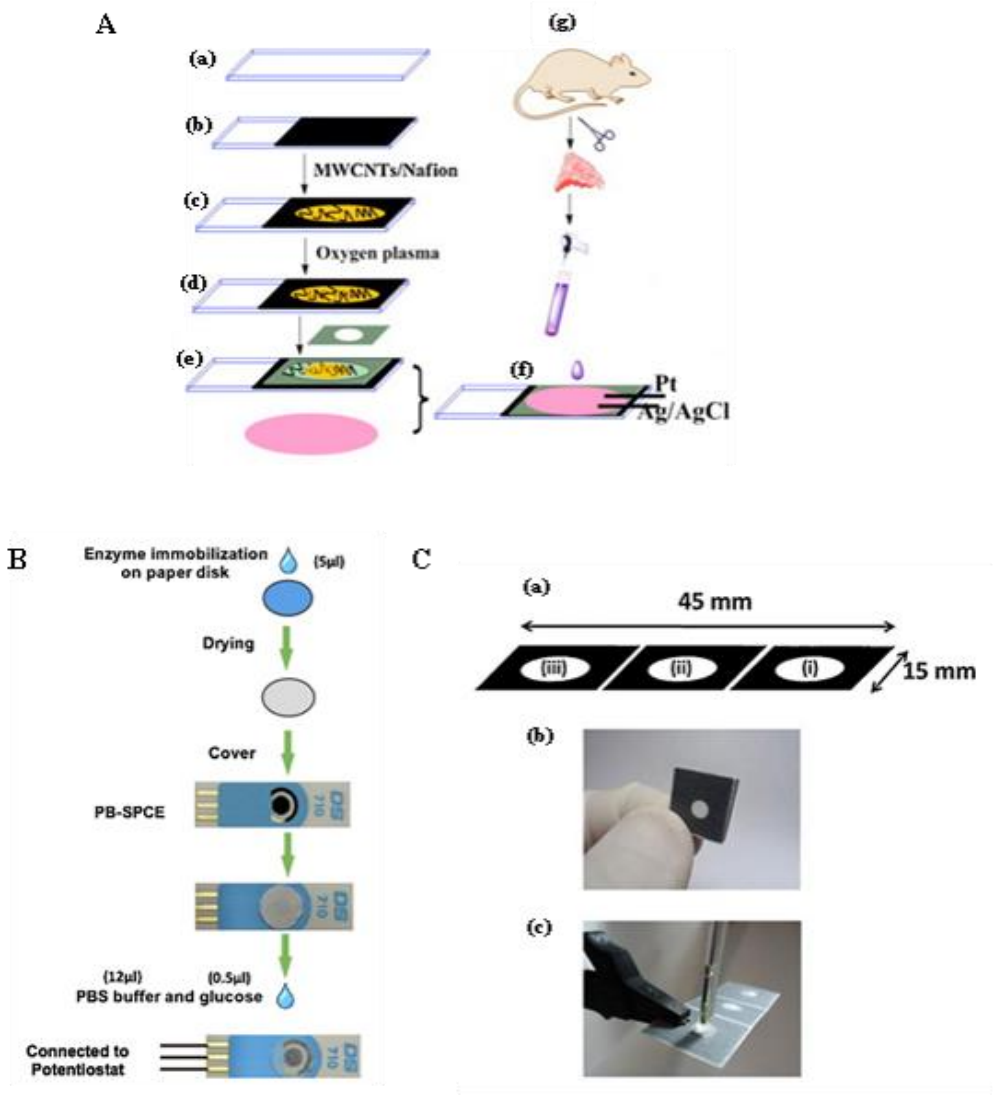

Figure A1.6: Biological applications of ePADs. (A) Multiwall carbon nanotubes and Nafion (MWCNTs/Nafion) modified carbon tape working electrode for determination of DA extracted from the striatum of rat; (a) ITO glass, (b) carbon tape electrode, (c) MWCNTs/Nafion carbon tape electrode, (d) treatment of oxygen plasma, (e) insulate plastic adhesive tape with a hole, (f) DA from striatum of rat and (g) the integrated ePAD. Reprinted with permission from [69]. Copyright 2015 Elsevier. (B) A GOX paper disc integrated with a PB SPE for electrochemical measurements of glucose. Reprinted with permission from [71]. Copyright 2014 Elsevier. (C) An ePAD glucose sensor; (a) wax-printed paper designed to have three hydrophilic working zones: (i) filtration step, (ii) reaction zone and (iii) electrochemical detection area, (b) a folded device and (c) Two electrode system fabricated from graphite pencil as a working electrode and silver ink as reference and counter electrodes for determination of glucose. Reprinted with permission from [20]. Copyright 2013 Elsevier.

doped diamond (AgNP/BDD) electrode. The favorable electrochemical properties of the BDD electrode in terms of stable and low background current enhanced the detection reproducibility and sensitivity by increasing the signal-to-noise ratio (S/N). AgNPs were used to modify the electrode in order to catalyze the reduction reaction of H_2O_2, and enhance signal while lowering the detection potential from unmodified electrodes. Cholesterol oxidase was directly drop-cast onto the hydrophilic area of the ePAD, and the H_2O_2 produced by the enzymatic reaction was monitored via reduction, which eliminated possible interference from other easily oxidized species in biological samples such as AA and UA

Cancer cells/markers

Cancer remains the second most common causes of death.[74] Early diagnosis of cancer is key to increasing survival prognosis, while providing effective and successful treatment for patients. Therefore, diagnostics providing rapid, sensitive and accurate detection of cancer cells or carcinogenic biomarkers have been an important area of research in ePAD development. A 3D ePAD capable of cancer cell detection was presented by Su *et al.*[75] The device contained four working electrodes all sharing a counter and reference electrode. A defined paper region was modified to create high surface area macroporous AuNP coated cellulose fibers to serve as a working electrode. Human acute promyelocytic leukemia cells (HL-60) were used as the cancer cell model, and a cell-targeting aptamer (KH1C12) was immobilized on the working paper electrode for detection. Using differential pulse voltammetry, detection of oxidized o-phenylenediamine from the reaction of hydrogen peroxide and HRP tagged to captured cells provided a linear range of 5.0×10^2 to 7.5×10^7 cells $mL^{-1}$for HL-60 detection with a LOD of 350 cells mL^{-1}. In addition, this research group recently reported an ePAD platform using trimetallic, dendritic PdPt nanodots on gold nanoparticles (Au@PdPt NPs) for detection of K-562 cells,

markers for early human chronic myelogenous leukemia diagnosis.[76] The Au@PdPt NPs possessed peroxidase-like activity and amplified signal by catalyzing the reduction of H_2O_2.When compared to the enzymatic peroxidase system previously reported,[75] this system exhibited more robust catalytic activity. The LOD of 31 cell mL^{-1} was found.

Aside from cancer cell detection, ePAD approaches for detection of cancer biomarkers have been developed. Li *et al.*[26] for example, proposed a 3D origami multiplexed electrochemical immunodevice for the simultaneous detection of carcinoembryonic antigen (CEA) and alpha-fetoprotein (AFP) using a nanoporous silver paper working electrode (PWE). A PANI-Au-PWE was also developed for quantification of CEA and AFP.[77] Electropolymerization of aniline was deposited on the Au-PWE layer, which served as a platform to absorb antibodies. This biosensor exhibited a detection limit of 0.5 and 0.8 pg mL^{-1} for CEA and AFP, respectively. Subsequently, highly sensitive determination of CEA was demonstrated using a novel 3D PWE fabricated from Au- core-shell-Pt nanoparticles possessing high conductivity and large surface area. This ePAD device showed high sensitivity with a detection limit of 0.4 pg mL^{-1} and a linear range of 1.0 pg mL^{-1}-100 ng mL^{-1} towards CEA detection. Moreover, a novel cuboid silver (CS) modified paper working electrode (CS-PWE) for determination of cancer antigen 125 (CA125) and carcinoma antigen 199 (CA199) was demonstrated by Li el al. Metal ion-coated nanoporous silver-chitosan was labeled on the CS-PWE to provide signal amplification. The detection limits of CA125 and CA199 were found to be 0.08 and 0.10 mU mL^{-1}, respectively. Furthermore, Ma *et al.*[78] presented an immunodevice based on a 3D origami platform for simultaneous detection of CEA and CA125 using Au nanorods modified paper working electrode (AuNRs-PWE) and metal ion-coated Au/bovine serum albumin (Au/BSA) nanospheres as tracing tags, as shown in Figure A1.7A. The introduction of AuNRs-PWE not only provided a biocompatible platform for immobilization of

antibodies, but also amplified the electrochemical signal of metal ions, such as Pb^{2+} and Cd^{2+}, which was carried by Au/BSA to form Au/BSA-metal ion tracer. This method provided high sensitivity with the detection limit of 0.08 pg mL^{-1} and 0.06 mU mL^{-1} for CEA and CA125, respectively. Additionally, an immunosensor for detection of prostate protein antigen (PSA), a biomarker of prostatic cancer, was introduced.[79] AuNPs were grown on the surface of screen-printed PWE and manganese oxide (MnO_2) was electrodeposited on the Au-PWE to form 3D nanowires. This immunoassay was based on enzymatic label redox cycling. GOx, 3,3',5,5'-tetramethylbenzidine (TMB) and glucose acted as an enzyme label, a redox terminator and a substrate, respectively. The proposed immunosensor provided high performance for PSA quantification with the detection limit of 0.0012 ng mL^{-1}.

Due to the problems associated with enzyme purification, immobilization, and denaturation, enzyme-free immunosensors were also developed as an alternative for detecting cancer biomarkers. Sun et al.[80] presented a novel enzyme-free electrochemical immunosensor constructed on an ePAD for detection of human chorionic gonadotropin, PSA and CEA using ZnO nanorods (ZNRs) on a modified reduced graphene oxide (rGO) working electrode on paper, as shown in Figure A1.7B. rGO improved the electron transfer rate, while ZNRs provided abundant binding sites for the capture probes. Due to the high catalytic activity of AgNPs toward H_2O_2 reduction, AgNPs mediated with bovine serum albumin (Ag-BSA) was employed for detection of H_2O_2. This proposed enzyme-free immunodevice exhibited high precision, sensitivity and stability and held great promise as a facile and cost-effective platform for clinical applications. Subsequently, this research group also presented an enzyme-free electrochemical immunodevice based on porous zinc oxide spheres (PZS) combined with silver nanoparticles (PZS-AgNPs) for selective determination of PSA.[81] In addition, a paper electrochemical sensor for selective

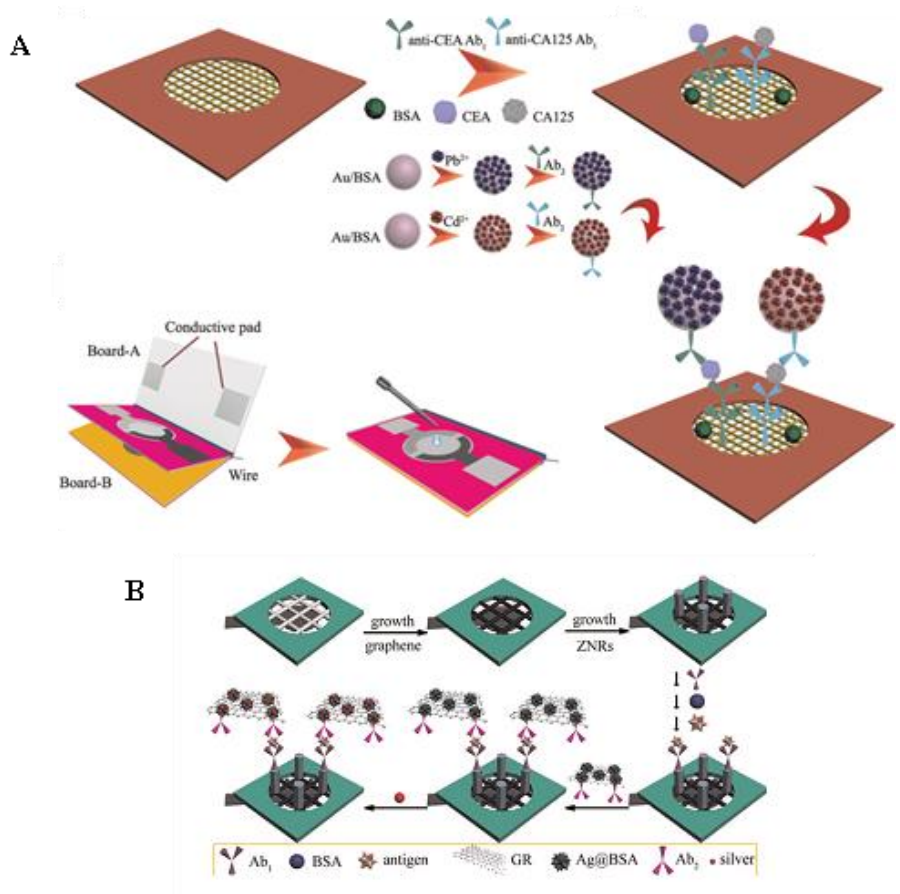

Figure A1.7: (A) Fabrication and operation of a 3D origami electrochemical immunosensor for detection of CEA and CA125. (a) Growth of AuNRs layer on bare PWE, (b) immobilization step (c) incubation of tracer and (d) electrochemical detection step. Reprinted with permission from [78]. Copyright 2015 Elsevier. (B) Schematic of the fabrication process of an enzyme-free electrochemical immunosensor on an origami ePAD; Ab and ZNRs are antibody and ZnO nanorods, respectively. Reprinted with permission from [80]. Copyright 2015 Elsevier.

determination of CEA was also developed using a poly(3,4-ethylen edioxythiophene):poly (styrene-sulfonate) (PEDOT:PSS) and rGO composite.[82] This paper electrode improved electrochemical performance when compared to the expensive conventional electrodes (ITO, gold and glassy carbon) and provided high sensitivity with the detection limit of 25.8 μA ng^{-1} mL cm^{-2} for CEA.

Summary and Outlook

Since its inception in 2009, ePADs have been widely used for a variety of applications in the fields of environmental monitoring, biomedical analysis, and POC diagnostics. Of particular

note is electrode fabrication which plays an essential role in electrochemical behavior and functionality and hugely impacts the performance of ePADs. Accordingly, electrode fabrication methods, materials and geometries have been continuously studied and developed to attain the highest level of ePAD performance. In addition, electrode modification, which can be simply performed using various substances/chemicals, can render ePADs more highly sensitive, selective and versatile. Moreover, multiplexed designs in 2D, 3D or origami configurations have proved to be more efficient and functional platforms where multiple or complicated reactions can be performed in a facile manner. Accordingly, a new generation of ePADs would be directed towards the development of integrated and automated devices, which possess more functions (e.g. sample preparation, separation, reaction and detection) in simplified platforms. This would drive ePADs into real-world analysis and open the door for applications in unexplored areas. To attain this feasibility, it would be necessary to develop a portable electrochemical reader for ePADs which is user-friendly and has an easy to interpret readout. In addition, self-powered ePADs should be considered for applications in remote or resource-limited areas. Recent advances in ePAD technologies hold great promise for transformation from proof-of-concept devices in laboratories to marketable and commercially fabricated devices, which are still rarely explored. Although the commercialization of ePADs looks to be a future route, fundamental studies and improvements should be ongoing to firmly strengthen and support ePAD technologies. Both scientific and industrial aspects will expedite ePADs for real-world analysis. With current and future endeavors, the coming years will not only be proof-of-principle ePAD platforms demonstrated in scientific journals, but they will be a practical technology, making the future full of possibilities and "nothing is impossible".

REFERENCES

1. J. Mettakoonpitak, K. Boehle, S. Nantaphol, P. Teengam, J. A. Adkins, M. Srisa-Art and C. S. Henry, *Electroanalysis*, 2016, **28**, 1420-1436.
2. A. W. Martinez, S. T. Phillips, M. J. Butte and G. M. Whitesides, *Angewandte Chemie-International Edition*, 2007, **46**, 1318-1320.
3. D. M. Cate, J. A. Adkins, J. Mettakoonpitak and C. S. Henry, *Analytical Chemistry*, 2015, **87**, 19-41.
4. J. Adkins, K. Boehle and C. Henry, *ELECTROPHORESIS*, 2015, **36**, 1811-1824.
5. A. K. Yetisen, M. S. Akram and C. R. Lowe, *Lab on a Chip*, 2013, **13**, 2210-2251.
6. W. Dungchai, O. Chailapakul and C. S. Henry, *Analytical Chemistry*, 2009, **81**, 5821-5826.
7. J.-M. Oh and K.-F. Chow, *Analytical Methods*, 2015, **7**, 7951-7960.
8. F. Sassa, K. Morimoto, W. Satoh and H. Suzuki, *Electrophoresis*, 2008, **29**, 1787-1800.
9. J. P. Metters, R. O. Kadara and C. E. Banks, *Analyst*, 2011, **136**, 1067-1076.
10. Z. Nie, C. A. Nijhuis, J. Gong, X. Chen, A. Kumachev, A. W. Martinez, M. Narovlyansky and G. M. Whitesides, *Lab on a chip*, 2010, **10**, 477-483.
11. A. Apilux, W. Dungchai, W. Siangproh, N. Praphairaksit, C. S. Henry and O. Chailapakul, *Analytical chemistry*, 2010, **82**, 1727-1732.
12. R. F. Carvalhal, M. S. Kfouri, M. H. Piazetta, A. L. Gobbi and L. T. Kubota, *Analytical chemistry*, 2010, **82**, 1162-1165.
13. S. N. Tan, L. Ge and W. Wang, *Analytical chemistry*, 2010, **82**, 8844-8847.
14. Z. Nie, F. Deiss, X. Liu, O. Akbulut and G. M. Whitesides, *Lab on a chip*, 2010, **10**, 3163-3169.

15. C. Hu, X. Bai, Y. Wang, W. Jin, X. Zhang and S. Hu, *Analytical chemistry*, 2012, **84**, 3745-3750.

16. A. Maattanen, P. Ihalainen, P. Pulkkinen, S. Wang, H. Tenhu and J. Peltonen, *ACS applied materials & interfaces*, 2012, **4**, 955-964.

17. G. Yang, L. Xie, M. Mantysalo, J. Chen, H. Tenhunen and L.-R. Zheng, *Ieee Transactions on Information Technology in Biomedicine*, 2012, **16**, 1043-1050.

18. N. Dossi, R. Toniolo, A. Pizzariello, F. Impellizzieri, E. Piccin and G. Bontempelli, *Electrophoresis*, 2013, **34**, 2085-2091.

19. N. Dossi, R. Toniolo, E. Piccin, S. Susmel, A. Pizzariello and G. Bontempelli, *Electroanalysis*, 2013, **25**, 2515-2522.

20. M. Santhiago and L. T. Kubota, *Sensors and Actuators B-Chemical*, 2013, **177**, 224-230.

21. N. Kurra and G. U. Kulkarni, *Lab on a chip*, 2013, **13**, 2866-2873.

22. P. Wang, L. Ge, M. Yan, X. Song, S. Ge and J. Yu, *Biosensors and Bioelectronics*, 2012, **32**, 238-243.

23. D. Zang, L. Ge, M. Yan, X. Song and J. Yu, *Chemical Communications*, 2012, **48**, 4683-4685.

24. H. Liu, Y. Xiang, Y. Lu and R. M. Crooks, *Angewandte Chemie*, 2012, **124**, 7031-7034.

25. N. Dossi, R. Toniolo, A. Pizzariello, E. Carrilho, E. Piccin, S. Battiston and G. Bontempelli, *Lab on a chip*, 2012, **12**, 153-158.

26. W. Li, L. Li, M. Li, J. Yu, S. Ge, M. Yan and X. Song, *Chemical communications*, 2013, **49**, 9540-9542.

27. D. D. Liana, B. Raguse, L. Wieczorek, G. R. Baxter, K. Chuah, J. J. Gooding and E. Chow, *RSC Advances*, 2013, **3**, 8683.

28. L. Ge, S. Wang, J. Yu, N. Li, S. Ge and M. Yan, *Advanced Functional Materials*, 2013, **23**, 3115-3123.

29. P. Wang, G. Sun, L. Ge, S. Ge, J. Yu and M. Yan, *Analyst*, 2013, **138**, 4802-4811.

30. M. Santhiago, J. B. Wydallis, L. T. Kubota and C. S. Henry, *Analytical chemistry*, 2013, **85**, 5233-5239.

31. G. P. M. K. Ciniciato, C. Lau, A. Cochrane, S. S. Sibbett, E. R. Gonzalez and P. Atanassov, *Electrochimica Acta*, 2012, **82**, 208-213.

32. Y. Wu, P. Xue, Y. Kang and K. M. Hui, *Analytical chemistry*, 2013, **85**, 8661-8668.

33. J. P. Metters, S. M. Houssein, D. K. Kampouris and C. E. Banks, *Anal. Methods*, 2013, **5**, 103-110.

34. N. Dossi, R. Toniolo, F. Terzi, E. Piccin and G. Bontempelli, *Electrophoresis*, 2015, **36**, 1830-1836.

35. J. Lankelma, Z. Nie, E. Carrilho and G. M. Whitesides, *Analytical chemistry*, 2012, **84**, 4147-4152.

36. H. Liu and R. M. Crooks, *Analytical chemistry*, 2012, **84**, 2528-2532.

37. J. Noiphung, T. Songjaroen, W. Dungchai, C. S. Henry, O. Chailapakul and W. Laiwattanapaisal, *Analytica chimica acta*, 2013, **788**, 39-45.

38. J. Szűcs and R. E. Gyurcsányi, *Electroanalysis*, 2012, **24**, 146-152.

39. P. Rattanarat, W. Dungchai, W. Siangproh, O. Chailapakul and C. S. Henry, *Analytica chimica acta*, 2012, **744**, 1-7.

40. N. Godino, R. Gorkin, 3rd, K. Bourke and J. Ducree, *Lab on a chip*, 2012, **12**, 3281-3284.

41. L. Y. Shiroma, M. Santhiago, A. L. Gobbi and L. T. Kubota, *Analytica chimica acta*, 2012, **725**, 44-50.

42. M. Novell, M. Parrilla, G. A. Crespo, F. X. Rius and F. J. Andrade, *Analytical chemistry*, 2012, **84**, 4695-4702.

43. H. Olsson, D. O. Carlsson, G. Nyström, M. Sjödin, L. Nyholm and M. Strømme, *Journal of Materials Science*, 2012, **47**, 5317-5325.

44. S. E. Fosdick, M. J. Anderson, C. Renault, P. R. DeGregory, J. A. Loussaert and R. M. Crooks, *Analytical Chemistry*, 2014, **86**, 3659-3666.

45. J. A. Adkins and C. S. Henry, *Analytica Chimica Acta*, 2015, **891**, 247-254.

46. N. Dossi, R. Toniolo, F. Impellizzieri and G. Bontempelli, *Journal of Electroanalytical Chemistry*, 2014, **722**, 90-94.

47. C. Renault, X. Li, S. E. Fosdick and R. M. Crooks, *Analytical Chemistry*, 2013, **85**, 7976-7979.

48. C. Renault, M. J. Anderson and R. M. Crooks, *Journal of the American Chemical Society*, 2014, **136**, 4616-4623.

49. S.-S. Chen, C.-W. Hu, I. F. Yu, Y.-C. Liao and J.-T. Yang, *Lab on a Chip*, 2014, **14**, 2124-2130.

50. S. Nantaphol, O. Chailapakul and W. Siangproh, *Sensors and Actuators B: Chemical*, 2015, **207**, 193-198.

51. J. Shi, F. Tang, H. Xing, H. Zheng, B. Lianhua and W. Wei, *Journal of the Brazilian Chemical Society*, 2012, **23**, 1124-1130.

52. G. Lisak, J. Cui and J. Bobacka, *Sensors and Actuators B: Chemical*, 2015, **207**, 933-939.

53. P. Rattanarat, W. Dungchai, D. Cate, J. Volckens, O. Chailapakul and C. S. Henry, *Analytical chemistry*, 2014, **86**, 3555-3562.

54. N. Ruecha, N. Rodthongkum, D. M. Cate, J. Volckens, O. Chailapakul and C. S. Henry, *Analytica chimica acta*, 2015, **874**, 40-48.

55. M. Santhiago, C. S. Henry and L. T. Kubota, *Electrochimica Acta*, 2014, **130**, 771-777.

56. M. Cuartero, G. A. Crespo and E. Bakker, *Analytical chemistry*, 2015, **87**, 1981-1990.

57. C. M. Cheng, A. W. Martinez, J. Gong, C. R. Mace, S. T. Phillips, E. Carrilho, K. A. Mirica and G. M. Whitesides, *Angewandte Chemie International Edition*, 2010, **49**, 4771-4774.

58. X. J. Li, Z. H. Nie, C.-M. Cheng, A. B. Goodale and G. M. Whitesides, *Proc. Micro Total Analysis Systems*, 2010, **14**, 1487-1489.

59. C. Tang, A. Vaze and J. Rusling, *Analytical Methods*, 2014, **6**, 8878-8881.

60. S. Wang, L. Ge, X. Song, J. Yu, S. Ge, J. Huang and F. Zeng, *Biosensors and Bioelectronics*, 2012, **31**, 212-218.

61. S. Wang, L. Ge, X. Song, J. Yu, S. Ge, J. Huang and F. Zeng, *Biosensors and bioelectronics*, 2012, **31**, 212-218.

62. S. K. Arya, G. Chornokur, M. Venugopal and S. Bhansali, *Biosensors and Bioelectronics*, 2010, **25**, 2296-2301.

63. A. Montrose, N. Creedon, R. Sayers, S. Barry and A. O'riordan, *J Biosens Bioelectron*, 2015, **6**, 1-7.

64. W. Liu, Y. Guo, M. Zhao, H. Li and Z. Zhang, *Analytical Chemistry*, 2015, **87**, 7951-7957.

65. J. C. Cunningham, N. J. Brenes and R. M. Crooks, *Analytical chemistry*, 2014, **86**, 6166-6170.

66. S. S. Mahshid, S. Camiré, F. Ricci and A. Vallée-Bélisle, *Journal of the American Chemical Society*, 2015, DOI: 10.1021/jacs.5b04942.

67. J. Lu, S. Ge, L. Ge, M. Yan and J. Yu, *Electrochimica Acta*, 2012, **80**, 334-341.

68. X. Li, K. Scida and R. M. Crooks, *Analytical chemistry*, 2015, **87**, 9009-9015.

69. Q.-M. Feng, M. Cai, C.-G. Shi, N. Bao and H.-Y. Gu, *Sensors and Actuators B: Chemical*, 2015, **209**, 870-876.

70. W. Kit-Anan, A. Olarnwanich, C. Sriprachuabwong, C. Karuwan, A. Tuantranont, A. Wisitsoraat, W. Srituravanich and A. Pimpin, *Journal of Electroanalytical Chemistry*, 2012, **685**, 72-78.

71. N. C. Sekar, S. A. M. Shaegh, S. H. Ng, L. Ge and S. N. Tan, *Sensors and Actuators B: Chemical*, 2014, **204**, 414-420.

72. N. Ruecha, R. Rangkupan, N. Rodthongkum and O. Chailapakul, *Biosensors & bioelectronics*, 2014, **52**, 13-19.

73. S. Nantaphol, O. Chailapakul and W. Siangproh, *Analytica Chimica Acta*, 2015, DOI: 10.1016/j.aca.2015.08.007.

74. Cancer Facts & Figures 2015, (accessed 1st December 2015).

75. M. Su, L. Ge, S. Ge, N. Li, J. Yu, M. Yan and J. Huang, *Analytica chimica acta*, 2014, **847**, 1-9.

76. S. Ge, Y. Zhang, L. Zhang, L. Liang, H. Liu, M. Yan, J. Huang and J. Yu, *Sensors and Actuators B: Chemical*, 2015, **220**, 665-672.

77. L. Li, W. Li, H. Yang, C. Ma, J. Yu, M. Yan and X. Song, *Electrochimica Acta*, 2014, **120**, 102-109.

78. C. Ma, W. Li, Q. Kong, H. Yang, Z. Bian, X. Song, J. Yu and M. Yan, *Biosensors and Bioelectronics*, 2015, **63**, 7-13.

79. L. Li, J. Xu, X. Zheng, C. Ma, X. Song, S. Ge, J. Yu and M. Yan, *Biosensors and Bioelectronics*, 2014, **61**, 76-82.

80. G. Sun, L. Zhang, Y. Zhang, H. Yang, C. Ma, S. Ge, M. Yan, J. Yu and X. Song, *Biosensors and Bioelectronics*, 2015, **71**, 30-36.

81. G. Sun, H. Liu, Y. Zhang, J. Yu, M. Yan, X. Song and W. He, *New Journal of Chemistry*, 2015, **39**, 6062-6067.

82. S. Kumar, S. Kumar, S. Srivastava, B. K. Yadav, S. H. Lee, J. G. Sharma, D. C. Doval and B. D. Malhotra, *Biosensors and Bioelectronics*, 2015, **73**, 114-122.